The enigma of plant tubulin detyrosination: lessons from a rice TTL family protein

Zur Erlangung des akademischen Grades eines

DOKTORS DER NATURWISSENSCHAFTEN

(Dr. rer. nat.)

von der KIT-Fakultät für Chemie und Biowissenschaften

des Karlsruher Instituts für Technologie (KIT)

genehmigte

DISSERTATION

von

Kunxi Zhang

aus

Henan, China

KIT-Dekan: Prof. Dr. Reinhard Fischer

Referent: Prof. Dr. Peter Nick

Korreferent: Prof. Dr. Reinhard Fischer

Tag der mündlichen Prüfung: 20. Juli 2020

Erklärung

Hiermit erkläre ich, dass ich die vorliegende Dissertation, abgesehen von der Benutzung der angegebenen Hilfsmittel, selbständig verfasst habe.

Alle Stellen, die gemäß Wortlaut oder Inhalt aus anderen Arbeiten entnommen sind, wurden durch Angabe der Quelle als Entlehnungen kenntlich gemacht.

Diese Dissertation liegt in gleicher oder ähnlicher Form keiner anderen Prüfungsbehörde vor.

Zudem erkläre ich, dass ich mich beim Anfertigen dieser Arbeit an die Regeln zur Sicherung guter wissenschaftlicher Praxis des KIT gehalten habe, einschließlich der Abgabe und Archivierung der Primärdaten, und dass die elektronische Version mit der schriftlichen übereinstimmt.

Karlsruhe, im June 2020

Kunxi Zhang

Acknowledgement

First of all, I have to express the depth of my gratitude to my supervisor Prof. Dr. Peter Nick. The most charming character of him is his approachable attitude, together with his highly positive attitude towards the work that I did, which always makes me free to speak to without being afraid and shy. I am also deeply impressed by his accessibility, no matter what results I had, negative or positive, he is always available for discussion. More importantly, he always gives me freedom and encouragement to explore my own ideas. When needed, he is always there for proposing his expert and constructive suggestion. I was like a piece of white paper that almost knew nothing about molecular biology when I came to our lab. Over the past 4 years, without his patient explainations, selfless dedication, support and professional guidance, this piece of white paper cannot be painted colourful. Beyond that, he always shows me how to propose scientific questions, how to handle it in the easiest way and how to persist on it. Without his enthusiasm and wisdom, I may not find the charm of academic research. I still remembered that the first lesson from him is unexpectedly not about research but about life: Real life helps to do good science, because it helps us to recognise what is important and real. Words cannot express how grateful I am for what he has done for me during these 4 years and he has shown me the model of a good teacher and scientist by himself.

I also want to express my special thanks to our stress group leader Dr. Michael Riemann, who helped me a lot both in research and life. Thanks for his expertise that helped me to solve several experimental problems, which saved up plenty of time for me. I still remembered the scene that he spent a lot of time sitting with me to give a pertinent suggestion to my Powerpoint presentation, from which I benefit a lot. I am really appreciated for his careful revision and

constructive suggestion on my thesis writing. Thanks a lot for his kind support.

A special thanks should also go to Dr. Sahi Vaidurya, who leads me to quickly adapt to lab life. I would also thanks Sabine Purper, Ernst Heene, Dr. Gabriele Jürges and Dr. Jan Maisch for their technical support, as well as Gero Kaeser for helping in protein related experiments and translating my abstract. Thanks for all colleagues and Azubis in the lab, with your selfless help, my work can go smoothly and my life can be easier.

I would like to thank Xiaobing Jiang, who is one of my best friends and sometimes acts as my tutor in life. Thanks for Dr. Huapeng Sun, Dr. Lixin Wang, Dr. Xiao Chen, Dr. Pingyin Guan and Dr. Gangliang Tang for treating me with beers, grapevine and Chinese wines, which enriches my part life about wine culture. Thanks for Xin Zhu, who gives her selfless dedication to my experiments especially in molecular biology. Thanks for Wenjing, who always treats me with her best dishes. Thanks for Lei Zheng and Weibin Wu, without you two, we cannot be ‘Big Three of Karlsruhe’.

At last, my heartfelt thank owes to my family. I have to thank my parents, my brother and sister-in-law for their unconditional loves on me. With your supports, I have the courage to pursue my dream. My heartfelt thank extends to Jinping Lu for true love and support, which changes me a lot and makes me better.

I would also thanks China Scholarship Council (CSC) for financial support on me to study in Germany.

Karlsruhe, 28/July/2020

Kunxi Zhang

Contents

Acknowledgement I

Abbreviations VI

Zusammenfassung VII

Abstract IX

1 Introduction 1

1.1 Overview of plant microtubules 1

1.2 Structural basis of plant microtubules 2

1.3 Functional diversity of plant microtubules 5

1.3.1 Functions of microtubules in cell expansion 6

1.3.2 Functions of microtubules in cell division 7

1.3.3 Functions of microtubules in signaling 9

1.4 Regulation of functional diversity of microtubules 11

1.4.1 Tubulin isotypes 11

1.4.2 Microtubule-associated proteins (MAPs) 12

1.5 Posttranslational modifications (PTMs) 14

1.5.1 Different posttranslational modifications 14

1.5.2 Functional diversity of differentially modified microtubules 16

1.6 Detyrosination/tyrosination cycle 17

1.7 Scope of this work 19

2 Materials and Methods 22

2.1 Multiple sequence alignment and phylogenetic analysis of TTL 22

2.2 Plant materials and cultivation 22

2.2.1 Rice materials and cultivation 22

2.2.2 Tobacco BY-2 cells and cultivation 23

2.3 Phenotyping of rice seedlings 24

2.4 Cell biological methods 25

2.4.1 Stable transformation of OsTTL-RFP into NtTUA3-GFP BY-2 cell line 25

2.4.2 Microtubule visualisation in rice tissues 26

2.4.3 Microtubule visualization in BY-2 cells 27

2.5 Molecular biological methods 29

2.5.1 RNA extraction and cDNA synthesis 29

2.5.2 Quantitative real-time PCR (qRT-PCR) analysis 29
2.5.3 Primers used in this work 30
2.5.4 Molecular cloning of construct of OsTTL fused with N-terminal His-tag 31
2.6 Biochemical methods 34
2.6.1 Protein extraction 34
2.6.2 SDS-polyacrylamide gel electrophoresis (SDS-PAGE) and Western blot analysis 34
2.6.3 EPC sepharose chromatography 37
2.6.4 Protein expression and purification in *E.coli* 38
2.7 Drug and cold treatment 40
2.7.1 Oryzalin treatment 40
2.7.2 Nitro-tyrosine treatment 40
2.7.3 Cold treatment 41
2.7.4 Extracellular alkalinisation 41
2.7.5 Determination of cell mortality 41
2.7.6 Butanol treatment 42
3 Results 43
3.1 Functions of OsTTL in rice growth and development 43
3.1.1 Plant TTLs cluster into a separate phylogenetic clade 44
3.1.2 Transcriptional level of OsTTL in OsTTL-RFP overexpressor rice lines 46
3.1.3 OsTTL-RFP decorates all microtubule arrays 46
3.1.4 Overexpression of OsTTL modulates orientation of microtubules, cell elongation, and cell division 49
3.1.5 Overexpression of OsTTL alters phenotypical changes of coleoptile and root 49
3.1.6 Overexpression of OsTTL promotes cell elongation and changes microtubule orientation in coleoptiles 50
3.1.7 Overexpression of OsTTL changes microtubule orientation in root elongation zone 52
3.1.8 Overexpression of OsTTL disorients cell walls in root meristem zone 53
3.1.9 Overexpression of OsTTL in BY-2 cell disorganizes phragmoplast microtubule 54
3.1.10 The organisation of phragmoplast microtubules is affected by nitrotyrosine .. 55
3.1.11 Overexpression of OsTTL confers a reduced sensitivity to oryzalin 56
3.1.12 Overexpression of OsTTL shifts α-tubulin into the detyrosinated form 57
3.2 Functions of OsTTL in cold stress 61

3.2.1 Overexpression of OsTTL reduces cold tolerance....61
3.2.2 Overexpression of OsTTL results in rapid cold induced microtubule disassembly 62
3.2.3 Overexpression of OsTTL results in more pronounced cold induced calcium influx....63
3.3 Functional interaction between OsTTL and OsPLDα1 65
3.3.1 Overexpression of OsTTL increases stability of cortical microtubules to 1% n-butanol treatment 66
3.3.2 OsPLDα1 co-localises with microtubules....67
3.3.3 Overexpression of OsPLDα1 results in higher abundance of detyrosinated α-tubulin....69
3.3.4 Overexpression of OsTTL increases the abundance of tyrosinated and detyrosinated α- tubulin (NtTUA3) contents....70
3.3.5 Overexpression of OsTTL results in higher transcripts of NtTUA3 and OsTTL71
4 Discussion....74
4.1 Why is it worth to study plant TTLs?....74
4.2 A role for tubulin tyrosination status in microtubule orientation?....76
4.3 Does tubulin re-tyrosination define functional subsets of microtubules? The case of the phragmoplast 78
4.4 Role of cotical microtubules that modified by OsTTL in cold perception....79
4.5 A role of posttranslational modification on autoregulation of tubulin synthesis 83
4.6 Is rice TTL a rice TTC?....87
4.7 Conclusion....91
References....94
Appendix....105

Abbreviations

+TIP	Plus-end tracking protein
BSA	Bovine serum albumin
CBB	Coommassie Brilliant Blue
cMT	Cortical microtubule
detyr	Detyrosinated α-tubulin
DTT	Dithiothreitol
E.coli	Escherichia coli
EPC	Ethy-N-phenylcarbamate
FITC	Fluorescein isothiocyanate
GDP	Guanosine-5’-diphosphate
GFP	Green fluorescent protein
GTP	Guanosine-5’-triphosphate
MAP	Microtubule associated protein
MT	Microtubule
NT	NitroTyrosine
PLD	Phospholipase D
PMSF	Phenylmethylsulfonyl fluoride
PTM	Posttranslational modification
RFP	Red fluorescent protein
ROS	Reactive oxygen species
TRITC	Tetramethylrodamine isothiocyanate
TTC	Tubulin tyrosine carboxypeptidase
TTL	Tubulin tyrosine ligase
tyr	Tyrosinated α-tubulin

Zusammenfassung

Der Detyrosinierungs- und Retyrosinierungszyklus ist einer der häufigsten posttranslationalen Modifikationsprozesse für α-Tubulin. Die Abspaltung eines konservierten, C-terminalen Tyrosins von α-Tubulin durch eine noch nicht bekannte Tubulin-Tyrosin-Carboxypeptidase (TTC) und die Religation dieses Tyrosins durch eine Tubulin-Tyrosin-Ligase (TTL) ist ein vermutlich gemeinsames Merkmal in allen Eukaryoten. Um diesen Zyklus der De- und Retyrosinierung genauer untersuchen zu können, wurden in unserem Labor transgene Linien erstellt, welche die Tubulin-Tyrosin Kinase aus Reis (nachfolgend als OsTTL bezeichnet) in sowohl Reis, als auch in Tabak BY-2 Zellen mit einem RFP-tag überexprimieren.

Überraschenderweise wurde herausgefunden, dass die Überexpression von OsTTL-RFP die relative Verweildauer von detyrosiniertem α-Tubulin in sowohl den Koleoptilen, als auch den Embryonalwurzeln erhöht ist und das dies mit stabileren und weniger transversal orientierten kortikalen Mikrotubuli einhergeht, die das Wachstums der Koleoptile und Seminalwurzeln beeinträchtigen. Pflanzen mit diesem Phänotyp zeigten eine gleichzeitig auftretende Störung in der Organisation der in den Phragmoplasten lokalisierten Mikrotubuli und eine fehlerhafte Orientierung der Zellwände. Folglich verändert die erhöhte Tubulin-Detyrosinierung, welche durch die Überexpression von OsTTL erreicht wurde, die strukturellen und dynamischen Eigenschaften von Mikrotubuli und beeinträchtigt damit die Axialität der Mittellamelle und schließlich das gesamte Pflanzenwachstum.

Die Überexpremierung von OsTTL-RFP in einer Mikrotubuli-Marker BY-2-Zelllinie, die NtTUA3-GFP exprimiert, veränderte die Kaltsensorfunktion der kortikalen Mikrotubuli, indem sie die kälteinduzierte Zerlegung der kortikalen Mikrotubuli beschleunigte, begleitet von einem ausgeprägten

Kalziumeinstrom, was schließlich zu einer verringerten Kälteakklimatisierung führte.

Der Abbau kortikaler Mikrotubuli, die durch die 1%ige n-Butanol induzierte Aktivierung der Phospholipase D (PLD) verursacht wurde, wurde durch eine Überexpression von OsTTL in der Zelllinie NtTAU3 BY-2 gemildert. OsPLDα1, eine Isoform der PLD-Familie aus Reis, die die gemeinsamen Funktionen der PLD vermittelt, wird vorzugsweise mit kortikalen Mikrotubuli, Spindel und Phragmoplastenmikrotubuli lokalisiert. Die Überexpression von OsPLDα1 erhöhte die Häufigkeit von detyrosiniertem α-Tubulin. Diese Ergebnisse deuteten auf eine funktionelle Interaktion zwischen OsPLDα1 und detyrosiniertem α-Tubulin hin.

Die Überexpression von OsTTL-RFP erhöhte nicht nur die Menge des α-Tubulin-Proteins, sondern auch die Transkription des α-Tubulin-Gens, sowie die Transkription von OsTTL, was auf eine gegenseitige Regulation der posttranslationalen Modifikation bei der Tubulinsynthese hindeutet.

Abstract

The detyrosination/retyrosination cycle is the most common posttranslational modification of α-tubulin. Removal of the conserved C-terminal tyrosine of α-tubulin by a still elusive tubulin tyrosine carboxypeptidase (TTC), and religation of this tyrosine by a tubulin tyrosine ligase (TTL) are probably shared between all eukaryotes. To get insight into the biological functions of this tubulin detyrosination/retyrosination cycle, in our lab, a tubulin tyrosine ligase family protein from rice (referred as OsTTL) was cloned, and overexpression OsTTL-RFP lines were generated in both rice and tobacco BY-2 cells.

It was found, unexpectedly, that overexpression of this OsTTL-RFP increased the relative abundance of detyrosinated α-tubulin in both coleoptile and seminal root, correlated with more stable microtubules and a less transverse orientation of cortical microtubule, followed by altered growth of coleoptiles and seminal roots. These phenotypes were accompanied by perturbed organisation of phragmoplast microtubules and disoriented cell walls. Thus, the elevated tubulin detyrosination in consequence of OsTTL overexpression affects structural and dynamic features of microtubule followed by changes in the axiality of cell plate deposition and consequently plant growth.

Overexpression of OsTTL-RFP in a microtubule marker BY-2 cell line expressing NtTUA3-GFP altered the cold sensing function of cortical microtubules by rendering more rapidly cold-induced disassembly of cortical microtubules, accompanied with a pronounced calcium influx, finally leading to reduced cold acclimation.

Disassembly of cortical microtubules caused by Phospholipase D (PLD) activation that induced by 1% n-butanol was mitigated by overexpressing

OsTTL in the NtTAU3 BY-2 cell line. OsPLDα1, one isoform of the PLD family from rice that conveys the common functions of PLD, preferentially localised with cortical microtubules, spindle and phragmoplast microtubules. Overexpressing OsPLDα1 increased the abundance of detyrosinated α-tubulin. These results indicated a functional interaction between OsPLDα1 and detyrosinated α-tubulin.

Overexpression of OsTTL-RFP inceased not only the amount of α-tubulin protein but also the transcripts of α-tubulin gene as well as transcripts of OsTTL gene, suggesting a mutual regulation of posttranslational modification on tubulin synthesis.

1 Introduction

1.1 Overview of plant microtubules

Apart from actin filaments, plant microtubules are one of the main components of the cytoskeleton, which was discovered in the 20th century with the development of high resolution of microscopy. In 1962, Paul Green predicted the existence of 'microtubules' by proposing that there must exist cortical proteins of spindle fiber nature which control the polar deposition of cellular fibrils to the plant cell wall (Green, 1962). Just one year later, the presence of 'microtubules' was proven by Keith Roberts Porter and Myron Ledbetter, who were inspired by Paul Green's prediction to search for the cellulose deposition mechanism. They termed 'microtubule' and showed that microtubules are the fine structures just beneath the surface of protoplasts with slender tubules that with a diameter of 230 to 270 Å and could mirror the orientation of the cellulose microfibrils of the adjacent cell walls. Since then, microtubules have become a new field of research and attracted more attention. Only a few years later, tubulin, the building block of microtubules, was isolated and identified as colchicine binding protein from mammalian brain (Weisenberg *et al.*, 1968). Although the cortical microtubule and mitotic microtubules in plant cells have been revealed by several immunofluorescence studies, due to the fixation methods that would kill cells, no living images would show the dynamic behaviors of microtubule were taken (Gunning and Wick, 1985; Hussey *et al.*, 1987; Lloyd, 1987). In 1990, the transition microtubules from static to dynamic structures in living dividing plant cells could be visualized and followed by microinjection of fluorescently labeled brain tubulin (Zhang *et al.*, 1990). With the development of the GFP technology and confocal microscopy, a GFP–MAP4 reporter gene was constructed to visualize microtubule in living plant cells (Marc *et al.*, 1998). Since then, with the development of advanced

technology, plant microtubules as well as their associated proteins have been found to not only influence cell morphology by controlling cell expansion and cell division but also function in signaling by responding to external environment stimuli (Nick, 2012; Nick, 2013; Parrotta *et al.*, 2014).

However, microtubules are endowed with different functions in different context: for instance, cortical microtubules in the interphase cells act as susceptors to respond to cold, whereas microtubules can arrange as mitotic microtubule arrays to control cell division, such as spindle and phragmoplast microtubules. How these functional different arrays of microtubules are formed is a central question of cell biology. To understand this, an overview of plant microtubules should be provided in advance here.

1.2 Structural basis of plant microtubules

Microtubule, one of the central building blocks of the plant cytoskeleton, is composed of heterodimers of α- and β- tubulin and each of them has similar molecular weight of about 50 kDa. In eukaryotic cells, microtubules comprise 13 parallel-aligned protofilaments that will assemble into a hollow cylinder structure with an average diameter of 25 nm. The heterodimers of α-tubulin and β-tubulin were stacked to generate protofilaments. It is commonly accepted that the protofilaments of MT are arranging in a B-type lattice where due to the lateral association a seam is generated representing three tubulin dimers (Fig. 1a) (Hashimoto, 2015). In addition, microtubules show structural polarity since they are assembled with head-to-tail structure of heterodimers of α- and β-tubulin where the heterodimers are asymmetrical and self-arranged in one direction, thus generating polar protofilaments. Actually, the β-tubulin which is the last dimer at the polar end is thought to be plus-end whereas the end of exposed α-tubulin is minus-end (Fig. 1b), due to their assembly into microtubules.

At the plus-end, microtubules can exhibit polymerization by addition of α- and β-tubulin heterodimers and each of them possesses one GTP-binding site (Fig. 1b). The N-site the GTP-binding site of α-tubulin is non-exchangeable such that GTP cannot be hydrolyzed and it plays a structural role within the heterodimers. However, the GTP exposed in the E-site of β-tubulin is changeable: GTP hydrolyzes to GDP when the β-tubulin exposed in the plus-end of microtubule is captured by the α-tubulin subunit of the incoming tubulin heterodimer, thus finally creating a GTP cap in the plus end of microtubule (Hashimoto, 2015). In contrast, after addition of a new α-tubulin and β-tubulin heterodimer, GTP is supposed to be hydrolyzed to GDP by releasing an inorganic phosphate and energy.

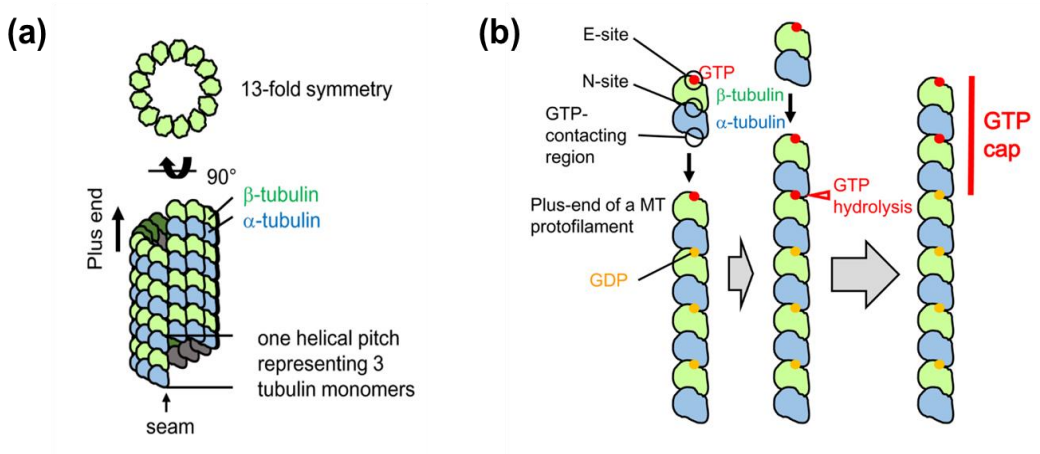

Fig. 1. (a) Microtubule structure. Microtubule is a hollow cylindrical structure with 13 parallel protofilaments generated by longitudinally stacked α- and β-tubulin heterodimers. Due to lateral association, one helical pitch representing 3 tubulin monomers is formed and called seam. (b) The assembly of α- and β-tubulin heterodimers to a microtubule and GTP hydrolysis. Within α- and β-tubulin heterodimers, GTP buried in the N-site of α-tubulin is unchangeable while it is changeable when exposed to the E-site of β-tubulin. When α- and β-tubulin heterodimers assemble into a growing plus-end of microtubule, GTP exposed in the E-site of β-tubulin in the plus-end of microtubule would hydrolyse to GDP. By this way, a small GTP-cap remains in a growing microtubule that promotes microtubule polymerisation. Image source: Hashimoto, 2015

Microtubules (and other cytoskeletal components) are not as static as the name cytoskeleton suggests but are highly dynamic in nature. The protofilament composed of a GTP cap structure is straight and can undergo polymerisation in the plus-end. However, due to the hydrolysis of GTP to GDP, the gradual loss of GTP cap structure will expose the labile inner core of GDP-tubulin that is structural curved and tends to outward peeling of protofilaments, thus leading to rapid depolymerization at the minus-end. As a consequence, the GDP-form of the β-tubulin subunit of an α- and β-tubulin heterodimer will be depolymerized from the microtubule into the cytoplasm (causing a microtubule catastrophe). This catastrophe of microtubule can be rescued by polymerisation where the microtubule recruits a small GTP cap at its plus-end by addition of newly formed GTP-bound β-tubulin that is exchanged from the GDP-form of the β-tubulin subunit in the cytoplasm. This property of microtubule exhibits both growing (polymerisation) and shrinking (depolymerization) in the plus- and minus-end at the same time, and the switching between growing and shrinking is termed ‘dynamic instability’ (Fig. 2a). However, when the net polymerisation in plus-end is equal to the net depolymerization in the minus-end, the length of a microtubule remains constant whereas the tubulin heterodimers are flowing form plus-end to minus-end. This is called ‘treadmilling’ (Fig. 2b).

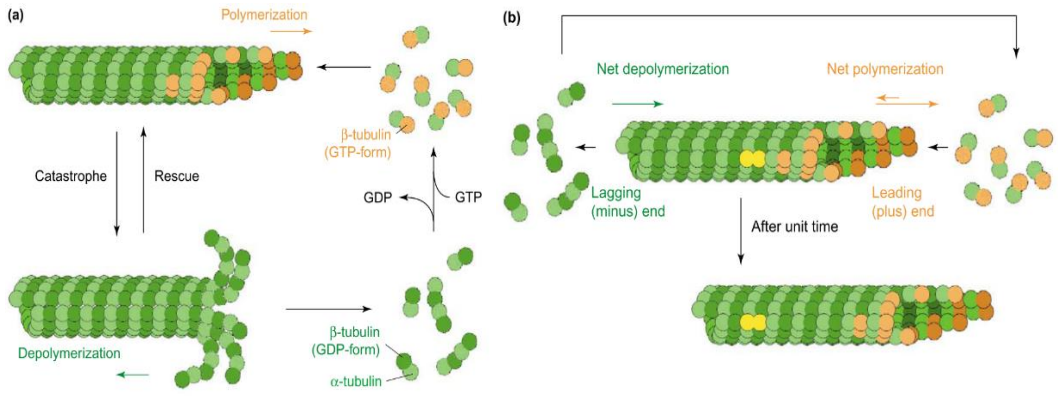

Fig. 2. (a) Dynamic instability of microtubules. Microtubules are not static but undergo

rapidly polymerisation and depolymerisation. Polymerisation is a process that GTP-formed α- and β-tubulin heterodimers in the cytoplasm assemble into a growing microtubule and GTP would hydrolysis to GDP. The GDP-bound β-tubulins are unstable and tend to bend outward. When microtubules lose their GTP-cap, that promotes stable polymerisation of microtubule, GDP-formed α- and β-tubulin heterodimers will be depolymerised from microtubules quickly, causing a catastrophe. This can also be rescued by recruiting a small GTP-cap. In addition, the dissociated GDP-formed α- and β-tubulin heterodimers will be exchanged with GTP in the cytoplasm pool. (b) Treadmilling. When the polymerization at the plus-end and the depolymerization at the minus-end is balanced, the net length of the MT remains constant but the individual tubulins in the polymer flow from the plus-end to the minus-end (a behaviour known as treadmilling). Image source: Hashimoto, 2003

1.3 Functional diversity of plant microtubules

Animals can move and escape from environmental stimuli whereas plants must adapt to their environment rather than escape. In this context, plants need to modulate their shape, for instance, to perform photosynthesis, they need to grow upward sending their leaves to the atmosphere while they send roots downwards to absorb water and nutrients. It seems that plant growth is directional. It is known, that the plant cell shape is controlled by cell division defining the geometry of cell axis followed by directional cell expansion. Both activities are requiring the function of microtubules. How would this be related? Indeed, plant microtubules can orient themselves into different arrays conveying different functions, such as cortical microtubules in interphase cells, preprophase band (PPB) in preprophase cells, spindle microtubules in metaphase cells as well as phragmoplast microtubules in anaphase cells (Nick, 2012).

1.3.1 Functions of microtubules in cell expansion

In interphase cells, cortical microtubules can orient to different arrays that control the preference of axial cell expansion, for instance, cortical microtubules can form parallel bundles that are perpendicular to the cell axis to maintain longitudinal cell expansion while the longitudinal bundles of cortical microtubules promote the lateral cell expansion (Fig. 3a). How does this happen?

Indeed, the driving force of cell expansion originates from turgor pressure. Cellulose microfibrils in the cell wall could resist the turgor pressure and transverse arrangement of cellulose microfibrils can resist the increase of cell diameter and transforms the turgor pressure thus leading to longitudinal expansion (Wymer and Lloyd, 1996). Indeed, a long time ago, cortical microtubules were reported to share the same direction of cellulose microfibrils and also mirror the directional depositions of cellulose microfibrils thus controlling the direct cell expansion (Ledbetter and Porter, 1963). How cortical microtubules control the orientation of cellulose microfibrils is giving rise to two models: the ‘monorail’ and ‘guard rail’ models (Fig. 3b). Monorails have been proposed to directly guide the movement of cellulose synthase along the cortical microtubules thus generating cellulose microfibrils with the same orientation of cortical microtubules (Heath, 1974). The alternative guard rail model proposes that cortical microtubules only function as guard rails to restrict the movement of cellulose synthase and the force that drives the movement of cellulose synthase comes from crystallization of cellulose (Herth, 1980; Staehelin *et* al., 1991). With the advance of fluorescent protein technology, the monorail model was widely accepted when the movement of a cellulose synthase subunits A6 (CESA6) fusion with YFP moving along individual microtubules labeled with α-tubulin fused with a blue fluorescent protein was observed and recorded (Paredez *et* al., 2006).

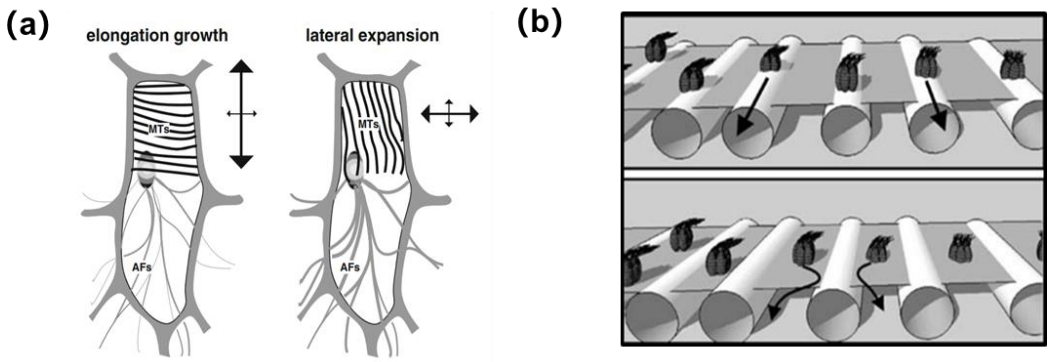

Fig. 3 (a). Microtubules orientation in interphase control relative direction of cell expansion. In interphase cells, cortical microtubules (MTs) can reorient either parallel transverse bundles or longitudinal bundles that are perpendicular to the cell axis to guide the cell expansion. Actin filaments (AFs) do not change orientation, but bundle in cells that cease elongation growth. (b). Models of microtubules control depositions of cellulose microfibrils: monorails (upper) and guard rails (bottom). Monorail model (upper one), where cortical microtubules directly guide the movement of cellulose synthase complexes via a microtubule-dependent motor. Guard rails, where cortical microtubules only function as guard rails to restrict the movement of cellulose synthase. Image source: Nick, 2007

1.3.2 Functions of microtubules in cell division

During cell cycle, cortical microtubules arrays in interphase cells are gradually replaced by PPB, spindle and phragmoplast microtubules arrays (Fig. 4). Just prior to mitosis, in the transition from G2 to M, as the nucleus moves to the cell center, a parallel microtubule array around cell equator called preprophase band (PPB) is formed, which is involved in microtubule disassembly, selective microtubule stabilization and re-assembly to a belt-like structure of the PPB. The PPB only exists shortly and later rapidly disappears upon nuclear envelope breakdown as the spindle forms. Simultaneously, it leaves an endosomic belt that persists through mitosis which is thought to be recognized by phragmoplast microtubules and guides the later expansion of phragmoplast

microtubule during cytokinesis, thus defining the organisation and position of phragmoplast and cell plate (Dhonukshe *et al.*, 2005). Later, after nuclear envelope breakdown, spindle microtubules are re-assembled to bipolar arrays, that are perpendicular to the plane of PPB, in metaphase. The minus-ends of spindle microtubules are anchored at two poles presumably by kinesins and plus-ends are stabilized and nucleated by kinetochores (Smirnova and Bajer, 1998). Together with kinesins and kinetochores, spindle microtubules are modulating the segregation of chromosomes into daughter nuclei. After anaphase, the phragmoplast microtubules originate from remnant spindle microtubules and organize to antiparallel arrays that are perpendicular to the division plane, predicted by the former PPB. The plus-ends of phragmoplast microtubules point towards the division plane and are overlapped by MAP65, while the minus-ends orient towards the distal zone. The formation of a new cell plate is guided by centrifugal expansion of phragmoplast microtubules which is involved in coordination of microtubule assembly and disassembly, vesicle trafficking and membrane dynamics (Smertenko *et* al., 2017).

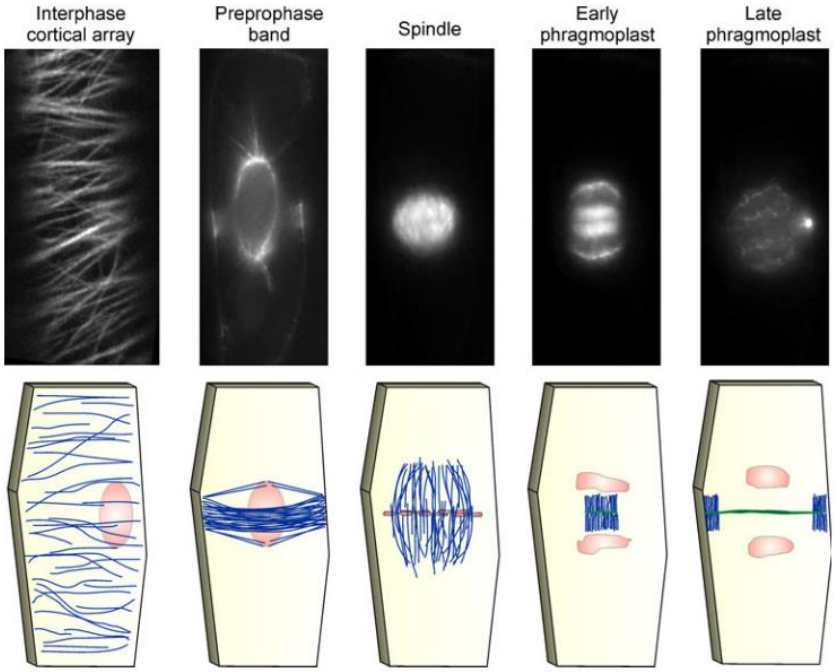

Fig. 4. Microtubule arrays during cell cycle, including interphase cortical microtubules,

preprophase band, spindle microtubules, early and late phragmoplast microtubules. Microtubule arrays on top are visualized by a marker tubulin fused with GFP in tobacco BY-2 cell. Schematic representations of microtubule arrays are shown below each image where microtubules are in blue and nucleus is in red. Image source: Zhu and Dixit, 2012

1.3.3 Functions of microtubules in signaling

Due to dynamic instability, cortical microtubules can form dynamically different population arrays to perform different functions in response to environmental stimuli, such as osmotic and cold stress (Nick, 2013). For instance, upon cold, the first physical input is the mechanical stress originating from membrane rigidification. Microtubules are thought to be the candidate that act as susceptors to transfer the physical input to a chemical signal since microtubules are of high rigidity that can rapidly process disassembly upon cold (Wang *et* al., 2020) (Fig. 5①). Indeed, microtubule disassembly can induce calcium influx, an important intracellular second messenger that takes part in numerous plant signaling pathways upon environmental stimuli. Then, the signal is amplified by a mechanism which involves in several molecular players, such as COLD1 phospholipase D (PLD), and apoplastic reactive oxygen species (ROS). COLD1 is a transmembrane protein playing an important role in signal amplification and during cold sensing, and interacts with a G protein to activate the Ca^{2+} channel. PLD, together with its product phosphotidic acid, are important signalling molecules under biotic and abiotic stresses and it can be triggered by the activation of a G protein. Apoplastic ROS are produced by a central input for plant stress signalling, the NADPH oxidase RbOH, and ROS would further amplify the opening of Ca^{2+} channel (Fig. 5②), and finally the amplification of signalling need. more stable microtubules to sustain efficient susceptors (Fig. 5③). In parallel, the signalling amplification components (such as COLD1, NADPH oxidase RbOH and calcium channel) are integral membrane proteins and they should be

synthesized and transported to the plasma membrane to maintain efficient amplification. In such a situation, not stable microtubule but a population of dynamic microtubules are needed to transport these components to the plasma membrane (Liu *et* al., 2013) (Fig. 5④).

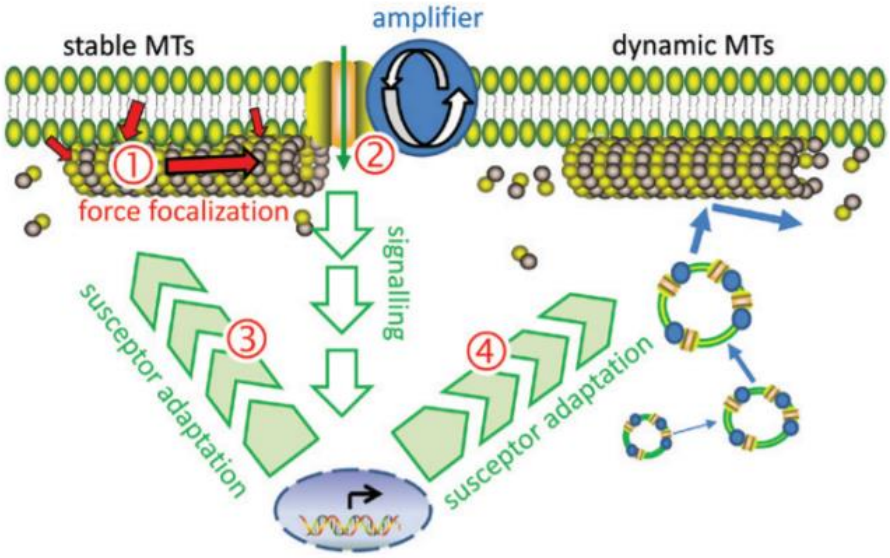

Fig. 5. Working model of the stability different populations of microtubules for cold acclimation. Under cold, membrane rigidification is the first physical input, which will be transmitted by cortical microtubules (①). To amplify the force, cold signalling is deployed, which is involved in the association with mechanosensitive calcium channels and other cold signalling molecular players, such as COLD1, phospholipids D (PLD) and ROS (②). This leads to the feedback on membrane, which will result in increased populations of stable microtubules that convey more efficient susception (③). In parallel, the dynamic microtubules are relevant for the long-term adaptation of the membrane and cold sensing system, because they control the integration of vesicles that contain important molecular components of cold signalling to the plasma membrane (④). Image source: Wang *et* al., 2020

Taken together, no matter if cortical microtubules function in cell expansion and sensing environmental stimuli or mitotic microtubules function in controlling cell

division, the premise is that microtubules should be reorganized dynamically to specific arrays in order to perform specific functions. How microtubules can be assigned to different functional arrays is a long-lasting question. It is commonly accepted that functional diversity of microtubules is regulated by a large number of microtubule-associated proteins that affect microtubule stability and organisation.

1.4 Regulation of functional diversity of microtubules

1.4.1 Tubulin isotypes

The original idea is that multifunctional microtubules are resulted from distinct tubulin gene sets of α- and β- tubulin that encode different polypeptides. Indeed, plant tubulin genes are not uniformly expressed and different plants have their own tubulin gene sets. For instance, in Arabidopsis, six α- tubulin genes and nine β-tubulin genes were identified. In rice, there exist three α-tubulin genes that are selectively expressed in different development stages where TubA3 gene accumulate throughout anthesis whereas TubA1 and TubA2 accumulate abundantly before flowering (Qin *et* al., 1997) and eight β-tubulin genes where seven of out of them are predominantly expressed in leaf sheaths whereas OsTUB8 is preferentially expressed in anthers (Yoshikawa *et* al., 2003). This indicates that even in one plant, tubulin genes are selectively expressed in different organs, developmental stages and different tissues. By transcriptional expressions of distinct tubulin genes, different types of α- and β- tubulin polypeptides are expressed and assemble to form structural different microtubules performing a variety of cellular functions.

1.4.2 Microtubule-associated proteins (MAPs)

The other hypothesis is that multifunctional microtubules are regulated by different microtubule-associated proteins (MAPs). A large number of MAPs play important roles in functional diversity of microtubules and most of the classical microtubule associated proteins are conserved throughout the eukaryotes. Apart from those, plants also have their own MAPs that are absent in animals (Gardiner, 2013).

One group of MAPs are motor proteins, which are thought to move along microtubules to transport cargoes, such as kinesins. Kinesins form a large protein family with 14 subfamilies. Kinesins with a calponin homology domain (KCHs) have been identified as plant unique motor proteins belonging to the kinesin-14 subfamily and they are moving to the minus-end of microtubules since they have a C-terminal motor (Richardson *et* al., 2006; Tamura *et* al., 1999). In interphase BY-2 cells, NtKCH is reported to not only associate with cortical microtubules but also co-localise to actin filaments, which is important for premitotic nuclear migration and mitosis (Frey *et* al., 2010). In addition, during cell division, NtKCH functions in cell division by specifically associating with only the PPB and phragmoplast microtubule, not with spindle microtubules (Klotz and Nick, 2012).

MAPs have influence on microtubule dynamic and organisation. For instance, microtubule plus-end tracking proteins (+TIPs) are a kind of plus-end binding proteins that localize to the plus-end of microtubules and regulate the phase of microtubule shrinking or growth, thus modulate the stability of microtubules by interactions of microtubule ends with other proteins. End binding protein-1 (EB1) is one of plant +TIPs and binds to plus-ends of microtubules that looks like ‘comets’ and affects polymerization rates of microtubules (Chan *et* al., 2003; Van Damme *et* al., 2004). The MAP65 family has been well described in plants and they are found to bind to the plus-end of antiparallel microtubules in

phragmoplasts and form an overlap in the division midzone that stabilizes and bundle phragmoplast microtubules, which is important for cell plate assembly (Murata *et* al., 2013).

Apart from those MAPs, there are also some multifunctional MAPs that have been identified functioning also in signalling, such as GAPDH, phospholipase D (PLD), Heat Shock Protein 70 (Hsp70) (Krtková *et* al., 2016). It has to be mentioned that PLD, a 90-kDa protein firstly isolated from tobacco membranes, is thought to be the linker between plasma membrane and microtubules and acts as a signalling hub in response to numerous stresses, such as cold, drought and salt (Abreu et al., 2018; Angelini et al., 2018; Gardiner *et* al., 2001; Zhang *et* al., 2012). PLD could transfer the posphatidyl groups to primary alcohol n-butanol forming phosphatidylbutanol (PBut), thus the output of PLD is blocked (Munnik *et* al., 1995). By adding n-butanol, cortical microtubules detach from the plasma membrane and partially depolymerise while the sec-butanol and tert-butanol, not capable of competing with trans-phosphatidylation, could not trigger microtubule reorganisation (Dhonukshe *et* al., 2003; Munnik *et* al., 1995).

However, the situation is more complicated as in some cases only selective expression of tubulin isotypes is not sufficient since microtubules are assembled in mixtures. Indeed, during their life, plants utilize more tubulin isoforms, which are different from those tubulin isotypes that originated from distinct gene sets. Those tubulin isoforms utilized by different tissues among different plants might be in relation to changes in structure and organisation of microtubules (Parrotta *et* al., 2014). In addition, microtubules have the ability to selectively bind specific MAPs and by binding MAPs, in turn, the stability and organisation of microtubules are affected or reconstructed so that they could perform special function that they should have in particular situations. However,

the premise is how tubulin isoforms are modified that would change structure of microtubules and how specific MAPs are recognized by specific microtubule arrays. The answer should be post-translational modifications that would increase functional diversity of tubulins, which would recruit specific MAPs leading to changes in structure and organisation of microtubules.

1.5 Posttranslational modifications (PTMs)

As mentioned above, there exist several tubulin isotypes although α- and β-tubulin are relatively conserved throughout the eukaryotes. However, there also exist tubulin isoforms through post-translational modifications. The first post-translational modification has been described by Barra and his colleagues that [^{14}C] tyrosine can be enzymatic incorporated into a soluble preparation of rat brain *in vitro*, which is independent from RNA (Barra *et* al., 1973). Later, a large numbers of tubulin modifications were gradually identified (Fig. 6), including detyrosination, tyrosination, acetylation, polyglutamation and polyglycylation.

1.5.1 Different posttranslational modifications

Acetylation is the only modification found at the N-terminus of α-tubulin. The enzymes responsible for N-terminal Lys 40 acetylation were identified including aTAT1 (Akella *et* al., 2010), NAA10 (Ohkawa *et* al., 2008) and ELP3 (Creppe *et* al., 2009) whereas the deactylases were identified as HDAC6 (Hubbert *et* al., 2002) and SIRT2 (North *et* al., 2003). The specific function of acetylation of α-tubulin is still unknown as acetylated tubulins are preferentially present in different tissues among different plant species as well as associates with preprophase band in maize leave cells (Gilmer *et* al., 1999; Wang *et* al., 2004). One experimental evidence argues that the acetylation is not important but the type of amino acid because the phenotype could be changed when Lys

40 is mutagenized to a glutamine while no phenotypical difference is observed when Lys 40 is mutagenized to an arginine that cannot be acetylated (Xiong *et* al., 2013).

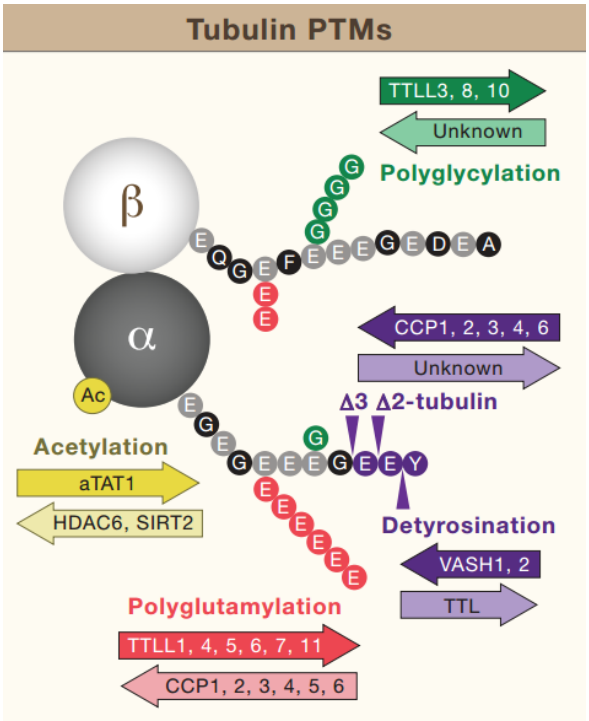

Fig. 6. Posttranslational modifications of α- and β-tubulin and corresponding enzymes. The detyrosination is enzymatic removal of C-terminal tyrosine of α-tubulin by vasohibin family protein (VASH1 and 2) and the readdition of tyrosine is catalyzed by tubulin tyrosine ligase (TTL). Upon detyrosination, the residue of glutamate can be further removed by cytosolic carboxypeptidases (CCPs) to generate Δ2- and Δ3- tubulin, whereas the reverse enzymes have not been identified. Polyglutamation and polyglycylation can occur on both α- and β-tubulin, which are catalyzed by the TTL-like protein family (TTLL) to produce a short chain of varying length of glutamate and glycine chains. The deglutamalases are enzymes from CCP family whereas the degylcylases have not been identified yet. Acetylation of α-tubulin takes place on lysine 40, is catalyzed by aTAT1, and is removed by HDAC6 or SIRT2. Image source: Magiera *et* al., 2018

Polymodifications, including polyglutamylation and polyglycylation, are

catalyzed by a large number of tubulin tyrosine ligase like (TTLL) family proteins that enzymatically add various length of glutamate and glycine chains to both C-terminus of α- and β-tubulin (Gardiner, 2019; Parrotta *et al.*, 2014). Tubulin polyglutamylation and polyglycylation often occur on the outer face of microtubules and are thought to affect microtubule dynamics by associating with MAPs, for instance, they can be regulated by katanin related microtubule severing activity (Parrotta *et* al., 2014; Sharma *et* al., 2007).

Apart from those modifications, there exists one common C-terminal detyrosination/tyrosination cycle of α-tubulin: the conserved C-terminal tyrosine of α-tubulin could be enzymatic cleaved off by a so called tubulin tyrosine carboxypeptidase (TTC) generating detyrosinated α-tubulin that further would be ligated a tyrosine by tubulin tyrosine ligase (TTL). In addition, upon detyrosination, by gradually losing one glutamate or two glutamate under the catalyzation of CCP family proteins, Δ-2 tubulin or Δ-3 tubulin is generated, however, the reverse enzymes were not identified yet (Cai, 2010; Gardiner, 2019; Parrotta *et* al., 2014).

1.5.2 Functional diversity of differentially modified microtubules

These various tubulin isoforms result from PTMs of α- and β-tubulin, which would generate so called ‘tubulin code’ for recognition by MAPs, leading to increase of structural and stability diversity of microtubules (Janke and Magiera, 2020; Magiera et al., 2018; Parrotta et al., 2014). For instance, tubulin acetylation is a well-known marker for stable microtubule and could enhance the binding of kinesin-1 to microtubule that participates in regulating kinesin-based motility (Gardiner et al. 2007). Katanin, a microtubule severing protein, has an effect on dynamic of microtubules that mainly associates with tubulin polyglutamylation and polyglycylation (Sharma et al. 2007).

Detyrosination/tyrosination cycles play important roles in dynamics and organisation of microtubules depending on the initial existence or loss of C-terminal tyrosine that differentially recuits different MAPs. For instance, in *Aspergillus nidulans,* a motor protein Kinesin-3 UncA is preferentially recruited to a specific microtubule during hyphae extension, which is strongly detyrosinated (Zekert and Fischer, 2009). The motor protein Kinesin-1 preferentially moves along detyrosinated microtubules to transport cargos rather than binds to tyrosinated microtubules (Reed *et* al., 2006). However, tyrosinated microtubules are preferentially recruit +TIP proteins that contain a CAP-Gly domain, which is important for neuronal development (Peris *et* al., 2006; Song and Brady, 2015). However, this cycle is elusive in plants and there is little information about tubulin detyrosination/tyrosination cycle.

1.6 Detyrosination/tyrosination cycle

The most common PTMs is the detyrosination and tyrosination cycle of α-tubulin (Fig. 7). Indeed, in most eukaryotes, almost all α-tubulins harbour a tyrosine as C-terminal amino acid. This C-terminal tyrosine can be enzymatically cleaved off by α-tubulin tyrosine carboxypeptidase (TTC, in animal models also abbreviated as TCP) generating detyrosinated α-tubulin. Subsequently, the detyrosinated α-tubulin can be enzymatically religated with a tyrosine by tubulin tyrosine ligase (TTL).

TTL had been first cloned and identified in porcine brain (Ersfeld *et* al., 1993). Later, structural analysis revealed that TTL preferentially binds to soluble tubulin dimers rather than to polymerized microtubules, and also inhibits the growth rate of microtubules in neurons (Prota *et* al., 2013). Overexpressed TTL was found to co-localise with microtubules of the mitotic spindle in animal cells (Barisic *et* al., 2015), whereas in TTL knockout mice, suppression of TTL

causes perinatal death that was accompanied by a poorly developed neuronal network, which may stem from a mislocalisation of the microtubule tip protein CLIP170 (Erck *et al.*, 2005). Recently, the hitherto elusive mammalian TCPs were identified as vasohibins (VASHs) and their regulators, as Small Vasohibin Binding Proteins (SVBPs) after 30 years of research (Aillaud *et* al., 2017; Nieuwenhuis *et* al., 2017). However, even in VASH knockout lines, a residual tubulin detyrosination activity remained, indicating that VASHs-independent TCPs are still to be found (Aillaud *et* al., 2017). Nevertheless, important molecular players of the tubulin detyrosination/retyrosination cycle have been partially identified, which paves the way to address the function of this cycle also on the molecular level. Unfortunately, very little information is available on plant homologues of these two key enzymes, or even the functions of this cycle.

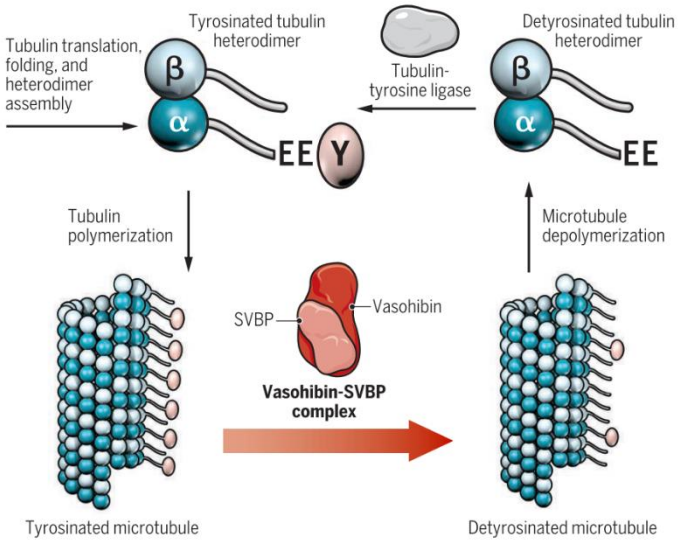

Fig. 7. The detyrosination and tyrosination of α-tubulin. All α-tubulins are encoded with a C-terminal tyrosine (Y). When α- and β- tubulin heterodimers assemble into microtubules, this would firstly generate a population of tyrosinated α-tubulin within microtubules. The tyrosine on microtubules can be enzymatic removed by Vasohibin- SVBP complex, resulting in detyrosinated α-tubulin in microtubules. After depolymerisation, detyrosinated α-tubulin can be retyrosinated by tubulin tyrosine ligase. Image source: Akhmanova and

Maiato, 2017

Despite the lack of molecular tools, pharmacological manipulation has revealed a role of the tubulin detyrosination cycle for plant growth and development. Nitro-tyrosine can be incorporated to detyrosinated α-tubulin by TTL, but cannot be cleaved off by TTC. By feeding nitro-tyrosine, the ratio of tyrosinated to detyrosinated α-tubulin was increased in tobacco BY-2 cells and in rice seedlings, accompanied by reduced mitosis, stimulation of cell elongation, and disorientation of cell walls (Jovanovic *et* al., 2010), indicating a role of the detyrosination/tyrosination cycle for cell elongation and cell division. Suppression of detyrosination by parthenolide, a bona-fide inhibitor of TTC, was shown to stimulate the association of the plant specific minus-end directed kinesin, KCH, to cortical microtubules. This was accompanied by impaired organisation of phragmoplast microtubules leading to a wavy and partially non-contiguous cell plate (Schneider *et* al., 2015), suggesting that the detyrosination/tyrosination cycle may regulate the recruitment of specific motor proteins to particular arrays of microtubules. A role of this cycle for microtubular organisation was also inferred from the observation that reorientation of cortical microtubules in maize coleoptiles induced by auxin depletion involved a transitional step, where transverse microtubules were predominantly tyrosinated, whereas longitudinal microtubules were mainly detyrosinated (Wiesler *et* al., 2002). These observations link the detyrosination/tyrosination cycle with the spatial organisation of specific microtubule arrays, possibly by recruiting specific kinesin motors.

1.7 Scope of this work

Since the detyrosination and tyrosination cycle plays important roles in modulation of stability and organisation of microtubules, to fully understand its functions, it is crucial to get molecular insight into the plant homologues of TTL

and TTC. VASH or SVBP homologues seem to be lacking, such that our understanding of the detyrosination/tyrosination cycle in plant cells is still in its infancy. However, in plants, there exists a homologue of TTL family proteins.

In our lab, a TTL family protein (referred as OsTTL, Q10QY4) from rice (*Oryza sativa* L. ssp. japonica cv. Dongjin) was cloned and overexpressed (referred to OsTTLox) several years ago. The overexpression line has been used to analyse the general physiological functions of OsTTL in plant growth and development. Indeed, it has been observed that several phenotypical changes occur due to overexpression of this OsTTL by a previous PhD student (Schneider, 2010, PhD thesis), indicating this OsTTL has real functions in affecting plant growth and development. Therefore, my work was trying to reveal how OsTTL affect plant growth and development as well as stress tolerance:

1. Since OsTTL is found to be a member of TTL family protein, one question was whether overexpression of OsTTL would have effects on the distribution of detyrosinated/tyrosinated α-tubulin?
2. If so, further question was, whether the shifted distribution of detyrosinated/tyrosinated α-tubulin due to overexpression of OsTTL would have effects on microtubule stability and orientation, thus leading to rice growth and developmental changes?

To address these two questions, the altered phenotypes of coleoptile and root due to overexpression of OsTTL-RFP were focused in this work since their growth is highly involved in microtubule-dependent cell expansion and cell division. In the following, microtubule orientation and organisation had to be analysed based on immuonofluorescence staining. In parallel, the biochemical detection of tubulin detyrosination and tyrosination had to be conducted to analysis the distribution of detyrosination/tyrosination

abundance.

3. If the stability of microtubule be affected by redistribution of detyrosination/tyrosination due to overexpression of OsTTL, whether the sensing functions of microtubules under cold stress would also be altered?
4. Is rice phospholipase Dα1 (OsPLDα1) a potential functional partner of OsTTL? Since EPC affinity chromatography approach had revealed phospholipase Dα1 as potential binding partner for detyrosinated tubulin in previous work in our lab.

To link the functions of OsTTL with cold stress as well as with OsPLDα1, it was necessary to view microtubules *in vivo*. Therefore, a transgenic line stably overexpressing OsTTL-RFP in a microtubule marker line NtTUA3-GFP BY-2 cell line (TTL+TUA3) was generated. The functions of OsTTL in cold stress could be dissected by following the microtubule responses *in vivo*. n-butanol, a PLD activator, was applied to dissect the functional linking between OsTTL and PLD. A transgenic BY-2 cell line overexpressing OsPLDα1-GFP as well as an overexpressor OsPLDα1-GFP rice line were used to view the localisation of OsPLDα1 and also used to test the functional interactions with tubulin detyrosination.

2 Materials and Methods

2.1 Multiple sequence alignment and phylogenetic analysis of TTL

Candidate proteins belonging to tubulin-tyrosine-ligase protein family from *Oryza sativa ssp. japonica* (Q8H022, Q10QY4 Q10QY3), *Vitis vinifera* (A5AQ23), *Nicotiana tabacum* (A0A1S4CWA5), *Arabidopsis thaliana* (Q6IDC7, Q9CAQ1), the lycophyte *Selaginella moellendorffii* (D8RZ55), the bryophytes *Marchantia polymorpha* (A0A2R6WBW4), and *Physcomitrella patens* (A0A2K1KGF1), the chlorophyte *Chara braunii* (A0A388KR02), versus homologues from animals, including *Danio rerio* (A0A0R4IKV1), *Homo sapiens* (Q14166), and *Mus musculus* (Q3UDE2), *Sus scrofa* (P38160); *Saccharomyces cerevisiae* (P38254) as representative of the fungi, and bacterial homologues from *Alkalilimnicola ehrlichii* (Q0AC43), and *Marinobacter hydrocarbonoclasticus* (A0A368V3Q9) were collected from Swiss-Prot via a BLAST search. The multiple sequence alignment was conducted by KALIGN (https://msa.sbc.su.se/cgi-bin/msa.cgi). The phylogenetic analysis was conducted by MEGA-6 (https://www.megasoftware.net/) using the Maximum Likelihood algorithm, and a bootstrap consensus tree inferred from 100 replicates to represent the evolutionary history of the deduced proteins analysed.

2.2 Plant materials and cultivation

2.2.1 Rice materials and cultivation

Rice caryopses (Table 2.1) were preselected for uniformity and proper filling, and sown equidistantly on a floating plastic mesh in a box filled with 100 mL ddH_2O and cultivated at 25 ℃ in photobiological darkness as described by

Frey *et* al., (2010) for different time intervals depending on the respective experimental purposes.

Table 2.1 Rice genotypes used in the study.

Name	Genotype
Dongjin	Wild type (WT), Oryza sativa L.ssp.japonica cv. Dongjin
TTLox	TTLox, Overexpression of OsTTL fused with RFP in Oryza sativa L.ssp.japonica cv. Dongjin
OsPLDα1	OsPLDα1, Overexpression of OsPLDα1 fused with GFP in Oryza sativa L.ssp.japonica cv. Dongjin

2.2.2 Tobacco BY-2 cells and cultivation

All the BY-2 cell lines used in this work were cultivated in MS liquid medium (containing 4.3 g/L Murashige and Skoog salts (Duchefa, Haarlem, The Netherlands), 30 g/L sucrose, 200 mg/L K_2HPO4, 100 mg/L inositol, 1 mg/L thiamine and 0.2 mg/L 2,4-dichlorophenoxyacetic acid (2,4-D), pH 5.8, supplemented with either 30 mg/L hygromycin (TTLox line), 50 mg/L kanamycin (TUA3 line and OsPLDα1 line) or 30 mg/L hygromycin and 50 mg/L kanamycin (TTL+TUA3 line), respectively) by continuously shaking at 150 rpm, 25 °C in darkness. For subcultivation, the cells were subcultured weekly (TTLox line and OsPLDα1 line) or twice a week (TUA3 line and TTL+TUA3 line) by inoculating 1.5 mL of stationary cells into fresh medium (30 mL) in 100 mL flasks. The cells were incubated at 26°C under constant shaking at 150 rpm.

Table 2.2 Transformed and non-transformed BY-2 cell lines used in the work.

Name	Genotype	Application	Source
WT	Wild Type (WT), *Nicotiana tabacum* L.cv. Bright Yellow 2	Control	
TTLox	TTLox, Overexpression OsTTL fused with RFP in *Nicotiana tabacum* L.cv. Bright Yellow 2	Localisation and phragmoplast analysis	Durst, Diploma thesis, 2009
OsPLDα1	OsPLDα1, Overexpression of OsPLDα1 fused with GFP in *Nicotiana tabacum* L.cv. Bright Yellow 2	Localisation and biochemical analysis	Jovanovic, PhD thesis, 2010
TUA3	NtTUA3-GFP BY-2 cell line, Overexpression NtTUA3 fused with GFP in *Nicotiana tabacum* L.cv. Bright Yellow 2	Microtubule marker line	Berghöfer *et* al., 2009
TTL+TUA3	Overexpression OsTTL-RFP in NtTUA3-GFP BY-2 cell line	Signaling analysis	This work

2.3 Phenotyping of rice seedlings

If not stated otherwise, coleoptiles and roots were imaged at day 6 after sowing as described above. Mean cell length and cell number were determined as described by Frey *et* al., (2010) with minor modifications. Briefly, basal and apical parts of the coleoptile were separately immersed with one drop of 1 g/L Calcofluor White (Sigma, Darmstadt, Germany) and one drop of 10% NaOH, and then the epidermal cells were imaged by fluorescence microscopy (AxioImager.Z1 Apotome, Zeiss, Jena, Germany, filter set 49 with excitation at 365 nm, beamsplitter at 395 nm, and emission at 445 nm at 10x

magnification). The mean cell length of epidermal cells in the basal and apical part of the coleoptile was determined as: Mean cell length = length of cell row / number of cross walls. The mean cell numbers were estimated by: Mean cell numbers = total length of coleoptile / mean cell length

To determine the orientation of cross walls, seminal roots were stained with 1% propidium iodide (Sigma, Steinheim, Germany) for 3 min, followed by washing twice with ddH_2O, before imaging the cells in the root apex by spinning disc microscopy. The angles between the cross wall and the side wall were measured by the angle tool of ImageJ (NIH, Bethesda, USA, https://imagej.nih.gov).

2.4 Cell biological methods

2.4.1 Stable transformation of OsTTL-RFP into NtTUA3-GFP BY-2 cell line

The construct of pH7WGR2-OsTTL [N-terminal fusion of the red fluorescent protein, the constitutive CaMV 35S promoter, hygromycin resistance; accession number of OsTTL: LOC_Os03g08140] from Durst, 2009 was used for stable transformation into NtTUA3-GFP BY-2 cell line to get a double expression OsTTL-RFP and microtubule marker NtTUA3-GFP by Agrobacterium-mediated transformation as described in Klotz & Nick, (2012). Briefly, the construct pH7WGR2-OsTTL was transformed into *Agrobacterium tumefaciens* strain LBA4404 (Invitrogen). Then the transformed LBA4404 was co-cultivated with 7 days NtTUA3-GFP BY-2 cells under continuous shaking at 150 rpm in dark room for 15min. The co-cultivated suspension droplets were plated on solid Paul's agar plate (4.3 g/L Murashige-Skoog salts and 30 g/L Sucrose) and incubated in totally dark condition for three days. After that, the

co-cultivated suspension droplets were transferred onto selective solid MS medium agar plate with antibiotics containing 100 mg/L cefotaxime, 100 mg/L kanamycin and 60 mg/L hygromycin. To make liquid cell suspension culture, after incubation in 25 °C darkness for 1-2 month, the newly formed resistant calli were transferred into liquid MS medium with 100 mg/L cefotaxime, 50 mg/L kanamycin and 30 mg/L hygromycin. To make the transformed cell line more stable in terms of expression, the cells in liquid MS medium were dropped back onto selective solid MS agar plate and incubated for 1-2 month at 25 °C in darkness. Then the newly formed calli were transferred into liquid MS medium to generate a suspension culture. After repeating 4 times, the stable culture was used to conduct different experiments.

2.4.2 Microtubule visualisation in rice tissues

Microtubules of rice coleoptiles and seminal roots were visualised by immunofluorescence as described by Abdrakhamanova *et* al. (2003) with minor modifications. Briefly, whole coleoptile and root segments (3-7 mm from root tip) were fixed by 3.7% w/v paraformaldehyde in microtubule stabilising buffer for 1 h, while gently shaking. After fixation, tangential sections were obtained using a vibratome as described in (Waller and Nick, 1997). The sections were collected and placed on a glass slide in a drop of 1.2% w/v agar dissolved in MSB and then incubated with block solution (Sigma, Neu-Ulm, Germany) in TBS buffer for 20 min at 25℃ to block non-specific interactions. After incubation overnight at 4℃ with mouse monoclonal antibodies directed against α-tubulin (DM1A, Sigma, Neu-Ulm, Germany; dilution 1:100 in TBS), the sections were washed 3 times for 5 min with TBS, and reincubated for 1 h at 37℃ with a fluorescein-isothiocyanate-(FITC)-conjugated secondary antibody (anti-mouse immunoglobulin G from goat; Sigma, Deisenhofen, Germany) diluted 1:20 in TBS. Sections were washed 3 times for 5 min in TBS

and then imaged immediately.

Table 2.3 Components for immunofluorescense staining microtubules in rice tissue

Substrate	Components	Concentration
Microtubule stablisation buffer (MSB buffer)	PIPES	0.05 M
	$MgSO_4$	1 mM
	EGTA	5 mM
	Triton X-100	0.25 % (v/v)
	Glycerol	1 % (v/v)
	pH=6.9	
Fixation	PFA in MSB	3.7 % (w/v)
Tris-buffered saline (TBS buffer)	NaCl	150 mM
	Tris-HCl	20 mM
	Triton-X 100	0.25 % (v/v)
	pH=7.4	
Block solution	BSA in TBS buffer	5 % (w/v)
Primary Antibody	DM1A in TBS buffer	1: 100 (v/v)
Secondary Antibody	FITC conjugated antibody (IgG) in TBS buffer	1: 20 (v/v)

2.4.3 Microtubule visualization in BY-2 cells

The microtubules in non-transformed or transformed BY-2 cells were visualised by immunofluorescence at the time of maximal mitotic activity, at day 3 after subcultivation as described in Schwarzerová *et* al (2006). 500 µL

cells were harvested and fixed by incubation in 500 µL 3.7 % PFA in MSB buffer. After 30 min fixation, the cells were washed for 3×5 min with MSB buffer, followed with incubation in cell wall digestion buffer for 20 min. After digestion, to block unspecific binding with antibody, BSA buffer was applied for incubation for 30 min in room temperature. After incubation overnight at 4℃ with mouse

Table 2.4 Components for immunofluorescence staining of microtubules in BY-2 cells

Substrate	Components	Concentration
Microtubule stablisation buffer (MSB buffer)	PIPES	0.05 M
	$MgSO_4$	2 mM
	EGTA	2 mM
	Triton X-100	0.1 %
	pH 6.9	
Fixation	PFA in MSB	3.7 % (w/v)
Phosphate buffer saline (PBS buffer)	NaCl	150 mM
	KCl	2.7 mM
	$KH2PO_4$	1.2 mM
	$Na2HPO_4$	6.5 mM
	pH=7.2	
Digestion solution	Macerozyme	1 % (w/v)
	Pectolyase	0.2 % (w/v)
Block solution	BSA in PBS	0.5 % (w/v)
Primary Antibody	ATT or DM1A in PBS	1: 500 (v/v)
Secondary Antibody	FITC or TRITC conjugated antibody (IgG) in PBS	1: 200 (v/v)

monoclonal antibodies directed against α-tubulin (DM1A, Sigma, Neu-Ulm, Germany; dilution 1:100 in TBS), the cells were washed 3 times for 5 min with PBS, and reincubated for 1 h at 37℃ with a fluorescein-isothiocyanate-(FITC)-conjugated secondary antibody (anti-mouse immunoglobulin G from goat; Sigma, Deisenhofen, Germany) diluted 1:20 in PBS. Cells were washed 3 times for 5 min in TBS and then imaged immediately.

2.5 Molecular biological methods

2.5.1 RNA extraction and cDNA synthesis

Total RNA was isolated using the innuPREP Plant RNA kit (Analytik Jena, Jena, Germany) according to the instructions of the manufacturer, and the quality of extracted RNA was verified by electrophoresis on a 1.0% agarose gel. cDNA was synthesized by using the M-MuLV cDNA Synthesis Kit (New England Biolabs) according to the instructions of the manufacturer. The amount of total RNA template was 1 µg.

2.5.2 Quantitative real-time PCR (qRT-PCR) analysis

Real time qRT-PCR was performed using a Bio-Rad CFX detection System (Bio-Rad). The reaction system and cycler conditions are shown in table 2.5 and table 2.6, respectively.

Table 2.5 qPCR mix per reaction

Component	Amount(μL)
5x GoTaq Puffer buffer	4
5 mM each dNTP Mix	0.4
10 μM primer forward	0.4
10 μM primer forward	0.4
0.5 U/μl GoTaq Polymerase (Promega)	0.1
SybrGreen	0.95
cDNA template (1:10)	1
MgCl2 (50mM)	1
dd H2O	11.75
Final volume	**20**

Table 2.6 Cycling conditions of qRT-PCR

Temperature (℃)	Time
95	3 min
95	15 s
60	40 s

2.5.3 Primers used in this work

Table 2. 7 Primers used in the study

Name	Sequence	Application
attB-TTL Fw	GGGGACAAGTTTGTACAAAAAAGCAGGCTTCATGTCGCCGGCCG	Recombinant expression of OsTTL
attB-TTL Rv	GGGGACCACTTTGTACAAGAAAGCTGGGTCTTACAGCGGCGATACATCTT	Recombinant expression of OsTTL

M13 Fw	TGTAAAACGACGGCCAGT	Standard sequencing primer, (GATC, Konstanz, Germany)
OsTTL-F622	GAATGTAGAAGGCTAAAGGC	Sequencing of Recombinant expression of OsTTL
OsTTL-F1338	CATGCCCGATGGTAAACTAG	Sequencing of Recombinant expression of OsTTL
pRSET-RP	ATGCTAGTTATTGCTCAGC	Standard sequencing primer, (GATC, Konstanz, Germany)
OsTTL Fw	GGGTTAGGTTAGCAAACAATCAGT	qPCR detection of OsTTL in rice
OsTTL Rv	GTATCATATCCCGTATGCGTCCA	qPCR detection of OsTTL in rice
OsTTL Fw	CCTCACCGGATGATCGCAT	qPCR detection of OsTTL in BY-2
OsTTL Rv	CAGGGCTCTACCGAGAAGGC	qPCR detection of OsTTL in BY-2
NtTUA3 Fw	TGAGCAAAGACCCCAACGAG	qPCR detection of GFP-NtTUA3
NtTUA3 Rv	TGAATACCGGCCTGACCAAT	qPCR detection of GFP-NtTUA3
GAPDH Fw	CTGATGATATGGACCTGAGTCTACTTTT	Reference gene
GAPDH Rv	CAACTGCACTGGACGGCTTA	Reference gene

2.5.4 Molecular cloning of construct of OsTTL fused with N-terminal His-tag

The construct for protein expression in *E.coli* was obtained by Gateway-cloning (Invitrogen) via two steps: BP and LR reaction to get entry clone and expression clone, respectively.

2.5.4.1 Cloning PCR of OsTTL

OsTTL was amplified by PCR from the plasmid OsTTL-RFP via the primer pair:

attB-TTL Fw and attB-TTL Rv and the PCR reaction system and cycling conditions are shown below:

Table 2.8 PCR mix per reaction

Component	Amount(μL)
5x Q5 buffer (NEB, Frankfurt, Germany)	10
10 mM each dNTP Mix	1
10 μM primer forward	2.5
10 μM primer reverse	2.5
Q5 polymerase (NEB, Frankfurt, Germany)	0.5
Nuclease free water	21.5
GC enhancer	10
Plasmid	1
Final volume	**50**

Table 2.9 Cycling conditions for PCR

Procedure	Temperature (℃)	Duration	Cycle
Initial Denaturation	98	3 min	
Denaturing	98	30 s	
Annealing	60	30 s	34
Elongating	72	3 min	
extension	72	5 min	
store	12	forever	

2.5.4.2 BP reaction

The PCR product of OsTTL was cloned into the pDONR/Zeo vector (Invitrogen) via BP reaction to get entry clone. The reaction contained the components shown below:

Table 2.10 Reaction system for BP reaction

Components	Amount (μL)
PCR product (50-150 ng)	1
pDONR/Zeo (150ng/μL)	1
BP clonase II enzyme	2
TE buffer	To 10

After incubation at 25℃ for 1h, 1μL proteinase K was added to end the reaction and incubate for 10min at 37℃. Then the mixture was proceeded to transform into *E.coli* DH5α competent cell by heatshock. The transformed cells were plated on LB plate containing 50 μg/mL zeocin and incubated at 37℃overnight under continuous shaking at 180 rpm. A single colony was selected and incubated in 5 mL liquid LB medium with 50 μg/mL zeocin at 37℃overnight at continuous shaking at 180 rpm. The plasmid was extracted using the Roth®-Prep Plasmid MINI kit (Roth, Germany) and then the insertion was verified by sequencing (GATC Biotech, Cologne, Germany). The entry clone was used in the LR reaction.

2.5.4.3 LR reaction

The expression clone of OsTTL fused with His-tag was cloned via a LR reaction as shown below:

Table 2.11 Reaction system for LR reaction

Components	Amount (μL)
Entry clone (50-150 ng)	1
pHGWA (150ng/μL)	1
LR clonase II enzyme	2
TE buffer	Adjust to 10

The rest of the process was same as described for the BP reaction apart from the selection antibiotic, which was 100 μg/mL ampicillin. After verification by sequencing, the plasmid (expression clone) with correct sequence was used in protein expression assay.

2.6 Biochemical methods

2.6.1 Protein extraction

Rice coleoptiles and primary root segments (0.5 mm from root tip to differentiation zone) were harvested 6 days after sowing. For BY-2 cells, 5 days cells of the OsTTLox line or 7 days cells of the TUA3 and TTL+TUA3 line were harvested by centrifugation at 8000 rpm for 3 min. Then the tissues or cells were ground to powder in liquid nitrogen, following by the same volume of cold extraction buffer (25 mM MES, 5 mM EGTA, 5mM $MgCl_2 \cdot 6H_2O$, pH 6,9 adjusted by KOH, 1 mM DTT and 1 mM PMSF) and vigorously mixed. After centrifugation at 13500 rpm for 30 min, the pellet that contained cell wall debris and other insoluble remains was discarded and the soluble protein in the supernatant was collected to perform Western blots or ethyl-N-phenylcarbamate (EPC) affinity chromatography.

2.6.2 SDS-polyacrylamide gel electrophoresis (SDS-PAGE) and Western blot analysis

The protein extracts were mixed with 3x loading buffer (Table 2.12) and denatured at 95℃ for 5 min. Equal amounts of total protein were loaded on different sets of 10% (w/v) SDS-polyacrylamide gels (Table 2.13). After running at a constant 25 mA for 60 min in a Mini Gel Tank (Life technologies, Thermo Fisher Scientific) filled with electrophoresis buffer, one set was used for Coomassie brilliant blue (CBB) staining for 1 h and the bands were visualized

by incubation with destainer buffer (Table 2.14).

Table 2.12 Compositions of 3x loading buffer

Substrate	Components	Concentration
3x loading buffer	Glycerol	30 % (w/v)
	DTT	300 mM
	SDS	6 % (w/v)
	Stacking gel buffer	48 % (w/v)
	Bromphenolblue	0.05% (w/v)
	Milli Q water	To 10 mL

Table 2.13 Compositions of 10% SDS-PAGE

Substrate	Components	Separation gel (10%)	Stacking gel (4%)
30% Acrylamide/Bis-solution	30 % (w/v) Acrylamid and 0.8 % (w/v) Bisacrylamid	8.2 mL	1.3 mL
Separation gel buffer	1.5 M Tris-HCl (pH=8.8) and 0.6 % (w/v) SDS	6.2 mL	
Stacking gel buffer	0.5 M Tris-HCl (pH=6.8) and 0.6% (w/v) SDS		2.3 mL
ddH2O		10.3 mL	
TEMED	40 % (w/v) N;N;N` ,N` ,-Tetramethylethylendiamin in milli Q water	108 µL	52.8 µL
APS	10 % (w/v) ammonium sulphatein milli Q water	215.9 µL	105.7µL

Table 2.14 Components of Coomassie Brilliant Blue (CBB) staining

Solution	Components	Concentration
Coomassie Brilliant Blue (CBB)	Coomassie Brilliant blue R250	0.04% (w/v)
	Methanol	40 % (w/v)
	Acetic acid	10% (w/v)
Destainer solution	Ethanol	30 % (w/v)
	Acetic acid	10 % (w/v)

The replicate gels were used to transfer proteins to a polyvinylidene fluoride (PVDF, Pall Gelman Laboratory, Dreieich, Germany) membrane by Trans-Blot® Semi-Dry Transfer (Bio-Rad). Before transferring, four layers of blotting papers (Whatman, Dassel, Germany) were soaked in transfer buffer containing 14.4 g/L glycine, 12.07 g/L Tris-HCl and 20% [v/v] MeOH. In parallel, a polyvinylidene fluoride (PVDF) membrane was activated in methanol (Roth, Germany). Two blotting papers were placed on the anode (positive), followed by PVDF membrane, the the SDS (separation gel part), the other two blotting papers and finally the cathode (negative). After running for 1 h at a voltage of 23, the proteins were transferred to a PVDF membrane, which was washed two times with TBS buffer (20 mM Tris-HCl, pH 7.6 and 150 mM NaCl) for 10 min. After washing, to avoid unspecific binding, the PVDF membrane was blocked in a 5 % milk buffer in TBS buffer for 1h, followed by 2 times TBST (TBS buffer with Tween-20) for 10 min washing away milk buffer. Then the PVDF membrane was incubated with primary antibody (Table 2.15, 1:2000 in TBS buffer) overnight at 4 ℃. The primary antibody was removed by 2 times washing for 10 min with TBST followed by washing with TBS for 10 min. Subsequently, the secondary antibody (anti-mouse IgG, alkaline

phosphatase-conjugated, 1:30000 in TBS buffer) was incubated at room temperature for 1 h. After rinsing 4 times in TBST buffer for 10 min, the membrane was ready for signal development. The signal was developed with 3 mL NBT/BCIP (Sigma, Germany) at room temperature. If necessary, the signal was quantified by using the plot profile function of ImageJ (NIH, Bethesda, USA), corrected for background, and the integrated density of each band was calculated relative to the value obtained for the control sample.

Table 2.15 Primary antibodies used in western blot.

Primary antibody	Target	Source
ATT	Detecting tyrosinated α-tubulin	Sigma-Aldrich
DM1A	Detecting detyrosinated α-tubulin	Sigma-Aldrich
Anti-GFP	Detecting GFP	Sigma-Aldrich

2.6.3 EPC sepharose chromatography

Tyrosinated and detyrosinated α-tubulin were fractionated based on their differential affinity with the antimicrotubular compound phenyl urethane (ethyl-N-phenylcarbamate, EPC) following the protocol described in Wiesler *et* al. (2002): an amino-ethyl group was linked to a CNBr-activated sepharose 4B matrix (purchased from Sigma-Aldrich, Darmstadt, Germany) by ethylene-diamine to yield amino-ethyl sepharose according to (Cautrecasas, 1970). The amino-ethyl sepharose was then coupled by carboxy-ethyl-N-phenylcarbamate that was synthesised from ethyl chloro-carbonate and 3-amino-benzoic acid as described in (Mizuno *et* al., 1981) to yield EPC sepharose. The fractionation was conducted in batch as described by Wiesler *et* al. (2002), by mixing first the extract with the matrix in

a reaction tube, and separating matrix and eluent by short centrifugation (1 min, 15000 g, 4°C) in a reaction tube (2 mL), using glass wool as filter to prevent that the supernatant was contaminated by the matrix. Then, the bound protein was eluted by increasing ionic stringency. For each elution step, the eluent was mixed with the matrix, and then re-separated by centrifugation. Ionic stringency was progressively increased by adding KCl (0 M, 0.05 M, 0.1 M, 0.15 M, 0.2 M, 0.25 M, 0.3 M, 0.35 M, 0.4 M, 0.45 M, 0.5 M, 1 M). The eluted fractions were precipitated by tri-chloro-acetic acid (Bensadoun and Weinstein, 1976), prior to processing for SDS-PAGE and Western blotting.

2.6.4 Protein expression and purification in *E.coli*

The expression clone (N-terminal His-tag fusion of OsTTL) was expressed in *E.coli* BL21 (DE3) or Rosetta-gami (DE3) via heat shock and the positive clone was selected and grown in LB medium at 37℃ overnight with 100 μg/mL ampicillin. Then the OD600 value was recorded followed by transferring the volume of culture needed into either 40 mL (small culture) or 3 L (large culture) LB medium for making original OD600 to 0.1 and then let cultures grew in 37° to OD600 between 0.6 to 0.8. To induce the expression of protein, the culture was induced with different concentrations of IPTG (20, 40, 80, 100, 200μM) and in parallel let grow in different temperature (18° for 2 days, 28° overnight, 37°overnight). The cells were harvested by centrifugation at 10000g for 10 min at 4℃ when the OD600 was above 2.0. The cells were resuspended with washing buffer (small culture) or ground buffer (large culture) and opened up by Frenchpress. After centrifugation at 10000g for 30 min at 4 ℃,

(a). for small culture, the supernatant was persevered on ice and the pellet was resuspended in 2 mL washing buffer and ready for SDS-PAGE to detect the expression of OsTTL.

or

(b). for large culture, the supernatant was collected, the volume measured, and precipitated with 70% Ammonium sulphate (without EDTA). Then solid ammonium sulphate was added to a final concentration of 93%. After dissolving

Table 2.16 The buffers used in protein expression and purification

Solutions	Components	concentration
Ground buffer	Tris (pH=7.8)	50mM
	EDTA	5mM
	NaCl	300mM
	glycerol	10%(w/v)
Washing buffer	Tris (pH=7.8)	50mM
	Imidazol	10mM
	NaCl	300mM
	glycerol	10%(w/v)
Elution buffer	Tris (pH=7.8)	50mM
	Imidazol	250mM
	NaCl	300mM
	glycerol	10%(w/v)
Ammonium sulphate buffer without EDTA	Ammonium sulphate	3.3 M
	Tris (pH7.8)	50 mM
Ammonium sulphate buffer with EDTA	Ammonium sulphate	3.3 M
	Tris (pH=7.8)	50 mM
	EDTA	5 mM

ammonium sulphate at 4 ℃, the pellet was dissolved in 30mL washing buffer and incubated with 5 mL HiTrap NiNTA column (GE, Healthcare). The proteins bound to column were eluted by elution buffer and precipitated with ammonium sulphate buffer containing EDTA at 70%. Again, solid ammonium sulphate was used at a final concentration of 93%. After centrifugation of 10000 g for 30 min at 4 ℃, the pellet was redissolved with 2 mL ground buffer and the resuspension was used for SDS-PAGE to detect purified OsTTL with His-tag subsequently.

2.7 Drug and cold treatment

2.7.1 Oryzalin treatment

Two sets of each, WT and TTLox seedlings, were imaged at day 5 after sowing and root length at this time point (L_0) was measured by the periphery tool of Image J (NIH, Bethesda, USA, https://imagej.nih.gov). Then, one set was subjected to treatment with 100 nM oryzalin (as treatment group), while the other set was cultivated without oryzalin (as control group) for additional 24 h, before roots were imaged and root length at this time point (L_1) determined. The relative growth rate (%) was determined as $\Delta L/L_0 \times 100\%$ where $\Delta L = L_1 - L_0$. The relative Inhibition was calculated as [relative growth rate of treatment – relative growth rate of control]/growth rate of control.

2.7.2 Nitro-tyrosine treatment

To assay the effect of nitrotyrosine on phragmoplast microtubules, NtTUA3-GFP cells were treated with 50 μM nitro-tyrosine for 2 h and then microtubules were imaged by spinning-disc confocal microscope that was equipped with a cooled digital CCD camera (AxioCamMRm; Zeiss), and two laser lines (488 and 561 nm, Zeiss, Jena, Germany)..

2.7.3 Cold treatment

All the experiments described below in this work were conducted with suspension cells cultured for 7 days, both for the TUA3 cell line and the TTL+ TUA3 cell line (almost all cells were in interphase, mainly containing cortical microtubule). To administer cold stress, flasks containing the cells were submerged into an ice-water bath (0℃) as shown in Wang et al. (2017)

2.7.4 Extracellular alkalinisation

Before applying cold stress, 4 mL of suspension cells were equilibrated on an orbital shaker for half an hour. After incubation on ice-water bath for 60 min, the cells were returned to room temperature for 1 h. The development of pH over the time was recorded by a pH meter (Schott handy lab, pH 12) combined with a pH electrode (Mettler Toledo, LoT 403-M8-S7/120) and by a paperless readout (VR06; MF Instruments GmbH, Albstadt-Truchtelfingen, Germany).

2.7.5 Determination of cell mortality

After cold treatment of 24h, cell mortality was assessed using 1 ml of 2.5 % (w/v) Evans Blue (Sigma-Aldrich) in aliquots of 200µl and using custom-made staining chambers to remove the medium. Following by 3 times washing with ddH_2O for 5 min per time, the dead cells (stained in blue) was scored using an AxioImager Z.1 microscope (Zeiss, Jena, Germany) as described in Gong *et* al., (2019). Mortality values were determined from 500 cells with three independent biological replicates.

2.7.6 Butanol treatment

For all treatments, 1% n-butanol, 1% sec-butanol and 1% tert-butanol treatment for 1h were used to see the differences of microtubules in TUA3 and TTL+TUA3 line, respectively. Images were taken every 30 min using a spinning disc confocal microscope that was equipped with a cooled digital CCD camera (AxioCamMRm; Zeiss), and two laser lines (488 and 561 nm, Zeiss, Jena, Germany).

3 Results

The key enzymes of tubulin detyrosination and tyrosination cycle have been identified in animals: Tubulin tyrosine ligase (TTL) for tubulin tyrosine and VASHs for tubulin detyrosination (Ersfeld *et* al., 1993; Aillaud *et* al., 2017; Nieuwenhuis *et* al., 2017). However, the homologue of VASHs seems lack in plants whereas only one homologue of TTL presents in plants. To obtain a better understanding the functions of the tubulin detyrosination and tyrosination cycle in plants, this homologue of TTL was focused as it has the maximum possibility to directly affect tubulin detyrosination and tyrosination.

Therefore, the present work started with the analysis of the phylogenetic position of plant TTLs, followed by a closer look into the alteration of phenotypes on coleoptiles and roots due to overexpression of a rice TTL fused with RFP (OsTTL-RFP). From the cellular and biochemical levels, a possible function of this rice TTL in tubulin detyrosination and tyrosination and its effect on microtubule stability and organisation were investigated. The second part focused on the role of OsTTL in the function of microtubule sensing under cold stress by overexpressing OsTTL-RFP in a microtubule marker BY-2 cells overexpressing NtTUA3-GFP that allowed to dissect the responses of microtubules to cold stress *in vivo*. Followed by the third part that attempted to dissect the interactions of OsTTL with PLD. In the end, a potential link between tubulin posttranslational modification with tubulin synthesis was analysed.

3.1 Functions of OsTTL in rice growth and development

In this part, the evolution analysis of plant tubulin tyrosine ligase family proteins versus TTLs from animals, fungi and bacteria was conducted. Next, by

analysing overexpression of an OsTTL-RFP rice line and a BY-2 cell line, the potential localisiation and phenotypical changes (mainly focusing on coleoptile and root) were observed. In the end, from the cellular and biochemical level, it was attempted to understand the role of OsTTL in tubulin detyrosiantion/tyrosination cycle as well as in microtubule stability and organisation, thus leading to alteration of phenotypes (mainly coleoptile and root).

3.1.1 Plant TTLs cluster into a separate phylogenetic clade

Since all α-tubulins from plants harbour the carboxy-terminal tyrosine, first, the putative plant homologues of tubulin-tyrosine ligase (TTL) was searched. For this purpose, a multiple sequence alignment of the deduced protein sequences of TTL from eukaryotes and prokaryotes was conducted. The three homologues of TTL proteins in rice: a hypothetical protein without annotated function (Q8H022, rice 1), a protein annotated as tubulin-tyrosine-ligase (Q10QY4, TTL, rice 2), and a tubulin-tyrosine-ligase like protein (Q10QY3, TTLL, rice 3), harboured a tubulin-tyrosine-ligase domain in their C-terminal region between amino-acid residue 534 and 862 (Fig. S1), which was conserved among *Arabidopsis thaliana*, *Vitis vinifera*, and *Physcomitrella patens*. Futhermore, all tested plant TTLs were endowed with a long N-terminal extension containing a leucin-rich repeat domain (Fig. S1), which was not found in the TTL homologues from animals, fungi, and bacteria.

To infer the phylogenetic relationship, 17 deduced amino acid sequences of TTL from animals, plants, fungi, and bacteria were analysed by the neighbour-joining (NJ) algorithm. As shown in Fig. 3.1, the phylogenetic tree was found to be divided into four main branches: All sequences from plants clustered into one clade, clearly separate from the representatives of

metazoan animals (*Danio rerio, Homo sapiens, Mus musculus*), *Saccharomyces. cerevisiae* as representative of the fungi was quite distant, and the bacterial sequences clustered into a separate group. Within the plant clade, the Angiosperms were forming a subclade supported by a high bootstrap value (98%), the Lycophyte *Selaginella moellendorfii* stood basal to this clade, while the two tested Bryophytes (*Marchantia polymorpha* and *Physcomitrella patens*) grouped into a well-supported (bootstrap value 89%) own subclade. As representative of the Chlorophytes, a sequence from *Chara braunii* could be recovered that located at the base of the plant clade, but remained clearly distinct (with a bootstrap value of 84%) from the metazoan clade.

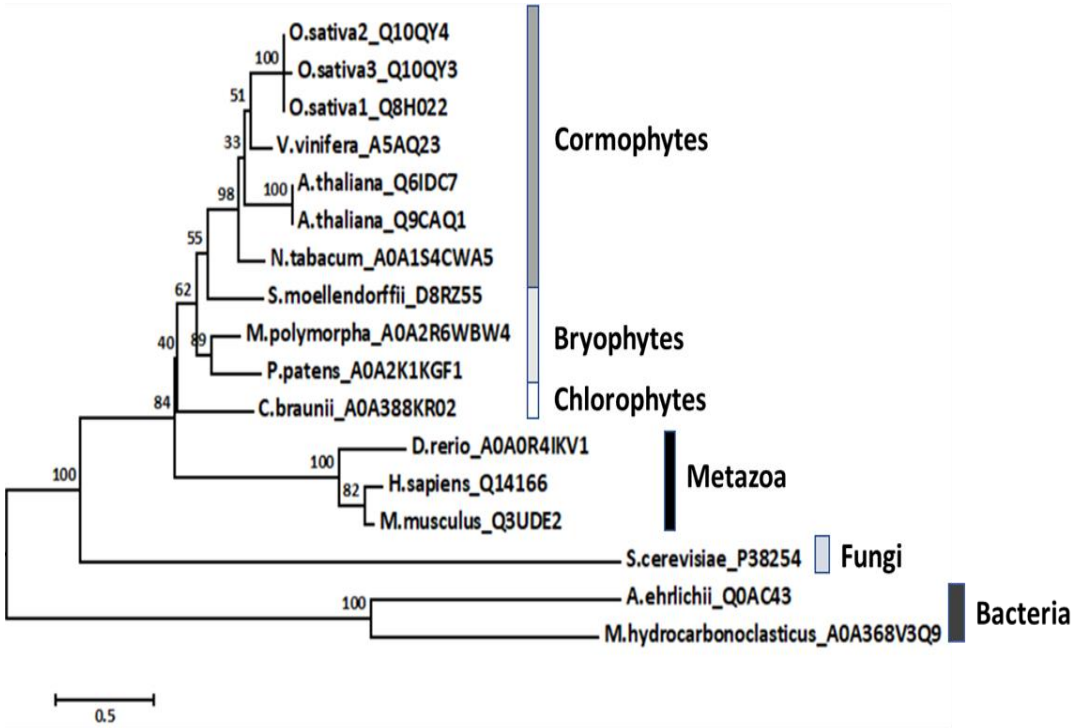

Fig. 3.1 Evolutionary relationships of plant tubulin tyrosine ligase homologues (TTLs) with TTLs from animals, fungi and bacteria. Phylogenetic tree for OsTTL was constructed using by the neighbour-joining based method. The bootstrap consensus tree inferred from 500 replicates is taken to represent the evolutionary history of the taxa analyzed. The tree is drawn to scale, with branch lengths in the same units as those of the evolutionary distances used to infer the phylogenetic tree.

3.1.2 Transcriptional level of OsTTL in OsTTL-RFP overexpressor rice lines

Three independent OsTTL-RFP overexpression rice lines were selected to check the expression levels by real-time RT-qPCR (Fig. 3.2). Compared to the wild type, steady-state transcript levels in these lines probed in the seminal root were elevated by 17, 12 and 7 times, respectively.

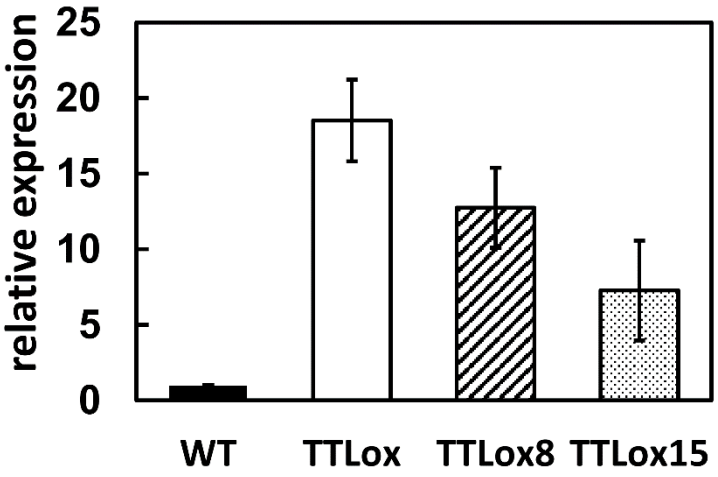

Fig. 3.2 Gene expression of OsTTL. Steady-state transcriptional levels of OsTTL in primary roots of different overexpressor lines as compared to the non-transformed wild type. Data represent mean values collected from three biological replicates.

To get clear phenotypic readouts, the line with the highest expression level (17-fold over the WT) was in the focus of the subsequent experiments, and is designated as OsTTLox in the following.

3.1.3 OsTTL-RFP decorates all microtubule arrays

In order to understand the potential function of OsTTL, the cellular localisation of its RFP-fusion was followed through the cell cycle in tobacco BY-2 cells by

visualisation of microtubules probing tubulin by indirect immunofluorescence using the monoclonal mouse antibody DM1A recorded by FITC as readout (Fig. 3.3), the results are from diploma thesis of Durst, 2009. OsTTL colocalised with all microtubule arrays, including cortical MTs in interphase cells, preprophase band and nuclear rim at the G2/M transition, spindle MTs during anaphase (preferentially the kinetochore microtubules), and the phragmoplast during telophase (Fig. 3.3), with no obvious preference for specific subsets of microtubules.

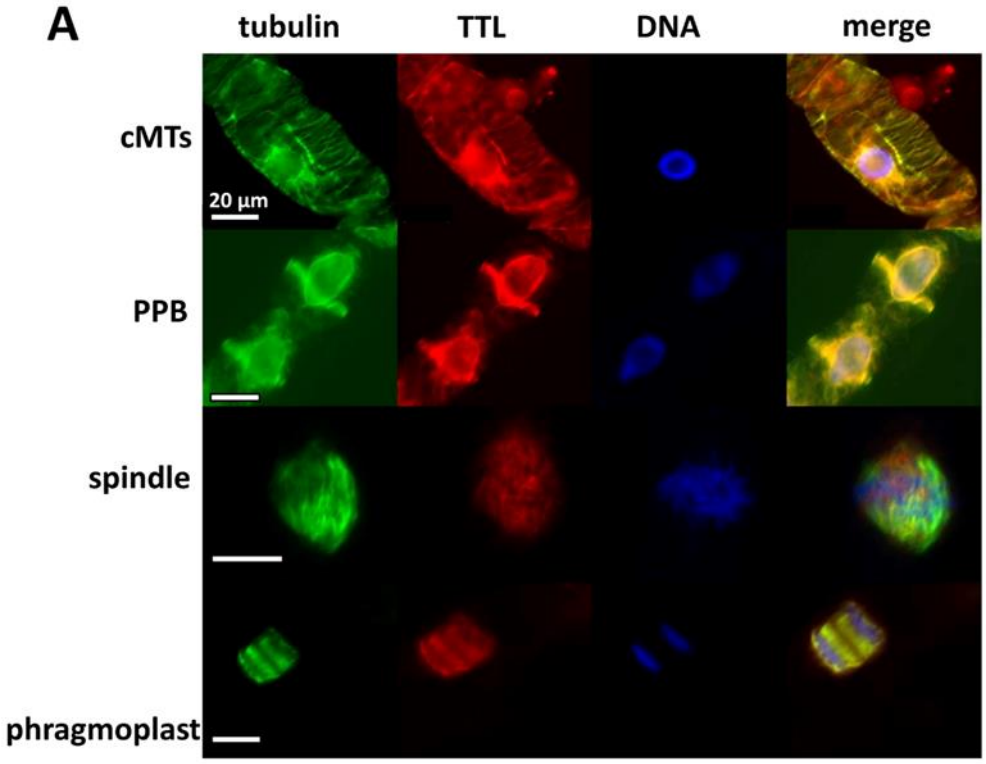

Fig. 3.3 Subcellular localisation of OsTTL in cycling BY-2 cells overexpressing OsTTL-RFP. Triple-staining of OsTTL-RFP in BY-2 cells in relation to different microtubule arrays. Microtubules are shown in green stained by immunofluorescence with DM1A and FITC as a readout and OsTTL-RFP is shown in red, DNA is shown in blue stained by Höchst 33258. In the merged images co-localized RFP and green fluorescent signals appear yellow as well as bule. Source: Durst, 2009.

To test the relationship between OsTTL and microtubules in the homologous system, rice, cortical MTs were visualised in root sections collected from OsTTLox. In contrast to tobacco BY-2, it was observed with a clear asymmetry for the two signals (Fig. 3.4) : while the dense and obliquely oriented cortical microtubules in the rhizodermal layer were strongly labelled by DM1A, but not decorated by RFP-OsTTL, the pattern was inverse for the cells of the subtending cortex layer, where microtubules were organised in transverse and looser arrays and were not recognized by DM1A, but clearly decorated by RFP-OsTTL. Since DM1A is preferentially binding to detyrosinated microtubules (Wiesler *et* al. 2002), while TTL is reported to prefer tubulin dimers (Kumar and Flavin, 1981), this observed asymmetry indicates that the oblique arrays in the rhizodermis harbour stable microtubules with a higher proportion of detyrosinated tubulin as compared to the loose arrays in the root cortex.

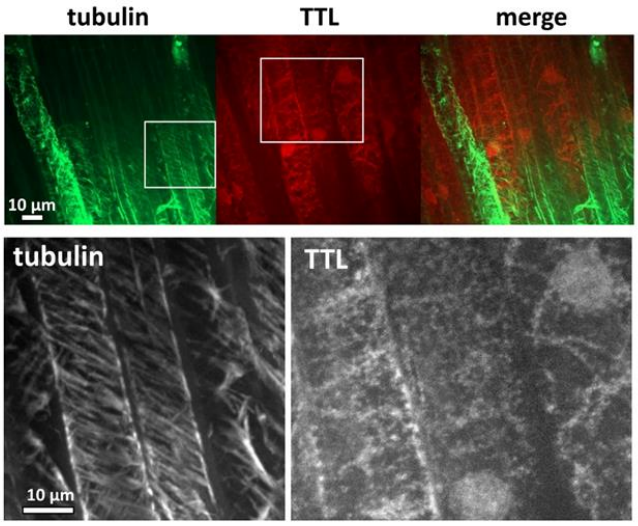

Fig. 3.4. Localisation of OsTTL (RFP) in rhizodermal cells of rice seminal roots of overexpressor OsTTL-RFP rice line in relation to cortical microtubules (tubulin, visualised by immunofluorescence using FITC as marker). Microtubules are shown in green stained by immunofluorescence with DM1A and FITC as a readout and OsTTL-RFP is shown in red. The zoom-in microtubules were shown in lower part from the rectangle in the upper images, respectively.

3.1.4 Overexpression of OsTTL modulates orientation of microtubules, cell elongation, and cell division

After germination, rice coleoptile growth is exclusively based on cell expansion, while for the rice root, growth starts with cell division in the meristem, followed by cell elongation in the elongation zone leading to cell differentiation in the maturation zone. Since cortical microtubules play an important role in directional cell expansion and different mitotic microtubule arrays control the process of correct cell division. In addition, detyrosination levels have been found to differ depending on the orientation of cortical microtubules (Wiesler *et* al., 2002). Therefore, phenotype should be focused since the overexpression of OsTTL would correlate with changes of microtubule orientation and, consequently, changes of organ growth.

3.1.5 Overexpression of OsTTL alters phenotypical changes of coleoptile and root

Here, after completion of coleoptile expansion, at day 6 after sowing, coleoptiles in OsTTLox appeared to be longer than in WT (Fig. 3.5 A) and the average length of coleoptiles was significantly increased by 28% due to overexpression of OsTTL (Fig. 3.5 B, left).

Interestingly, a reduced root length was also observed in OsTTLox compared to WT as the root length of OsTTLox was 0.7 cm shorter than WT 6 days after germination (Fig. 3.5 B, right).

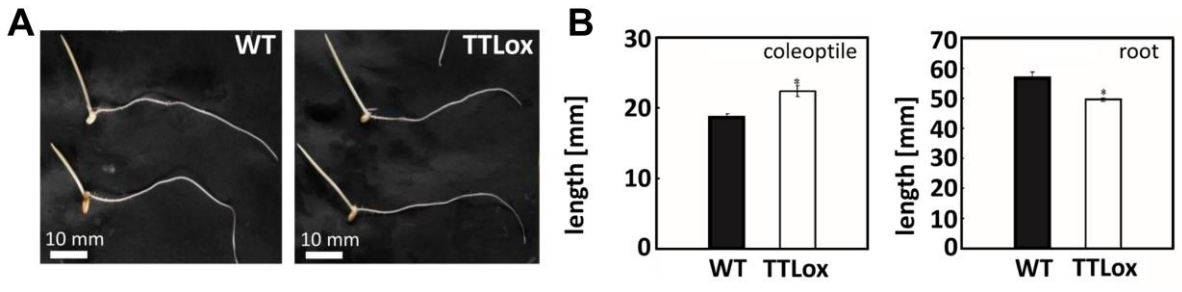

Fig. 3.5. Phenotype of OsTTLox rice seedling compared with wild type (Dongjin). A. Representative image of root and coleoptile of WT (left) and OsTTLox (right) 6 days after germination, Scale bar: 10 mm. B. Coleoptile and root length (mm) of WT and OsTTLox (n=15).

3.1.6 Overexpression of OsTTL promotes cell elongation and changes microtubule orientation in coleoptiles

In order to find out whether the longer coleoptile phenotype in OsTTLox was caused by enhanced cell expansion or increased cell numbers, mean cell length and cell numbers were determined from epidermal cells over the entire length of the coleoptile. As shown in Fig. 3.6 B, the mean cell length in OsTTLox clearly exceeded those in the WT, while the mean cell number in OsTTLox was decreased compared to in WT. The difference in elongation was most pronounced in the basal part of the coleoptile (Fig. 3.6 A), where the cells of OsTTLox appeared extremely long and rectangular, while WT cells of the same region were much shorter and still more rhomboid in shape. Thus, the observed increment in coleoptile length was caused by a strong stimulation of cell elongation, which was partially compensated by a strong decrease in cell number in OsTTLox.

To find out whether the stimulated cell elongation by overexpression of OsTTL is correlated with a changed orientation of cortical microtubules, the cortical

microtubules of epidermis cells of 6 days coleoptiles were visualised by immunofluorescence (Fig. 3.6 C) and frequency distributions over orientation constructed (Fig. 3.6 D). Here, for OsTTLox coleoptiles, the distribution was shifted towards the left as compared to the WT, which means that microtubules assumed more shallow angles with the short cell axis, while in the WT, microtubules were mostly oriented in steeply oblique arrays.

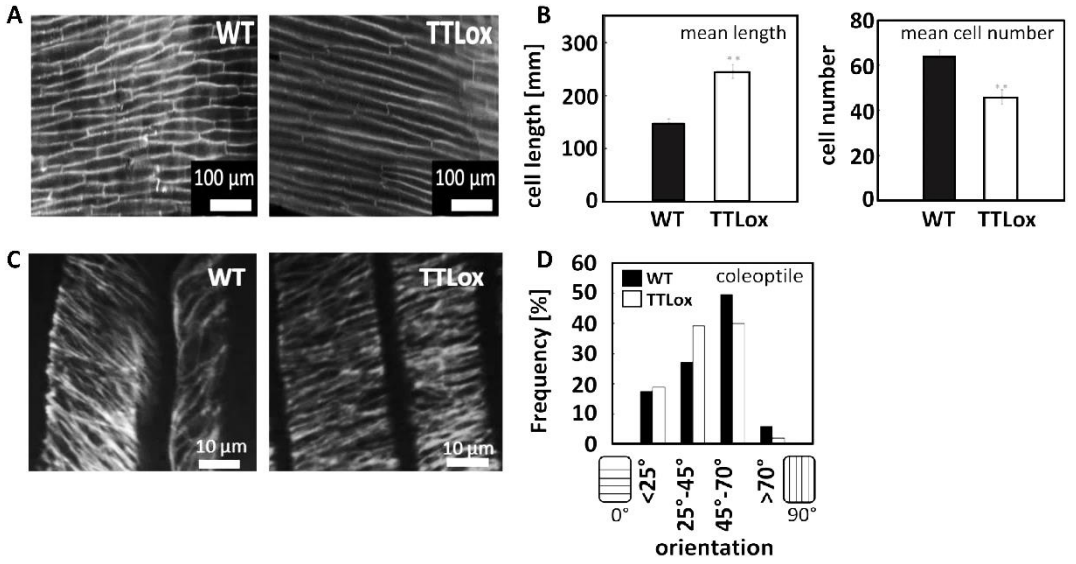

Fig. 3.6. A. Representative images of epidermis cells visualised by the autofluorescence of their cell walls in the coleoptile base of WT and OsTTLox. Scale bar: 100 µm. B. Mean length of cell and mean cell number in coleoptile of WT and OsTTLox. C. Microtubule were visualised by immunofluorescence using a FITC-conjugated secondary antibody. Scale bar: 10 µm. D. Frequency of distributions of MTs orientation in epidermis of coleoptile. The angle of microtubule defined as 0° when microtubule perpendicular to the side wall whereas 90° represented microtubule parallel to the side wall.

3.1.7 Overexpression of OsTTL changes microtubule orientation in root elongation zone

In order to test whether the difference of root growth between WT and OsTTLox was related to potential differences of microtubule orientation in the cortex of the root elongation zone, microtubules were visualised in longitudinal sections by immunofluorescence at the same time point, at day 6 after sowing. In the WT, cortical microtubules were mostly transverse or slightly oblique, while in OsTTLox, their orientation appeared shifted to steeper angles (Fig. 3.7 A). This impression was also supported by the frequency distributions over the angle with the transverse axis (Fig. 3.7 B). Here, for OsTTLox roots, the distribution was shifted towards the right as compared to the WT, which means that microtubules assumed steeper angles with the short cell axis, while in the WT, microtubules were mostly oriented in shallower arrays.

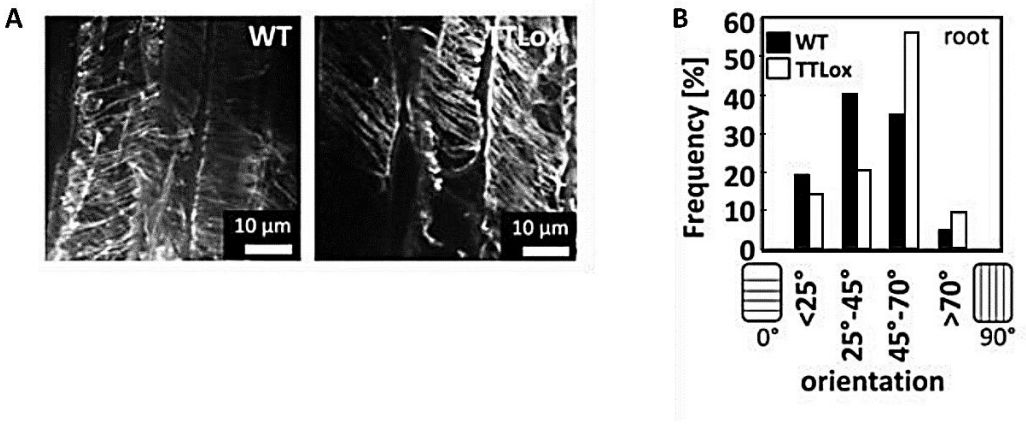

Fig. 3.7. Microtubule orientation in root elongation zone of WT and TTLox. A. Microtubules were visualised by immunofluorescence using a FITC-conjugated secondary antibody. Scale bar: 10 µm. B. Frequency of distributions of MTs orientation in epidermis seminal root elongation zone. The angle of microtubule defined as 0° when microtubule perpendicular to the side wall whereas 90° represented microtubule parallel to the side wall.

3.1.8 Overexpression of OsTTL disorients cell walls in root meristem zone

To get insight into the reduced root growth in rice OsTTLox, the apical region of the seminal root was stained with propidium iodide at day 6 after sowing to visualise the cell walls for confocal microscopy. Here, a distinct and specific phenotype was observed in the transition zone between meristem and distal elongation zone (Fig. 3.8 A): While in the WT cross walls were strictly perpendicular with the root axis, and evenly spaced, in the overexpressor they were oblique, in some cases even wavy, and spaced unevenly. This phenotype was seen in all tested lines overexpressing OsTTL (Fig. 3.8 A). A frequency distribution constructed over the incidence of normally and abnormally oriented cell walls (Fig. 3.8 B, C) confirmed that the frequency of the abnormally oriented cell walls was significantly increased from around 20% in the WT to around 50% in all scored lines overexpressing OsTTL. Thus, overexpression of OsTTL leads to disordered cell wall orientation.

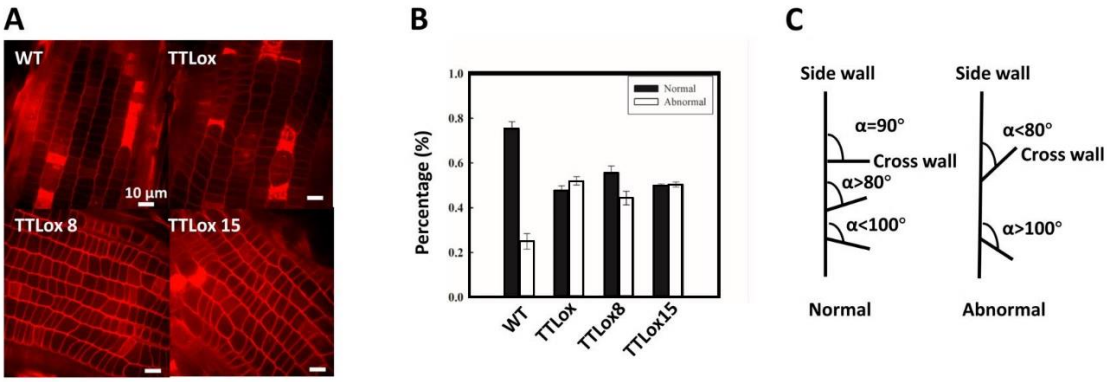

Fig. 3.8. Cell wall orientation in seminal roots of WT and three independent overexpression of OsTTL-RFP lines. A. Representative images of cell walls in the root apex stained by propidium iodide in different overexpression OsTTL lines and WT. Scale bar: 10 µm. B. Frequency distribution over the orientation of cross walls in the root apex, data represent mean values ± SE of 3 replicates. Each replicate represents at least 150

cells from 15 roots. C. Schematic representation of normal and abnormal cross wall orientation. Cell walls that were perpendicular with the root axis, i.e. representing the angle ⩾80° or ⩽100° were scored as normally oriented, while angle < 80° or >100° were scored as abnormal orientations.

3.1.9 Overexpression of OsTTL in BY-2 cell disorganizes phragmoplast microtubule

The precise construction of cell plate during cytokinesis is built up by phragmoplast that consists of microtubule, actin and other cellular components. The phragmoplast microtubules perpendicular to the cell axis and align two

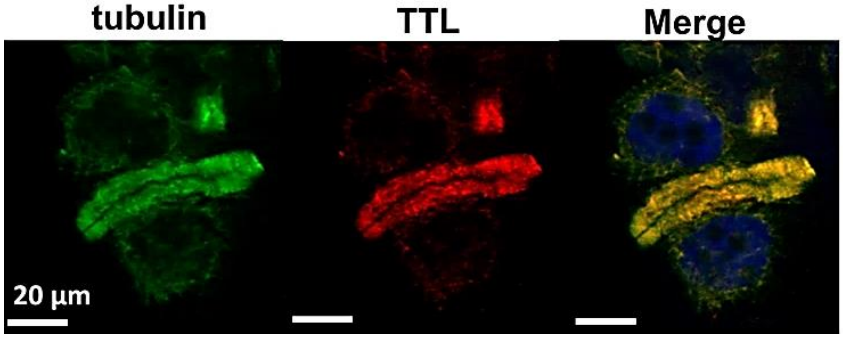

Fig. 3.9. Phragmoplast microtubule in OsTTLox BY-2 cell. Microtubules are shown in green stained by immunofluorescence with DM1A and FITC as a readout and OsTTL-RFP is shown in red. In the merged images co-localized RFP and green fluorescent signals appear yellow, while nuclei stained with Höchst appear in blue. Scale bar: 20 µm.

sides of the phragmoplast midzone, where the cell plate assembly occurs. The assembly of cell plate requires phragmoplast expansion which is driven by the dynamic instability of microtubules (Smertenko et al, 2017). It was therefore asked, whether overexpression of OsTTL would affect the organisation of phragmoplast microtubules. This was tested in the OsTTL BY-2 cell line by immunofluorescent staining of advanced phragmoplasts. As shown in Fig. 3.9,

OsTTL colocalised tightly with phragmoplast microtubules. In addition, the phragmoplast showed perturbations of alignment, with a wavy and even not fully contiguous cell plate in OsTTLox BY-2 cells when compared with NtTUA3-GFP BY-2 cells (Fig. 3.10, control) where the phragmoplast microtubule was aligned properly and perpendicular to the cell axis.

3.1.10 The organisation of phragmoplast microtubules is affected by nitrotyrosine

In order to check, whether perturbations of tubulin tyrosination can interfere with phragmoplast organisation, the NtTUA3-GFP BY-2 cells were treated with nitrotyrosine (NT) that is incorporated into detyrosinated α-tubulin and cannot be cleaved off by TTC (Jovanovic *et* al., 2010). As shown in Fig. 3.10, in untreated cells, the phragmoplast is oriented strictly perpendicular to the side wall, and the cell plate appeared as straight line of even thickness. However, after treatment with 50 µM nitrotyrosine for 2 h, phragmoplasts were laid down in an aberrant manner: some phragmoplasts were correctly oriented, but lined a wavy cell plate, others deviated from the short axis of the cell, even to the degree that they were oriented parallel to side walls, and some were bent and positioned asymmetrically separating a small lens-shaped area of the cell from a much larger region (Fig. 3.10, right hand).

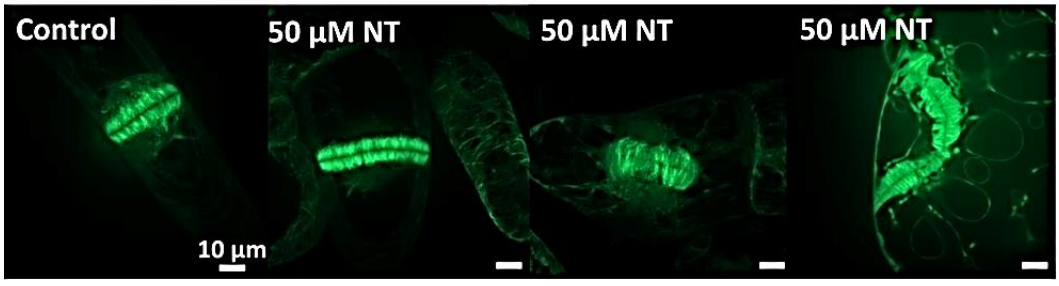

Fig. 3.10. Phragmoplast microtubule in overexpressing NtTUA3-GFP BY-2 cell. Representative images of phragmoplast microtubules in NtTUA3-GFP cell with or without treatment of 50 µM nitro-tyrosine (NT). Scale bar: 10 µm.

3.1.11 Overexpression of OsTTL confers a reduced sensitivity to oryzalin

Since the stability of microtubules correlates with the abundance of detyrosinated α-tubulin, it was wondered, whether overexpression of TTL would be accompanied by higher dynamics of microtubules. This should become physiologically manifest as an increased sensitivity towards oryzalin, a dinitro aniline herbicide that sequesters tubulin dimers and, thus, eliminates microtubules depending on their innate turnover. To test this, seedlings of WT and OsTTLox were grown in presence of 100 nM oryzalin to determine the relative growth rate (ΔL/L in % per day, during the period of maximal elongation, between day 5 and day 6). In the absence of oryzalin, the growth rates were

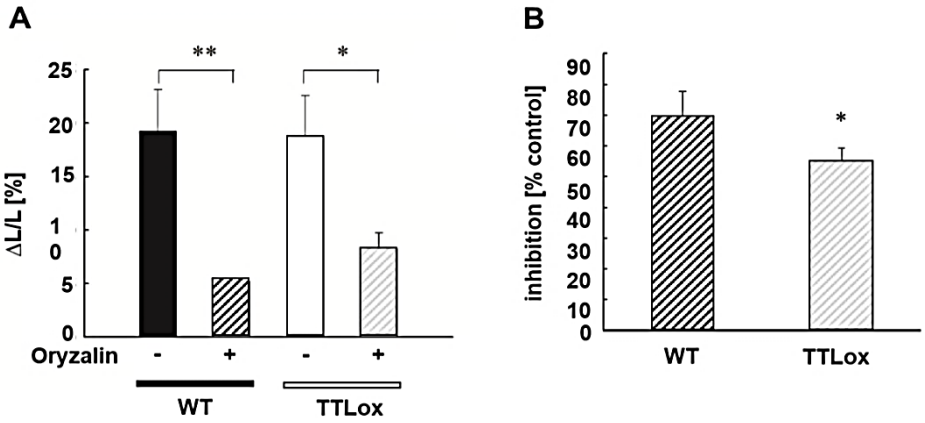

Fig. 3.11. A. Comparison of relative growth rate of seminal roots between WT and OsTTLox seedlings after treatment with 100 nM oryzalin. B. Comparison of relative inhibition of root growth rate between WT and OsTTL overexpressor seedlings after treatment with 100nM oryzalin. Asterisks (**) indicate significant differences ($P < 0.01$) from 3 independent replicates in Student *t*- tests for paired data and each replicate represents 9 seedlings.

identical (around 19% per day). As expected, the growth rates of both, WT and

OsTTLox roots, decreased significantly in presence of 100 nM oryzalin (Fig. 3.11 A). However, this reduction was significantly more pronounced in the WT (from 19.2% to 5.2%, corresponding to 70% inhibition, Fig. 3.11 B) when compared to OsTTLox (from 19.2% to 8.2%, corresponding to only 55% inhibition, Fig. 3.11 B). Thus, OsTTLox roots did not show the expected increase in oryzalin sensitivity, but a significant increase.

3.1.12 Overexpression of OsTTL shifts α-tubulin into the detyrosinated form

In order to test, whether the modulations of microtubule orientation and the reduced sensitivity of microtubules to oryzalin were accompanied by modulations in the ratio of tyrosinated/detyrosinated α-tubulin due to overexpression OsTTL-RFP, total proteins extracted from coleoptiles and roots of WT and OsTTLox at day 6 after sowing were separated by SDS-PAGE (Fig. 3.12 A and C, CBB) and probed by Western blotting using two monoclonal antibodies: ATT detecting tyrosinated α-tubulin (Fig. 3.12 A and C, tyr-tubulin), and DM1A detecting detyrosinated α-tubulin (Fig. 3.12 A and C, detyr-tubulin). The resulting signals were then quantified and compared on a relative scale (Fig. 3.12 B and D). In coleoptiles, the relative content of tyrosinated α-tubulin was not affected by overexpression of OsTTL, while the relative content of detyrosinated α-tubulin increased by 70% in OsTTLox compared to the WT (Fig. 3.12 B). The same phenomenon of an increased detyrosinated α-tubulin content was also found in roots, albeit less pronounced (Fig. 3.12 D). Here, the value for OsTTLox was 30% higher when compared with the WT. Again, there was no difference of tyrosinated α-tubulin between the roots from WT and OsTTLox (Fig. 3.12 D). In conclusion, overexpression of OsTTL did not lead to higher proportions of tyrosinated α-tubulin, but, opposite to the expectation, increased detyrosinated α-tubulin content in both, coleoptile and root. The

same pattern was also seen in BY-2 cells overexpressing OsTTL (Appendix Fig. S2). Here, the upper band detected by ATT representing tyrosinated α-tubulin was stronger in WT BY-2 cells, while the (somewhat smaller) band detected byDM1A representing detyrosinated α-tubulin was stronger in the line overexpressing OsTTLox.

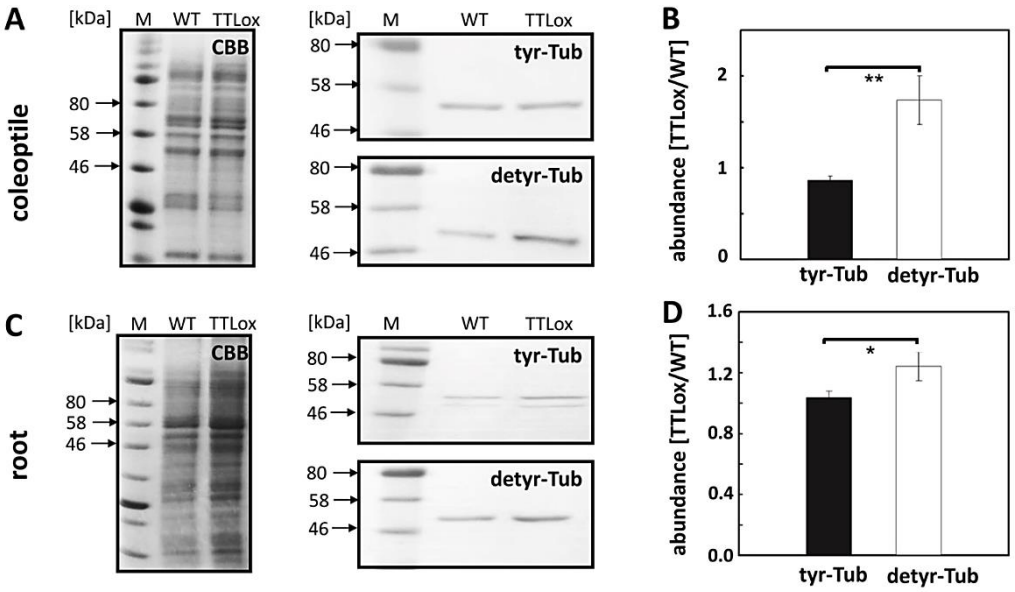

Fig. 3.12. Detection of tyrosinated and detyrosinated α-tubulin by antibodies ATT and DM1A in total extracts from coleoptiles and seminal roots of WT and OsTTLox at day 6 after germination. A and C, representative images of Western blots obtained from coleoptile and root extracts. Left, Coomassie Blue stained gel (CBB); right, tyrosinated α-tubulin detected by ATT (upper part), and detyrosinated α-tubulin detected by DM1A (lower part). B and D, relative content of tyrosinated (tyr-tub) and detyrosinated (deTyr-tub) α-tubulin in coleoptiles (B) or seminal roots (D) of OsTTLox in comparison to the WT (defined as 1).

In order to further validate the perturbed ratio of tyrosinated/detyrosinated α-tubulin seen in the OsTTLox, EPC affinity chromatography was adopted to separate tyrosinated and detyrosinated α-tubulin in one step, due to a higher affinity of detyrosinated α-tubulin for this antimicrotubular compound (Wiesler

et al., 2002). After incubation of coleoptile (Fig. 3.13 A, B) and root (Fig. 3.13 C, D) extracts with EPC sepharose, the bound proteins were eluted by a gradient of increasing ionic strength, and the fractions were collected, separated by SDS-PAGE, transferred to a membrane, and probed by antibodies: ATT (directed to tyrosinated α-tubulin) and DM1A (directed to detyrosinated α-tubulin). Tyrosinated α-tubulin detected by ATT had a lower affinity with EPC sepharose and could be eluted at lower ionic stringency, by lower concentrations of KCl (Fig. 3.13 A, C, tyr-Tub), whereas detyrosinated α-tubulin could only be eluted by higher concentration of KCl (Fig. 3.13 A, C, detyr-Tub), which was consistent with the previous report (Wiesler *et* al., 2002). The signals detected by ATT and DM1A were quantified (Fig. 3.13 B, D). In coleoptiles of OsTTLox (Fig. 3.13 B), the abundance of tyrosinated α-tubulin was the same as in the WT, while the abundance of detyrosinated α-tubulin was strongly increased (with a surplus of 150% for coleoptiles over the values found in the WT). In the roots (Fig. 3.13 D), both, the abundance of tyrosinated α-tubulin as well as of detyrosinated α-tubulin were increased by 70% in OsTTLox, as compared to the wild type. However, the ratio of the two tubulin forms was not significantly different. In summary, the more sensitive approach to purify the two tubulin pools by affinity chromatography, confirmed that tubulin in OsTTLox coleoptiles was significantly more detyrosinated, while tyrosinated α-tubulin remained at the same level as in the WT (note: it did not decrease to compensate the higher level of detyrosinated tubulin). In the root, the situation differs: here both pools of tubulin were increased to the same degree over the values seen in the WT.

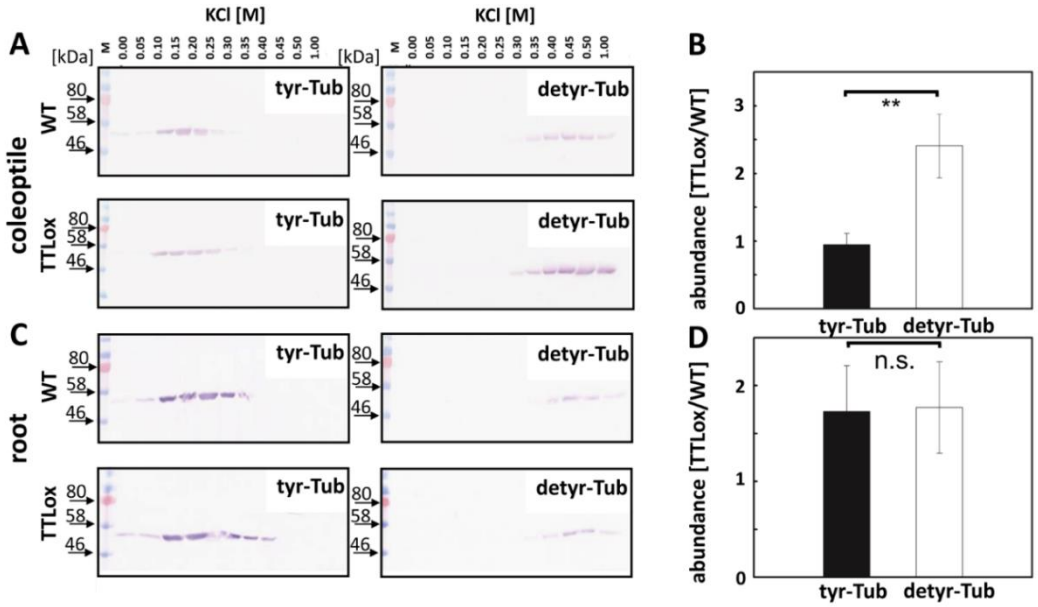

Fig. 3.13. Separation of tyrosinated and detyrosinated α-tubulin in extracts from coleoptile and root of WT and OsTTLox by EPC sepharose affinity chromatography. A and C, representative images of tyrosinated α-tubulin (detected by ATT) and detyrosinated α-tubulin (detected by DM1A) in the fractions from coleoptile and root extracts eluted by a gradient of concentrations of KCl. B and D, quantification of tyrosinated and detyrosinated α-tubulin content from coleoptiles and seminal roots of OsTTLox relative to WT (defined as 1).

Taken together, overexpression of OsTTL resulted in an increase in detyrosinated α-tubulin, instead of expected increase in tyrosinated α-tubulin. The unexpected increase of detyrosinated α-tubulin was corelated with enhanced stability of microtubules upon treatment with oryzalin, cortical microtubule reorientation in the respective tissue and reorganisation of phragmoplast, affecting rice cell wall orientation and coleoptile and root growth.

3.2 Functions of OsTTL in cold stress

As predicted above, OsTTL would participate in regulation of detyrosination and tyrosination cycle that would affect microtubule stability. Moreover, cortical microtubules play important roles in cold stress, act not only as cold perception but also as cold signalling (Wang and Nick, 2017). Thus, this part was focusing on dissecting the role of OsTTL in microtubule-based responses to cold stress. To test whether cold induced cortical microtubule disassembly would be affected by overexpression of OsTTL, it was urgent to visualize the responses of microtubules *in vivo*. Therefore, in this part, OsTTL was overexpressed into a microtubule-marker BY-2 cell line overexpressing NtTUA3-GFP to generate a double overexpression line (referred as TTL+TUA3, whereas NtTUA3-GFP was referred as TUA3). Thus, the responses of microtubules under cold stress could be followed to analyse the functions of OsTTL in cold-induced microtubule responses.

3.2.1 Overexpression of OsTTL reduces cold tolerance

First, whether OsTTL participates in modulation of cold tolerance was investigated. Both TUA3 and TTL+TUA3 were subjected to cold (0℃) for 24 h and the cell mortality was recorded. The result showed that cold treatment for 24 h could induced cell death in both lines, however, the relative percentage of cell mortality of the TTL+TUA3 cell line was significantly higher (around 78%) than in the TUA3 cell line, where only 10 % of cells were dead, which suggested that overexpression of OsTTL resulted in less cold tolerance (Fig. 3.14).

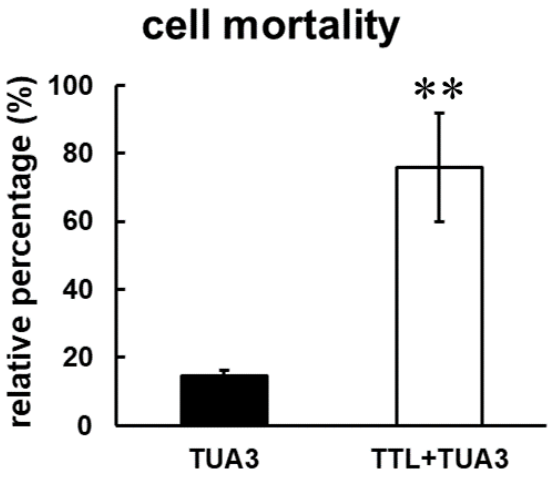

Fig. 3. 14. Comparation of cold induced cell mortality in overexpression of NtTUA3-GFP BY-2 cell line (TUA3) and overexpression of OsTTL-RFP in NtTUA3-GFP BY-2 cell line (TTL+TUA3). Relative percentage of cell mortality of TUA3 and TTL+TUA3 cell lines under cold treatment (0℃ water ice bath) for 24 h are shown by mean values collected from three biological replicates. Asterisks (**) indicate significant differences (P <0.01) between TUA3 and TTL+TUA3 overexpressor as assessed by a Student *t*- test for unpaired data.

3.2.2 Overexpression of OsTTL results in rapid cold induced microtubule disassembly

Since cortical microtubules disassembled rapidly under cold shock, it was important to know whether cold induced disassembly of cortical microtubules was affected by overexpression of OsTTL. To test it, microtubules in both cell lines were marked with GFP that allowed to visualise the responses of cortical microtubules to cold *in vivo*. It was found, without cold, cortical microtubules in TUA3 as well as in TTL+TUA3 cell lines, were almost intact and mainly oriented as parallel bundles that aligned perpendicular to the long cell axis (Fig. 3.15, 0 min). Upon cold stress, in TUA3 cell line, cortical microtubules partially disassembled within 5 min, even after 15 min, partial cortical microtubules

remained still stable, although some of cortical microtubules disassembled. However, in comparison, cortical microtubules in TTL+TUA3 almost totally disappeared in 5 min of cold stress (Fig. 3.15), suggesting that cortical microtubules modified by OsTTL would undergo rapid depolymerisation upon cold treatment.

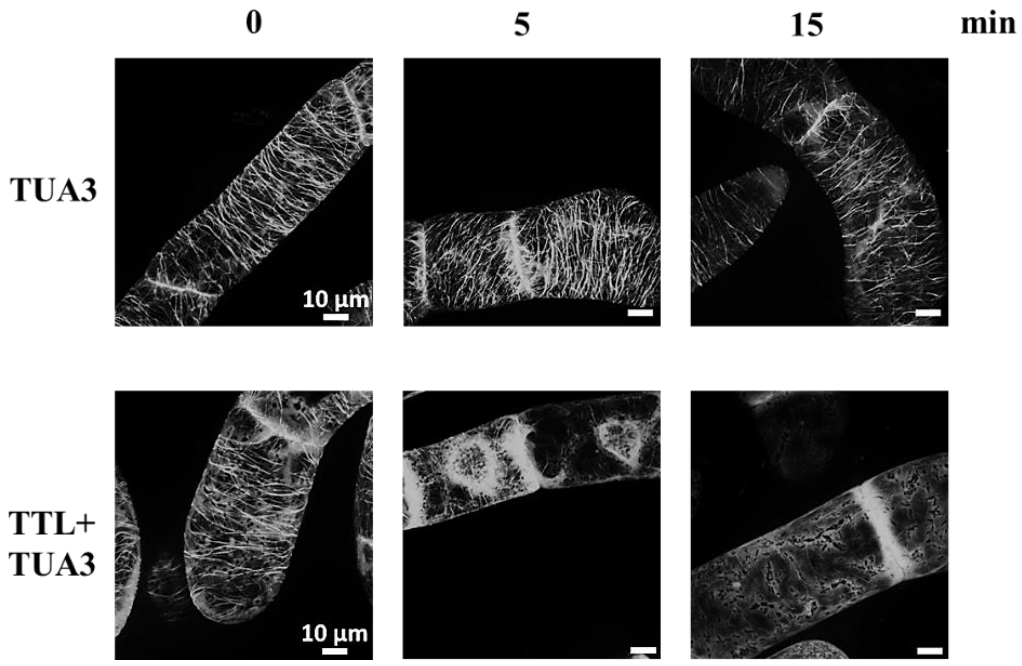

Fig. 3.15. Cold triggered MT disassembly. The response of cortical microtubules in overexpression of NtTUA3-GFP BY-2 cell line (TUA3) and overexpression of OsTTL-RFP in NtTUA3-GFP BY-2 cell line (TTL+TUA3) to cold (0 °C) treatments at different time points. Scale bar: 10 µm.

3.2.3 Overexpression of OsTTL results in more pronounced cold induced calcium influx

Calcium is an important second messenger that triggers intercellular processes to respond to numerous external stimuli such as cold, drought and high salinity. Different types of stresses cause a transient increase of Ca^{2+}, which is thought to be triggered by a transient disruption of cortical

microtubules (Nick, 2013; Thion *et* al., 1996). Therefore, it was assumed that more rapid disassembly of cortical microtubules induced by cold in TTL+TUA3 BY-2 cell line would also trigger rapid increase of Ca^{2+} influx. To test the idea, the extracellular alkalisation, a readout of potential Ca^{2+} influx, was recorded in a time series under cold stress for 60 min followed within another 60 min of recovery to room temperature.

As expected, in both TUA3 and TTL+TUA3 cell lines, extracellular alkalisation was triggered after onset of cold treatment (Fig. 3.16).

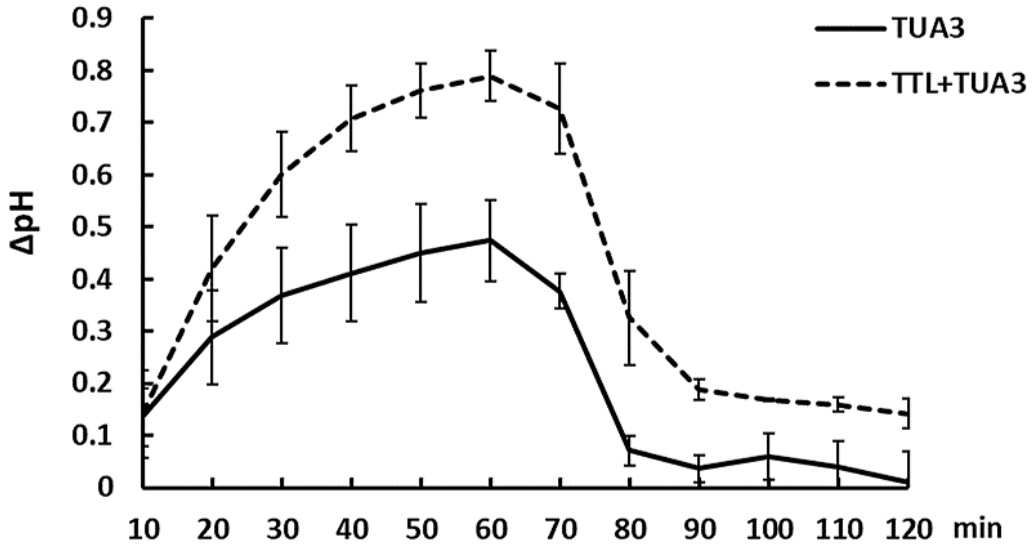

Fig. 3.16. Response of extracellular alkilization to cold. Comparison of changes of extracellular alkalisation during cold (0 ℃) for 60 min and recovery to room temperature from 60 min to 120 min in overexpression of NtTUA3-GFP BY-2 cell line (TUA3) and overexpression of OsTTL-RFP in NtTUA3-GFP BY-2 cell line (TTL+TUA3). Data represent mean values ±SE of 3 biological replicates.

However, in the TTL+TUA3 cell line, cold induced extracellular alkalisation was increased more rapidly in 60 min from a pH of 0.15 to around 0.8 compared with readily increase from a pH gradient of 0.1 to around 0.45 of TUA3 cell line. The same trend could also be observed, when recovering from cold to room

temperature, the extracellular alkalisation of the TTL + TUA3 cell line dropped faster than that of the TUA3 cell line (Fig. 3.16). This indicated that overexpression of OsTTL resulted in more pronounced calcium influx under cold stress.

Thus, overexpression of OsTTL resulted in more rapidly cold-induced depolymerisation of cortical microtubules, accompanied with more pronounced calcium influx under cold stress. These early signals might lead to reduced cold tolerance, manifested by more relative cell death under cold stress.

3.3 Functional interaction between OsTTL and OsPLDα1

Phospholipase D (PLD), a 90-kD protein isolated from tobacco membranes, is thought to be the linker between plasma membrane and microtubules and acts as a central signalling hub in plant stress (Dhonukshe *et* al., 2003; Gardiner *et* al., 2001; Munnik *et* al., 1995). Indeed, PLD activation could induce microtubule reorganization (Angelini *et* al., 2018; Dhonukshe *et* al., 2003). However, how PLD associates with microtubule is still unknow.

Here, in this part, it was attempted to understand whether PLD would interact with microtubules that were modified by overexpressing OsTTL. PLD activation can be mimicked by different alcohols due to their specific functions: n-butanol acts as PLD activator. It not only activates PLD but also consumes the product PA such that the PA-dependent signalling pathway will be blocked; in parallel, sec- and tert- butanol can act as negative control since sec-butanol can also activate PLD but is unable to act as the transphosphatidylation substrate such that PA-dependent signalling pathway can still go on, while, tert- butanol can do neither (Munnik *et* al., 1995). To further test whether PLD interacts with detyrosinated α-tubulin, an overexpression of OsPLDα1 fused

with GFP was used.

3.3.1 Overexpression of OsTTL increases stability of cortical microtubules to 1% n-butanol treatment

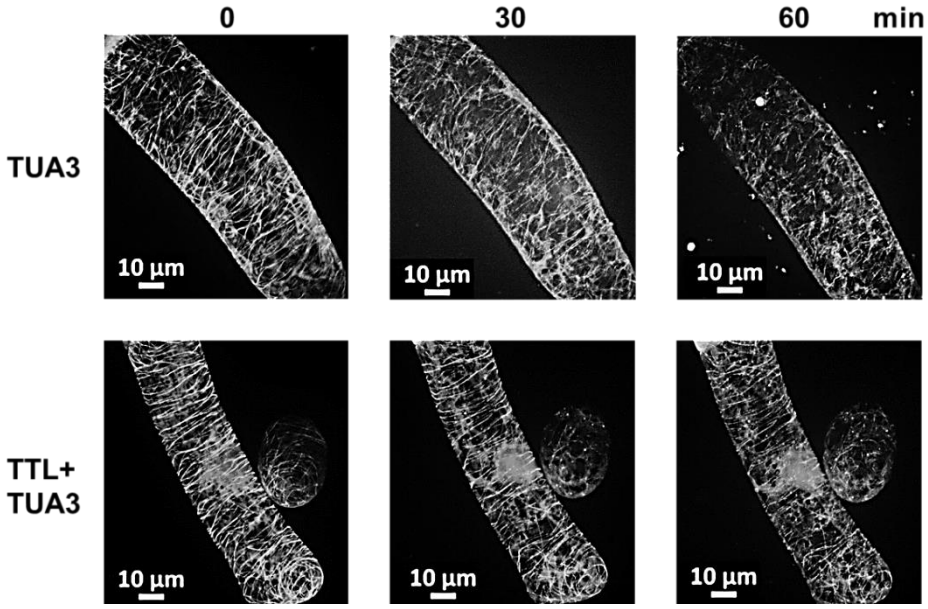

Fig. 3.17. Comparation of microtubular responses to 1% n-butanol in BY-2 cell expressing NtTUA3-GFP (TUA3) and overexpression of OsTTL-RFP in NtTUA3-GFP BY-2 cell line (TTL+TUA3). Representative images of responses of cortical microtubules to 1% n-butanol in both BY-2 cell lines are shown in a time series, respectively. Scale bar: 10 µm.

As shown in Fig. 3.17, after 30 min of 1% n-butanol treatment, cortical microtubules in both TUA3 and TTL+TUA3 cell lines started to depolymerize with no obvious difference, which is consistent with a previous report that PLD activation triggers the reorganization of plant microtubules (Dhonukshe *et* al., 2003). However, after 60 min, the cortical microtubules in the TTL+TUA3 cell line still sustained the microtubule structures whereas cortical microtubules in TUA3 cell line were completely depolymerized or fragmented, which indicated

that overexpression of OsTTL rendered cortical microtubules more stable towards 1% n-butanol treatment.

As expected, neither 1% sec- butanol nor 1% tert- butanol treatment for 60 min had effects on microtubule reorganisation or disassembly in both TUA3 and TTL+TUA3 cell lines (Fig. 3.18 and Fig. S3).

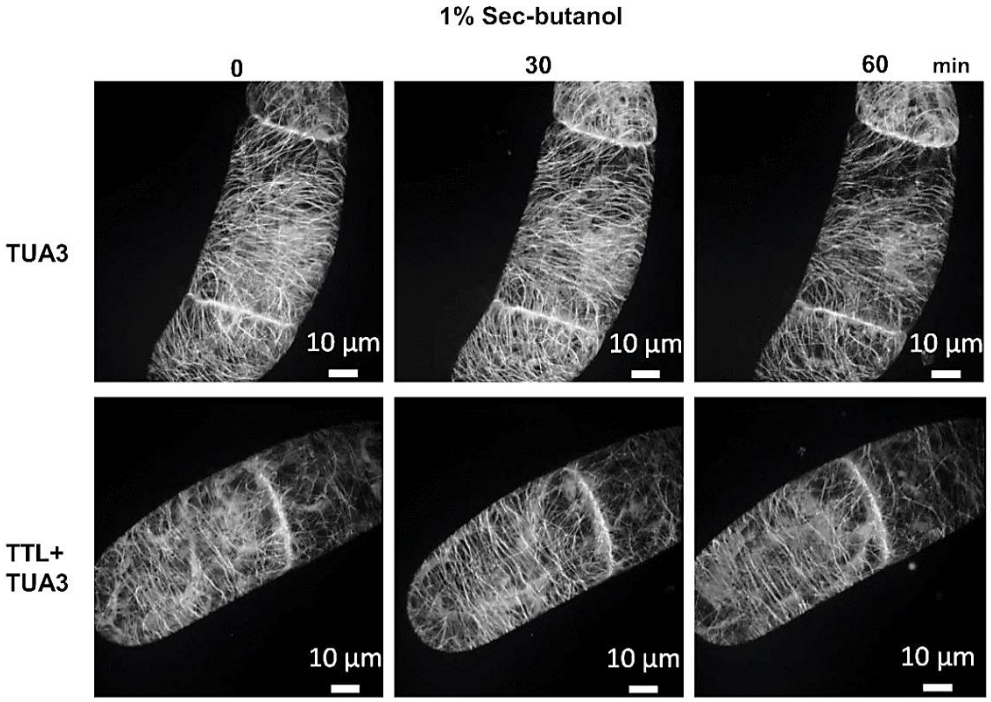

Fig. 3.18 Comparation of microtubular responses to 1% sec-butanol in BY-2 cell expressing NtTUA3-GFP (TUA3) and overexpression of OsTTL-RFP in NtTUA3-GFP BY-2 cell line (TTL+TUA3). Representative images of responses of cortical microtubules to 1% n-butanol in both BY-2 cell lines are shown in a time series, respectively. Scale bar: 10 µm.

3.3.2 OsPLDα1 co-localises with microtubules

In order to test whether PLD binds to microtubules, the localisation of OsPLDα1, an isoform of PLD from rice, was checked by immunofluorescence staining of microtubules in a tobacco BY-2 cell line overexpressing OsPLDα1

fused with GFP and coleoptiles of a rice line expressing the same fusion protein. In epidermis cells of coleoptiles overexpressing OsPLDα1-GFP, it was observed that OsPLDα1 localised to cortical microtubules (Fig. 3.19 A). Apart from that, OsPLDα1 also bound to mitotic microtubules in BY-2 cells overexpressing OsPLDα1-GFP, including spindle microtubules in metaphase and phragmoplast microtubules in anaphase (Fig. 3.19 B).

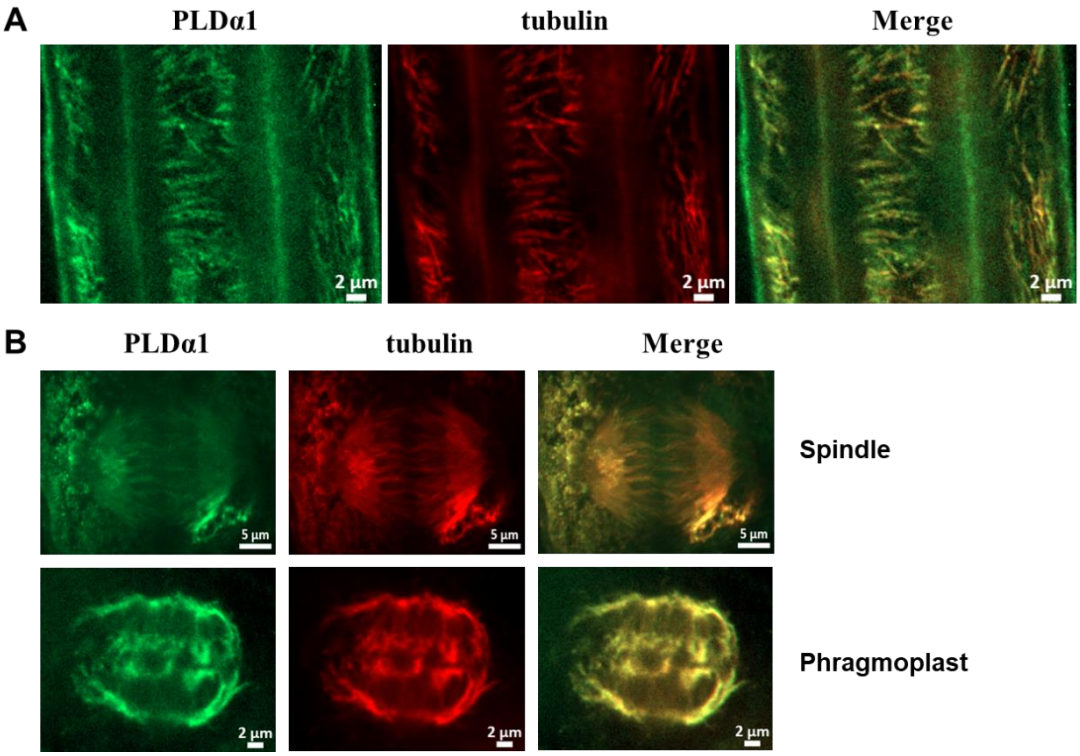

Fig. 3.19. Subcellular localisation of OsPLDα1 in cycling and non-cycling cells. A. Subcellular localisation of OsPLDα1 in epidermis cells of root in overexpression of OsPLDα1-GFP rice line. Size bar: 2 μm. B. Double-staining of OsPLDα1 in BY-2 cells in relation to different mitotic microtubule arrays (spindle and phragmoplast). Size bar: 5 μm in upper and 2 μm in below. Tubulin represented microtubules that visualised by immunofluorescence using TRITC as a marker; OsPLDα1 visualized by the signal of GFP and merged pictures showed green GFP and red TRITC siganls appear yellow.

3.3.3 Overexpression of OsPLDα1 results in higher abundance of detyrosinated α-tubulin

The above results showed that OsPLDα1 not only decorated microtubules (Fig. 3.19) but also preferentially associated with stable microtubules (Fig. 3.18), indicating a possible link between OsPLDα1 and detyrosinated α-tubulin since stable microtubules enriches in detyrosinated α-tubulin. Indeed, OsPLDα1 has been co-purified from the same fraction of detyrosinated α-tubulin by EPC affinity chromatography indicating OsPLDα1 might associate with detyrosinated α-tubulin (Krtková *et* al., 2012). If OsPLDα1 functionally interacts with detyrosinated α-tubulin, the detyrosinated α-tubulin would be changed when OsPLDα1 is overexpressed. To test it, Westernblot analysis was applied to dissect the abundance of detyrosinated α-tubulin in OsPLDα1-GFP overexpressing BY-2 cells. As shown in Fig. 3.20, it could be observed that in comparison with WT, overexpression of OsPLDα1 increased abundance of detyrosinated α-tubulin, which suggested that OsPLDα1 functionally interacted with detyrosinated α-tubulin.

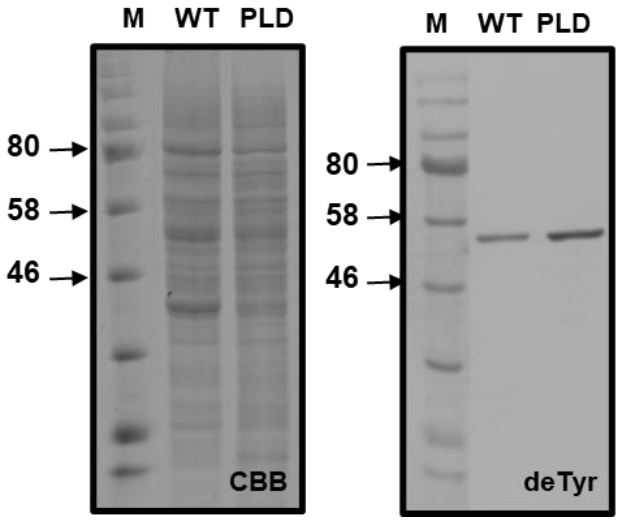

Fig. 3.20. Comparation of detyrosinated α-tubulin abundance in BY-2 cells overexpressing OsPLDα1-GFP and in wild type (WT) BY-2 cells. The abundance of detyrosinated

α-tubulin was detected by Western blot using antibody DM1A. M: marker of protein size in the first lane; WT: proteins extracted from WT in second lane; PLDα1: proteins extracted from OsPLDα1-GFP BY-2 cell; CBB: coomassie brilliant blue staining gel as control; deTyr: detyrosianted α- tubulin detected by antibody DM1A.

3.3.4 Overexpression of OsTTL increases the abundance of tyrosinated and detyrosinated α- tubulin (NtTUA3) contents

Since microtubules play two different roles depending on the stability. For instance, the stable microtubules help to sense membrane fluidity and transfer the force to the channel whereas the dynamic microtubules are relevant for the long-term adaptation of membrane due to their roles in controlling the integration of vesicles in plasm membrane (Wang *et* al., 2020). Therefore, in the following, the question was to know which population of microtubules was relevant here, since the stability of microtubules differed in populations of tyrosinated and detyrosinated α-tubulin (Wiesler *et* al., 2002). Therefore, Western blot was used to detect the abundance of tyrosinated and detyrosinated α-tubulin that probably be affected by overexpression of OsTTL.

The tyrosinated and detyrosinated α-tubulin seemed not to be affected by overexpression of OsTTL (Fig. 3.21 B and C, the lower bands). However, unexpectedly, a protein of approximately 80 kDa in size was detected by both antibodies, ATT and DM1A (upper bands in Fig. 3.21 B and C). Interestingly, the abundance of this 80 kDa protein was elevated in the TTL+TUA3 cell line compared with the TUA3 cell line. Since the weight of GFP is around 28 kDa and α- tubulin is around 55 kDa, it was proposed that the 80 kDa protein is NtTUA3 fused with GFP. To verify it, the monoclonal anti-GFP antibody was used. As expected, the upper one around 80 kDa could be detected as well by anti-GFP antibody, indicating that this 80 kDa protein is the NtTUA3 fused with

GFP. The central band, around 55 kDa in size, probably is an uncompletely translated version of NtTUA3 fused with GFP (Fig. 3.21 D). Therefore, the results suggested that overexpression of OsTTL resulted in more abundance of both tyrosinated and detyrosinated α-tubulin (NtTUA3).

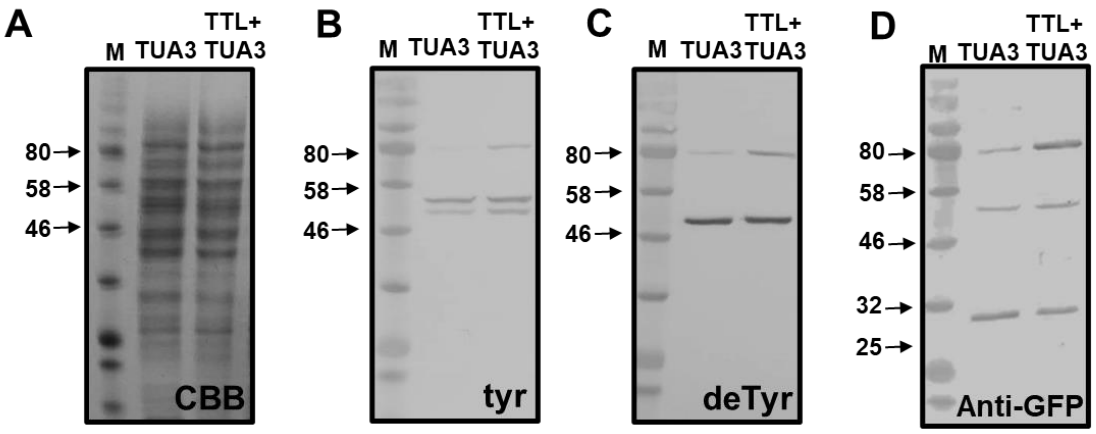

Fig. 3.21. Comparation of tyrosinated and detyrosinated α-tubulin abundance in BY-2 cell expressing NtTUA3-GFP (TUA3) and overexpression of OsTTL-RFP in NtTUA3-GFP BY-2 cell line (TTL+TUA3). Tyrosinated and detyrosinated α-tubulin were detected by Western blot using ATT and DM1A antibodies, respectively. A. CBB: comassie brilliant blue staining gel as control; B. tyrosinated α- tubulin detected by ATT; C. detyrosianted α-tubulin detected by DM1A; D. Anti-GFP was used to detect NtTUA3, since the NtTUA3 was fused with GFP. M: Marker of protein size; TUA3: overexpression of NtTUA3-GFP BY-2 cell line; TTL+TUA3: overexpression of OsTTL-GFP in NtTUA3-GFP BY-2 cell line.

3.3.5 Overexpression of OsTTL results in higher transcripts of NtTUA3 and OsTTL

Interstingly, it was found that overexpression of OsTTL increased in abundance of NtTUA3-GFP, both tyrosinated and detyrosinated, indicating the total content of NtTUA3-GFP was elevated due to overexpression of OsTTL. Based on that, whether higher tubulin synthesis of NtTUA3-GFP is caused by higher transcription of NtTUA3-GFP should be investigated. To test it, real-time

RT-qPCR was applied to detect the transcriptional level of NtTUA3-GFP. Here, it was found the transcripts of NtTUA3-GFP in OsTTL-RFP/NtTUA3-GFP BY-2 overexpression was 3 times higher than in NtTUA3-GFP BY-2 cell line. More interestingly, when tested the transcriptional level of OsTTL in OsTTL-RFP/NtTUA3-GFP BY-2 overexpression, transcripts of OsTTL in OsTTL-RFP/NtTUA3-GFP BY-2 overexpression was highly elevated by about 20 times compared to the BY-2 cells overexpressing only OsTTL-RFP.

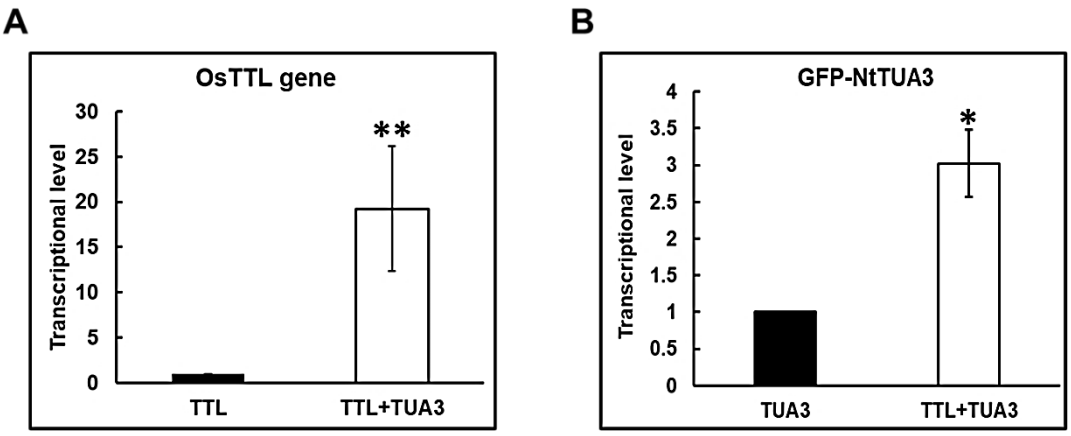

Fig. 3.22. Gene expression of OsTTL and GFP-NtTUA3. A. Real time RT-qPCR detecting transcriptional level of transformed OsTTL gene in overexpression of OsTTL-RFP in NtTUA3-GFP BY-2 cell line (TTL+TUA3) compared with the BY-2 cell line overexpressing OsTTL-RFP (TTL). B. Real time RT-qPCR detecting transcriptional level of NtTUA3 gene in overexpression of OsTTL-RFP in NtTUA3-GFP BY-2 cell line (TTL+TUA3) compared with in BY-2 cell overexpressing NtTUA3-GFP (TUA3). Data represent mean values collected from four replicates. Asterisks (*) and (**) indicate significant differences ($P < 0.05$) and ($P < 0.01$) from 4 independent replicates in Student *t*-tests for paired data, respectively.

Thus, overexpression of OsTTL resulted in enhanced tolerance to 1% n-butanol. OsPLDα1, one isform of PLD family protein, showed tightly colocalisation to mitotic microtubule arrays including spindle and phragmoplast

microtubules in cycling cells of the BY-2 cells overexpressing OsPLDα1-GFP as well as cortical microtubules in non-cycling cells of rice overexpressing OsPLDα1-GFP. When OsPLDα1 was overexpressed in BY-2 cell, the abundance of detyrosinated α-tubulin was elevated as well, indicating an interaction of OsPLDα1 with detyrosianted α-tubulin. In addition, overexpression of OsTTL in a microtubule marker line expressing NtTUA3-GFP resulted in accumulation of both tyrosinated and detyrosinated NtTUA3-GFP, accompanied with higher transcripts of NtTUA3-GFP as well as higher transcripts of OsTTL.

4 Discussion

In the current study, overexpressing a rice tubulin tyrosine ligase (TTL) family protein (Q10QY4, OsTTL) shifts the distribution of tubulin detyrosination/tyrosination, accompanied with alteration of the stability and orientation of microtubules, leading to changes in plant growth and development as well as stress tolerance.

Therefore, in the following section, it is firstly discussed the significant findings due to overexpressing OsTTL with respect to the functional differentiation of different microtubule arrays, the role of post-translational modifications for the reorientation of cortical microtubules, and the organisation of the phragmoplast. As most specific phenotype, it can be pinpointed a perturbed organisation of the phragmoplast (in tobacco cells), and a perturbed organisation of cross walls (in rice roots).

This is followed by a discussion on the role of OsTTL modified microtubules for early cold sensing. Subsequently the interaction of PLD and detyrosinated α-tubulin, and interesting findings about effects of posttranslational modifications on autoregulation of tubulin synthesis are discussed.

At the end is discussed whether OsTTL might be the elusive plant version of a tubulin tyrosine (de) carboxylase (TTC) or plant TTL, and how these possibilities could be followed up in the future.

4.1 Why is it worth to study plant TTLs?

Plant microtubules undergo a dynamic reorganisation that is functionally linked with the axiality of cell division, cell growth and differentiation (reviewed in Nick,

2007). This leads to the question, how tubulins are assigned to the different microtubule arrays that partially coexist in the same cell. The original idea that different arrays are composed of different tubulin isotypes has been discarded, based on the finding that microtubules utilise different isotypes simultaneously (Hussey *et* al., 1987). However, tubulin post-translational modification would provide an alternative mechanism to assign different functionalities to different microtubules occurring in the same cell. The highly conserved tyrosine at the carboxy-terminus of all eukaryotic tubulins (with exception of the slime mold Physarum, Watts *et* al., 1988) is evidence for the importance of tubulin detyrosination and tyrosination.

Plant TTLs cluster into a separate phylogenetic clade, and harbour a long N-terminal extension that is absent from mammalian TTLs: a leucine-rich repeat (LRR) domain (Fig. 3.1, Appendix. Fig. S1). In animals, the TTL protein family contains one *bona-fide* TTL protein and 13 subgroups referred as TTL-like (TTLL) proteins. Among them, the *bona-fide* TTL is the only identified enzyme that retyrosinates α-tubulin, while the others are either glutamylases (TTLL1, 2, 4, 5, 6, 7, 9, 11, 13) or glycylases (TTLL 3, 8, 10) (Janke and Magiera, 2020). Especially, human TTLL12 is identified as atypical TTL family protein not functioning as TTL, glutamylase or glycylase but affects detyrosination levels while both SET domain and TTL-like domain are lacking enzymatic activities *in vitro* (Brants *et* al., 2012; Wasylyk *et* al., 2010). Interestingly, plants only have one TTL family protein that is mostly similar to animal TTLL12 protein (Janke *et* al., 2005). However, since the N-terminal region of plant TTLs is different to the N-terminal SET like domain of animal TTLL12 as plant TTLs have one LRR domain instead, their functions are probably different due to N-terminal domain. The LRR domain occurs in a large number of proteins and functions for specific protein-protein interactions, for instance in receptors (reviewed in Kobe and Kajava, 2001). This would

indicate that the ligase function, located in the C-terminal half of the protein is recruited to specific interaction partners. These partners remain to be identified, for instance by pull-down assays using recombinantly expressed rice TTL, but already from the structural features a scenario emerges, where the tubulin ligase activity can be recruited to specific sites in the cell through this LRR domain. Such a working hypothesis will be pursued in future studies.

4.2 A role for tubulin tyrosination status in microtubule orientation?

In epidermal cells of maize coleoptiles, stimulation of cell growth by auxin was not only accompanied by a reorientation of cortical microtubules to more transverse orientations, but also by a higher proportion of tyrosinated α-tubulin (Wiesler *et* al. 2002). Even within the same cell, during the reorientation, transverse microtubules were preferentially composed of tyrosinated α-tubulin, while detyrosinated α-tubulin was more abundant in longitudinal microtubules. The differential modification of microtubules, depending on their orientation, might be caused by differences in turnover that would recruit TTC preferentially to the longitudinal microtubules (Kumar and Flavin, 1981), such that tubulins integrated into these longitudinal microtubules would get a higher chance to become detyrosinated (“stability first” model). However, there might as well be an inverse causality, where the detyrosinated α-tubulin would confer higher stability to the longitudinal arrays (“tubulin modification first” model).

The analysis of the OsTTL overexpressor lines allows to discriminate between the two possibilities: the overexpression results (unexpectedly) in a significant increase of detyrosinated over tyrosinated α-tubulin (Fig. 3.12 and 3.13), as well as in a reduced sensitivity to oryzalin (Fig. 3.11). Since oryzalin eliminates microtubules by sequestering tubulin heterodimers from integration into growing microtubules (Morejohn *et* al., 1987), it can be concluded that

microtubules are endowed with a higher stability, which would correlate with a more pronounced detyrosination status, consistent with the results of Wiesler *et* al. (2002). Beyond the further confirmation of the correlation between detyrosinated α-tubulin and a more longitudinal orientation of microtubules, the observation bears on the differentiation between the “stability first” versus the “tubulin modification first” models. The genetically caused increase in tubulin detyrosination is probably the cause for the observed, altered orientation of cortical microtubules in the overexpressor, and not its consequence.

Interestingly, the effect of OsTTL overexpression was different between coleoptile and root: in the coleoptiles, microtubules were shifted into a more transverse orientation (Fig. 3.6 C and D), which was linked with increased mean cell length and longer coleoptiles (Fig. 3.5, Fig. 3.6 A and B). The stimulation of cell elongation was accompanied by a decreased cell number (Fig. 3.5 B). In the root, the situation was inverse – here, microtubules were shifted into a steeper orientation (Fig. 3.7), followed by a reduction of growth.

From these patterns, two conclusions can be drawn: 1. No matter, into which direction microtubule orientation shifts as a result of OsTTL overexpression, the resulting organ growth remains linked with this orientation – the more transverse microtubules in the coleoptile support a stimulation of growth, the more longitudinal microtubules in the root inhibit growth. 2. The elevated detyrosination seen as result of OsTTL overexpression does not necessarily result in the same reorientation (steeper angles) of microtubules, but depends on the context. In the root, longitudinal arrays are favoured, in the coleoptile, it is transverse arrays that are favoured. Thus, detyrosination per se does not confer a particular orientation, it just seems to stabilise the respective orientation prevailing in the respective cells. This finding represents a kind of extension of previous results (Wiesler *et* al. 2002), where detyrosination was

associated with longitudinal microtubules that had been induced by auxin depletion. It would have been interesting to test, whether a reversion of this experiment, where microtubules are shifted from an originally longitudinal into a prospective transverse orientation by re-incubation with auxin, would have led to the same outcome, or whether under these conditions it would have been the transverse microtubules that would have been detyrosinated preferentially.

4.3 Does tubulin re-tyrosination define functional subsets of microtubules? The case of the phragmoplast

Since plant cell shape is mainly controlled by cell wall, the abnormal cell wall orientations in the root meristem of OsTTL overexpressor lines are expected to lead to reduced root growth, which was actually observed (Fig. 3.8). The data are also consistent with the previous report by Jovanovic *et* al., (2010), where nitro-tyrosine, that can be ligated to detyrosinated tubulin but cannot be cleaved off, subsequently affected cell wall organisation in rice roots. The correct orientation of the new cell wall is predefined by the preprophase band as shown by elegant centrifugation experiments in fern protonemata (Murata and Wada, 1991), because the phragmoplast is organised by spatial cues from an endosomal belt organised by the preprophase band and persisting through mitosis (Dhonukshe *et* al., 2005).

In the present work, it is shown that overexpression of OsTTL in BY-2 cells leads to a wavy and non-contiguous cell plate (Fig. 3.9), contrasting with the strictly perpendicular and non-interrupted cell plate found in BY-2 cells expressing just NtTUA3-GFP (Fig. 3.10, control), indicating that overexpression of OsTTL affects the structure of phragmoplast MTs. This

phenotype could be phenocopied by feeding 50 µM nitro-tyrosine to NtTUA3-GFP (Fig. 3.10), indicative of a role for balanced tubulin detyrosination and retyrosination for a normal organization of the phragmoplast. This finding has to be seen in the context of a report, which showed that during expansion phragmoplast microtubules differing in dynamics act in concert: whereby dynamic microtubules mainly orient oblique to the cell plate and nucleate via γ-tubulin on stable microtubules that are oriented mainly perpendicular to the cell plate. Thus, treadmilling of the dynamic microtubule population will drive the expansion of phragmoplasts (Murata *et* al., 2013). Furthermore, phragmoplast microtubules interact with kinesin motors. For instance, mutations of class-IV kinesins in the moss *Physcomitrella patens* results in extended overlaps of MT plus-ends in the midplane of the phragmoplast followed by oblique orientation of cell plate (de Keijzer *et* al., 2017). Also, class-XII kinesins (Lee *et* al., 2007), and several class-XIV kinesins (Buschmann et al., 2015; Klotz and Nick, 2012) seem to participate in the organisation of the phragmoplast. Since parthenolide, a drug that blocks the detyrosination function, promotes binding of the class-XIV kinesin KCH to microtubules (Schneider *et* al., 2015), the observed perturbations of phragmoplast organisation in the OsTTL overexpressor might be linked with a perturbed recruitment of specific kinesin motors to the phragmoplast. This would mean that tubulin tyrosination might define functional subpopulations of microtubules.

4.4 Role of OsTTL in cold perception

Since TTL prefers to modify cytoplasmic α- and β- tubulin heterodimers (Burns, 1987) whereas TTC prefers to modify α- and β- tubulin heterodimers that already assembled into microtubule (Gundersen *et* al., 1987), it creates a situation that a stable microtubule has priority to be detyrosinated whereas a dynamic microtubule would have more chance to escape from TTC activity. In

addition, the stability of cortical microtubules is well described in relation to early cold sensing: On the one hand, microtubules act as susceptor, which needs a population of stable microtubules to sustain efficient cold sensing to transfer the information from decreased membrane fluidity to cellular chemical signalling. On the other hand, dynamic microtubules are needed to integrate vesicles with signalling compounds to membrane lipids to readjust the highly dynamic plasma membrane (Guo *et* al., 2018; Nick, 2013; Wang *et* al., 2020). In addition, the stability of microtubules is correlated with the proportion of tyrosinated and detyrosinated α-tubulin (Wiesler *et* al., 2002), which is catalysed by TTL or TTC, respectively, indicating a role of tubulin detyrosination and tyrosination in modifying the sensing functions of cortical microtubules. In maize, cold-induced rapid and transient disassembly of microtubules is initialized with higher population of tyrosinated α-tubulin in cold-resistant species (Abdrakhamanova *et* al., 2003). Moreover, parthenolide, a TTC inhibitior that decreases tubulin detyrosination contents, would trigger an increase in calcium influx (Schneider et al., 2015), a important second messager under various stresses.

In the present work, overexpression of OsTTL results in more rapid disassembly of cortical microtubules (Fig. 3. 15). This leads to a pronounced increase in apoplastic alkalinisation indicative of an activation of calcium channels (Fig. 3. 16), which is observed in several cases where cold can induce rapid disassembly of cortical microtubules, which modulates opening of calcium channels (Abdrakhamanova *et* al., 2003; Thion *et* al., 1996; Wang and Nick, 2017; Wang *et* al., 2019). Both these activities are pronounced due to overexpression of OsTTL, leading to the possible interpretation that OsTTL renders cortical microtubules more dynamic by increasing the level of its direct product tyrosinated α-tubulin. During long-term cold chilling, overexpression of OsTTL might not sufficiently from a population of stable microtubules to sustain

efficient cold signalling amplification, which might be the reason why overexpression of OsTTL leads to reduced cold acclimation (Fig. 3.14). However, it can not be concluded which population of microtubules predominant in the corresponding position since the Western blot analysis reveals that overexpression of OsTTL increases both tyrosinated and detyrosinated α-tubulin (Fig. 3. 21). However, these results indicate overexpression of OsTTL could modify functions of cold perception of microtubules. Further experiments should analyse the relative contents of changes in population of tyrosinated and detyrosinated α-tubulin under prolonged cold chilling to understand how OsTTL modifies microtubules under prolonged cold.

Microtubules also act as a target of phospholipid D (PLD) in the early perception process (Wang and Nick, 2017). PLD, a 90-kDa protein isolated from tobacco membranes, is identified as the linker between plasma membrane and microtubules (Gardiner *et* al., 2001). By association with membrane and microtubules, PLD acts as a signalling hub involved in signal transduction, stress responses and membrane metabolism (Abreu *et* al., 2018; Angelini *et* al., 2018; Guo *et* al., 2018; Nick, 2013). PLD is an enzyme that can catalyze hydrolysis of structural phospholipids to phosphatidic acid (PA). It is commonly accepted that PA confers the signal of PLD activation that further activates NADPH oxidase respiratory burst oxidase homologue (RboH) to trigger ROS accumulations. PA derived from PLDα1 can stabilise microtubules by binding to a microtubule associate protein MAP65-1 in responses to salt stress (Nick, 2013; Wang and Nick, 2017; Zhang *et* al., 2012). However, recently microtubules have been determined as downstream target of PLD activation which is parallel with PA-dependent signalling (Wang and Nick, 2017), as observed by the effects of different alcohols: n-butanol not only activates PLD but also acts as a trans-phosphatidylation substrate such that

the PA-dependent signalling will be blocked, while sec-butanol only activates PLD but not acts as a substrate such that the PA-dependent signalling can occur. As a control, tert-butanol neither activates PLD nor acts as a substrate (Dhonukshe *et* al., 2003; Munnik *et* al., 1995; Wang and Nick, 2017). 1% n-butanol can induce disassembly of microtubules whereas sec- and tert-butanol have no effects on microtubules, indicating that microtubules are a downstream target of PLD activation (Wang and Nick, 2017), which is actually observed in my work where cortical microtubules gradually disassemble to small fragments in the TUA3-GFP BY-2 cell line (Fig. 3.17). Moreover, the same concentration of n-butanol causes less disassembly of cortical microtubule in the double overexpressor OsTTL-RFP and TUA3-GFP BY-2 cell line (Fig. 3.17), further suggesting PLD is mainly associated with stable microtubule that are modified by OsTTL. However, how PLD associates with microtubules is still unknown. Since detyrosinated α-tubulin enriches in stable microtubules, my observation linked the PLD to detyrosinated α-tubulin, which is consistent with previous work in our lab, where they have showed that a rice PLDα1 can be co-purified with fractions of detyrosinated α-tubulin by EPC affinity chromatography, indicating OsPLDα1 is probably linked to detyrosinated α-tubulin (Krtková *et* al., 2012).

Indeed, plant PLDs form a large family and among the super-family of PLDs, PLDα1 is the predominated isoform that conveys the common functions of PLD (Zhang *et* al., 2017). In present work, OsPLDα1 is found to localise with different arrays of microtubules, including spindle microtubules and phragmoplast microtubule as observed in BY-2 cells ovexpressing OsPLDα1-GFP (Fig. 3.19 A), as well as preferentially with cortical microtubules in the elongating epidermis cells in roots of rice overexpressing OsPLDα1-GFP (Fig. 3.19 B). Western blot analysis shows that overexpression of OsPLDα1 could also lead to increase in detyrosinated α-tubulin abundance, indicating

that there exists a functional interaction of OsPLDα1 and detyrosinated α-tubulin (Fig. 3.20). These results not only support that microtubules act as the downstream of PLD activation that is independent of PA signalling (Wang and Nick, 2017), but also extend the knowledge that OsPLDα1 might associate with specific microtubules, which are detyrosinated. However, whether they are physically interacted is still unknown. To further test this possibility, recombinant expression of OsPLDα1 should be conducted and later the purified OsPLDα1 can be used to further *in vitro* studies.

4.5 A role of posttranslational modification on autoregulation of tubulin synthesis

Apart from those, another interesting result is observed when overexpressing OsTTL-RFP into a microtubule marker line NtTUA3-GFP BY-2 cell line, a protein band with 80 kDa size is developed by both ATT and DM1A antibodies during Western blot (Fig. 3.21). This 80 kDa protein later turns out to be GFP fused α-tubulin as manifested by anti-GFP antibody and the specificity of anti-GFP antibody is also confirmed by the lowest band with 28 kDa of GFP. Therefore, overexpression of OsTTL increases not only tyrosinated NtTUA3 but also detyrosinated NtTUA3 fused with GFP, without changing the content of endogenous α-tubulin, indicating that overexpression of OsTTL leads to increase in GFP fused NtTUA3 content.

The simplest way to provide the accumulation of GFP fused NtTUA3 proteins would be that they are originated from the simultaneously transcriptional expression of GFP-NtTUA3 gene. This idea is confirmed in present work, where the transcriptional level of GFP-NtTUA3 is highly elevated in overexpression of OsTTL-RFP in NtTUA3-GFP BY-2 cell line than in NtTUA3-GFP BY-2 cell line. However, the expression of NtTUA3 fused with GFP is driven by 35S constitutively such that the expression level should be at

the same transcriptional level. Why mRNA level of OsTTL is also induced and how could this observation happen?

A likely explanation of high abundance of NtTUA3-GFP due to overexpression of OsTTL would be an autoregulation mechanism between tubulin stability and tubulin expression, which might involve in the functions of tubulin posttranslational modification (Breviario and Nick, 2000). In mammalian cells, increase of unassembled tubulin dimers by colchicine or microinjection of pure tubulin can suppress the tubulin synthesis rates while decrease of unassembled tubulin dimers by taxol could stimulate the rate of new tubulin synthesis (Cleveland, 1988; Cleveland *et* al., 1983). The original model proposes that unpolymerised tubulin dimers bind directly to the nascent amino terminal MREI motif (Met-Arg-Glu-lle) to regulate the degradation of β-tubulin mRNAs (Cleveland, 1988). However, how to regulate the corresponding tubulin degradation is unknown at that time. How to control the balance of α-tubulin and β-tubulin since microtubules are assembled with α- and β-tubulin heterodimers? Indeed, apart from post-transcriptional regulation of β-tubulin mRNAs, α-tubulin can act as a repressor of its own translation that would trap α-tubulin mRNA in the untranslated form, which would lead to degradation of α-tubulin protein until the level of α- tubulin is balanced with β-tubulin (Gonzalez-Garay and Cabral, 1996). These evidences indicate the presence of an autoregulatory mechanism between tubulin synthesis and the stability of ribosome-bound tubulin mRNAs.

However, a different regulation of tubulin synthesis is observed in *T. thermophila* where colchicine and oryzalin cause an increase in α-tubulin synthesis accompanied with an increase in tubulin mRNA accumulation (Stargell *et* al. 1992), which indicates a possibility that the autoregulation mechanism is self regulated. One possible explanation proposed by author

would be that the rapidly degradation of depolymerised tubulin caused by colchicine and oryzalin would results in a substantial decrease in the amount of the monomer pool, which would in turn lead to an increase in the synthesis of tubulin mRNA and protein (Stargell *et* al. 1992).

In plant, the situation is again different. In rice, oryzalin treatment leads to a decrease in tubulin protein without changing the level of tubulin mRNA while abscisic acid treatment has no effects on tubulin protein but shows a strong reduction of tubulin mRNA (Gianì *et* al., 1998). Since oryzalin is a microtubule-depolymerisation agent that would cause an increase of unpolymerized tubulin heterodimers while abscisic acid induces a reorientation of microtubules without affecting their integrity, the possible explanation would be the autoregulation of tubulin synthesis and tubulin mRNA depends on the assembly state of MTs (Gianì *et* al., 1998). In present work, it is observed with an increase in NtTUA3-GFP protein and NtTUA3-GFP transcripts due to overexpression of OsTTL (Fig. 3. 21 and Fig. 3. 22 B). More interesting is transcriptional level of OsTTL in overexpression of OsTTL-RFP in NtTUA3-GFP BY-2 cell line than in BY-2 cells only overexpressing OsTTL-RFP (Fig. 3. 22 A). The possible explanation would be that overexpression of OsTTL modifying NtTUA3-GFP protein leads to a decrease in monomer pool, which would intensify the accumulation of NtTUA3-GFP mRNA as well as proteins to compensate it. In turn, the accumulation of NtTUA3-GFP proteins would lead to transcriptional accumulation of OsTTL as well as translation that ensure the process of tubulin posttranslational modification going on.

Taken together, these observations propose a model here (Fig. 4.1): (1) posttranslational modification of α-tubulin firstly leads to reduced tubulin dimers, which would premote an increase in transcriptional expression of

tubulin gene that sustains sufficient tubulin synthesis to compensate; (2) the accumulation of new synthesis tubulin accelerates the process of posttranslation modification of α-tubulin by feeding back on transcriptional expression of the correspondence enzymes to sustain efficient posttranslational modification.

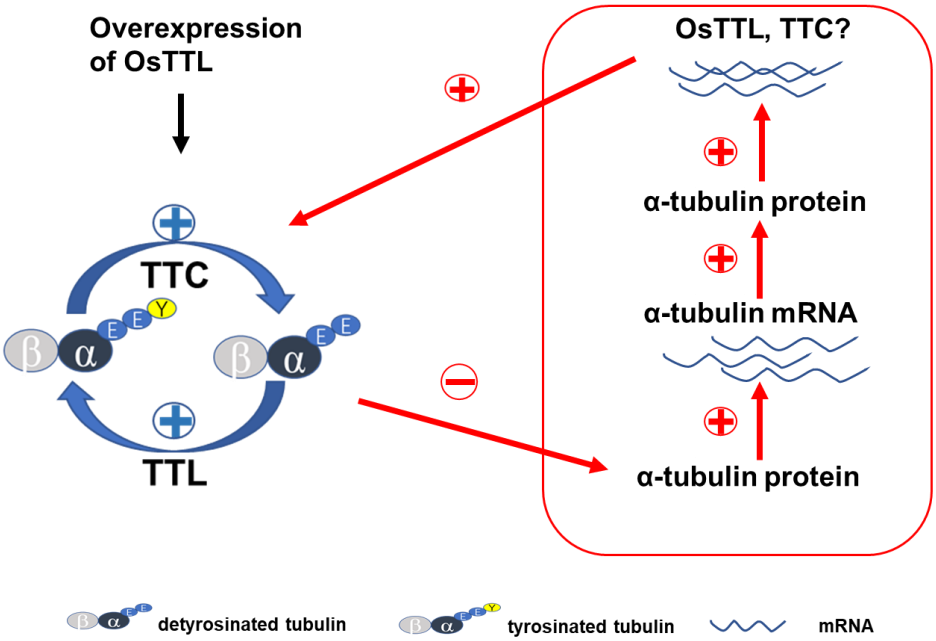

Fig. 4.1. Proposed functions of OsTTL in autoregulation of tubulin synthesis. Overexpression of OsTTL-RFP in a microtubule marker line expressing NtTUA3-GFP BY-2 cell line results in both tyrosinated and detyrosinated tubulin abundance, indicating a total content of tubulin protein is elevated, which would result in decrease in the pool of monomer dimer. The decreased tubulin dimer would accelerate translation from tubulin gene leading to an increase in NtTUA3-GFP transcripts that further promotes new synthesis of tubulin; in turn, the new tubulin synthesis would accelerate the process of posttranslational modification of α-tubulin, thus leading to increase in transcriptional accumulation of OsTTL as well as the still mysterious TTC to sustain efficiency of posttranslational modification of α-tubulin.

However, whether the modified tubulin or the unassembled tubulin dimers would act as the initial signal of this circuit is still unknown. To test it, further

experiments would be to measure transcripts of NtTUA3-GFP a few hours later either by giving taxol that reduces dimers, or by giving oryzalin that induces tubulin dimers.

4.6 Is rice TTL a rice TTC?

While TTL could be purified and cloned from porcine brain, the TTC had remained enigmatic over 30 years (Ersfeld *et* al., 1993). Only very recently, the vasohibins (VASHs) and their regulators, the Small Vasohibin Binding Proteins (SVBPs) were identified as the long-time elusive TCPs (Aillaud *et* al., 2017; Nieuwenhuis *et* al., 2017). However, to the best of my knowledge, plant homologues of these animal TCPs could not be found, which means that plant TTC remains to be found, in contrast to TTL that deviates by their N-terminal extension, but otherwise are present in plants.

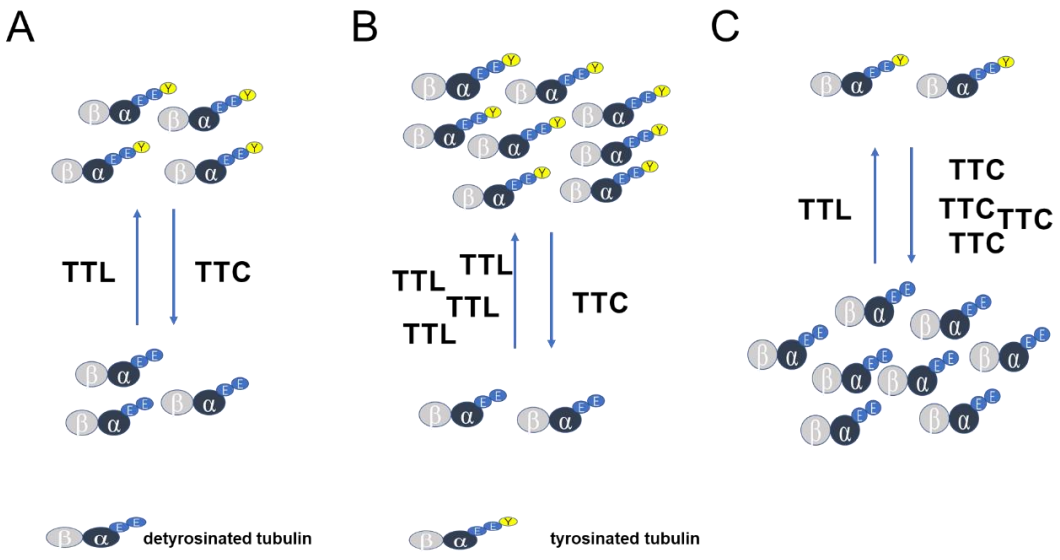

Fig. 4.2 Schematic model for proper functions of TTL and TTC in theory. A. Under normal condition, tyrosinated and detyrosinated α-tubulin coexist in plant cells but with slightly higher amount of tyrosinated α-tubulin; B. When TTL is overexpressed, tyrosinated α-tubulin will be increased while the antagonistic TTC is somehow blocked leading to decrease in detyrosinated α-tubulin; C. If TTC exists, overexpression of TTC would lead to

the distribution of detyrsoianted/tyrosinated α-tubulin to detyrosinated α-tubulin.

As shown in Fig. 4.2, the direct product of a TTL should be tyrosinated α-tubulin, while the antagonistic TTC is defined as enzymatic activity that yields detyrosinated α-tubulin. In theory, overexpression of TTL would shift the distribution of detyrosinated/tyrosinated α-tubulin to tyrosinated α-tubulin form whereas detyrosinated α-tubulin would be predominated when overexpression of TTC, if TTC exists in plant. TTL has been reported to preferentially bind to tubulin dimer (Kumar and Flavin, 1981) whereas TTC prefer assembled microtubule (Gundersen *et* al., 1987). These binding characteristics lead to the implication that the products of these two enzymes accumulate differently depending on the dynamics of microtubules. Stable microtubules should be enriched in detyrosinated α-tubulin, whereas dynamic MTs harbour more tyrosinated α-tubulin.

However, in the present work, overexpression of OsTTL-RFP in rice and BY-2 cells unexpectedly shifts α-tubulin into detyrosinated form. The higher abundance of detyrosinated α-tubulin is accompanied with a higher stability against oryzalin treatment, indicative of reduced turnover of microtubules. While the link between higher detyrosination levels and higher microtubule stability would be expected from the differential binding of TTL and TTC to dynamic versus static microtubule populations, the outcome that overexpression of OsTTL correlates with increased detyrosination, is unexpected. These results are not consistent with the retyrosinate function of overexpressing OsTTL as a ligase but in the contrary, more compitable with detyrosinate function of overexpressing a TTC. The most straightforward interpretation would be that OsTTL is not TTL but TTC (Fig. 4.3 ①). If this holds true that OsTTL is a TTC, aforementioned results seem reasonable.

However, when overexpressing OsTTL in a microtubule marker line expressing NtTUA3-GFP BY-2 cell line, the situation is different that both detyrosinated and tyrosinated α-tubulin are increased. In addition, increased detyrosinated and tyrosinated α-tubulin seem to have different effects on microtubules: in one hand, OsTTL modified microtubules form cold-sensitive arrays while OsTTL modified microtubules could also form stable arrays that tightly associates with PLD, which are less affected by 1% n-butanol treatment. In this context, together with the hypothesis that OsTTL acts as TTC, the possible explanation would be that the increased content of tyrosinated α-tubulin is achieved by the mutual regulation between tubulin posttranslational modification and tubulin synthesis as discussed in part **4.5** (Fig. 4.1), where α-tubulin detyrosination probably acts as initial signal to trigger transcriptional accumulation of α-tubulin that enables efficiency translation of tubulin protein, finally the new synthesis α-tubulin promotes the process of tubulin posttranslational modification as well as its key enzymes to sustain the efficiency, which finally would increase α-tubulin tyrosination as well. The proposed interpretation is shown in the model (Fig. 4.3).

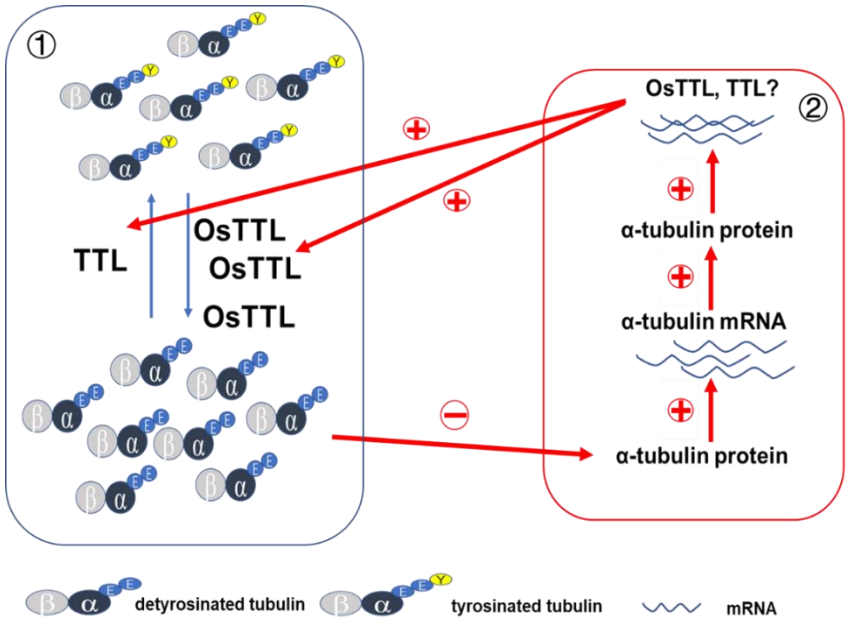

Fig. 4.3 Schematic model for the proposed OsTTL as TTC and the mechanism for

regulation of tyrosinated α-tubulin. ① OsTTL acts as TTC. If OsTTL is TTC, TTC level will be higher due to overexpression of OsTTL, the direct output of TTC: detyrosinated α-tubulin is highly elvated. ② Proposed mechnism for regelation of tyrosinated α-tubulin content as shown already in Fig. 4.1. Here, the elvated detyrosinated α-tubulin probably acts as initial signal to trigger this process.

However, one has to keep in mind that there also exists a possibility that OsTTL might not only retyrosinate α-tubulin but also detyrosinate α-tubulin just depending on the initial stability of microtubules. Because the microtubules in overexpressing NtTUA3-GFP BY-2 cells are initially with higher stability than in the nontransformed WT rice and BY-2 cells, when overexpressed OsTTL in this line, the OsTTL only has the chance to retyrosinate α-tubulin whereas when overexpressed OsTTL in rice and BY-2 cells that microtubules are more dynamic, OsTTL would detyrosinate α-tubulin firstly.

In this context, the leucine-rich-repeat domain (Appendix Fig. S1) characteristic for plant TTLs might become interesting, because it implies that OsTTL can form complexes with other proteins. It is conceivable that the direction of the enzymatic reaction (ligation of a tyrosine versus cleavage of a tyrosine) might be modulated by such interactions. To get biochemical access to the enzymatic activity conferred by TTL and potential binding partners, several attempts have been tried through recombinant expression of OsTTL in different strains of *E. coli* under various temperature by induction with different concentrations of IPTG. Unfortunately, recombinant OsTTL was mainly expressed in inclusion body such that purification of OsTTL failed (Fig. S4). In future, recombinant expression of OsTTL in insect and yeast cells should be conducted to try to get high amounts of protein such that *in vitro* studies could be launched.

4.7 Conclusion

The detyrosination/retyrosination cycle, one of the most common posttranslational modifications of α-tubulin, is conserved also in plants. Removal of the conserved C-terminal tyrosine of α-tubulin by a still elusive tubulin tyrosine caboxypeptidase (TTC), and religation of this tyrosine by a tubulin tyrosine ligase (TTL) are probably shared between all eukaryotes. To obtain the functions of tubulin detyrosination in plant, the only strategy is through genetic manipulation of TTL since TTC has remained elusive. Therefore, a rice TTL homoluohue was cloned and overexpressed to reveal some functions of elusive tubulin detyrosination.

By analysing an overexpression of OsTTL-RFP rice line and BY-2 cell line, unexpectedly, overexpression of this OsTTL-RFP shifts α-tubulin to detyrosinated form in both coleoptile and seminal root, correlated with more stable microtubules, independently of the respective orientation of cortical microtubule, followed by correspondingly changing growth of coleoptiles and seminal roots. These phenotypes are accompanied by perturbed organisation of phragmoplast microtubules and disoriented cell walls (Fig. 4.4 ①). These outcomes due to overexpression of OsTTL points towards the likely that OsTTL is not a ligase but the so far unknow plant TTC.

Overexpression of OsTTL-RFP in a microtubule marker lline NtTUA3-GFP BY-2 cells allows to dissect the functional interaction of OsTTL and microtubules in responses to cold *in vivo*. It shows that OsTTL renders cortical microtubule more sensitive to cold, correlated with a pronounced cold induced calcium influx as well as a reduced cold acclimation. 1 % n-butanol, a PLD activator, is not sufficient to trigger reorganization of cortical microtubules that modified by OsTTL. By further analysis of a rice OsPLDα1, a common PLD family protein, it can be found out that OsPLDα1 preferentially binds to

microtubules that might act as a possible interaction partner of detyrosinated α-tubulin (Fig. 4.4 ②).

Overexpression of OsTTL-RFP increased not only abundance of NtTUA3-GFP protein but also the transcriptional expression of NtTUA3-GFP gene as well as the transcripts of itself OsTTL. Based on that, it can be proposed with a likely mechanism for mutual regulation between posttranslational modification of α-tubulin and tubulin synthesis (Fig. 4.4 ③).

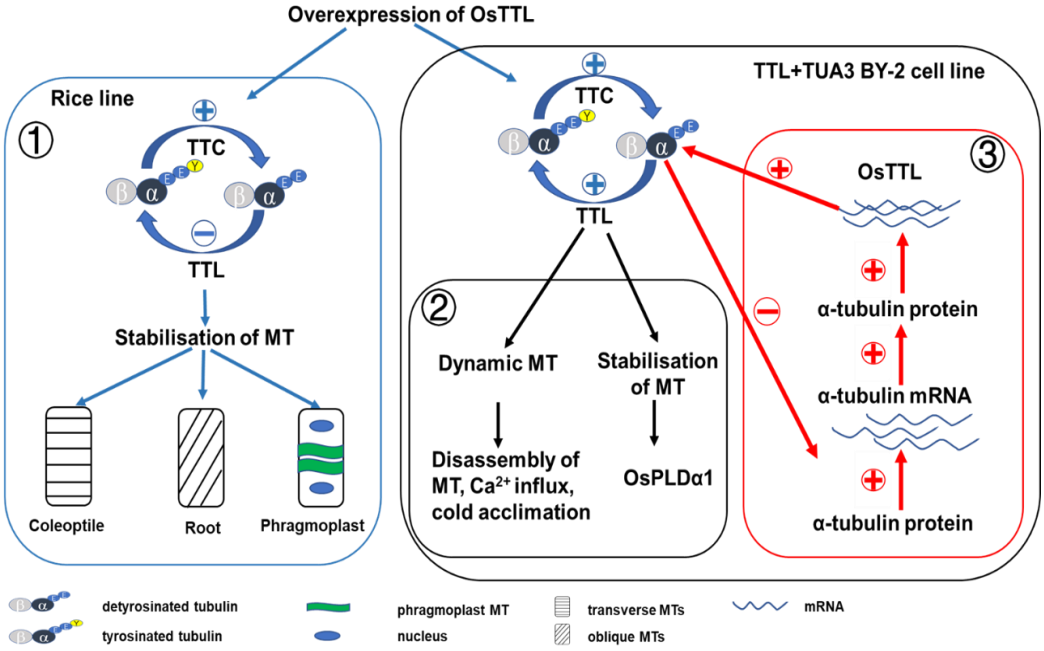

Fig. 4.4. Model of functions of OsTTL.

① Functions of OsTTL in rice growth and development. Overexpression of OsTTL-RFP in rice results in predominant detyrosinated tubulin content, leading to more stable MT that correlates with alteration of MT orientation and disorganisation of phragmoplast MT, futher affects rice growth and development;

② Functions of OsTTL in cold perception. Overexpression of OsTTL-RFP in a microtubule marker line expressing NtTUA3-GFP BY-2 cell line results in both tyrosinated and detyrosinated tubulin. However, under cold stress, OsTTL modified microtubules are more sensitive leading to rapid disassembly. This is accompanied with a pronounced

calcium influx as well as reduced cold acclimation. In addition, OsTTL modified microtubules are functional asscociated with phospholipis D (D), especially a rice PLDα1 functional interacts with detyrosinated tubulin.

③ Functions of OsTTL in autoregulation of tubulin synthesis. Overexpression of OsTTL-RFP in a microtubule marker line expressing NtTUA3-GFP BY-2 cell line results in increase in both tyrosinated and detyrosinated tubulin abundance, indicating a total content of tubulin protein is elevated, while the pool of monomer dimer is decreased. The decreased tubulin dimer would accelerate translation from tubulin gene leading to an increase in α-tubulin transcripts to sustain efficiency translation of α-tubulin to compensate; in turn, the new tubulin synthesis would have feedback on the process of posttranslational modification of α-tubulin by OsTTL, leading to increase in transcriptional accumulation of OsTTL that would promote efficiency of posttranslational modification.

References

Abdrakhamanova A, Wang QY, Khokhlova L, Nick P. 2003. Is microtubule disassembly a trigger for cold acclimation? *Plant Cell and Physiology*. **44**, 676-686.

Abreu FRM, Dedicova B, Vianello RP, Lanna AC, de Oliveira JAV, Vieira AF, Morais OP, Mendonça JA, Brondani C. 2018. Overexpression of a phospholipase (OsPLDα1) for drought tolerance in upland rice (*Oryza sativa* L.). *Protoplasma* **255**, 1751-1761.

Aillaud C, Bosc C, Peris L, Bosson A, Heemeryck P, Van Dijk J, Le Friec J, Boulan B, Vossier F, Sanman LE. 2017. Vasohibins/SVBP are tubulin carboxypeptidases (TCPs) that regulate neuron differentiation. *Science* **358**, 1448-1453.

Akella JS, Wloga D, Kim J, Starostina NG, Lyons-Abbott S, Morrissette NS, Dougan ST, Kipreos ET, Gaertig J. 2010. MEC-17 is an α-tubulin acetyltransferase. *Nature* **467**, 218-222.

Akhmanova A, Maiato H. 2017. Closing the tubulin detyrosination cycle. *Science* **358**, 1381-1382.

Angelini J, Vosolsobe S, Skupa P, Ho AYY, Bellinvia E, Valentova O, Marc J. 2018. Phospholipase Ddelta assists to cortical microtubule recovery after salt stress. *Protoplasma* **255**, 1195-1204.

Barisic M, e Sousa RS, Tripathy SK, Magiera MM, Zaytsev AV, Pereira AL, Janke C, Grishchuk EL, Maiato H. 2015. Microtubule detyrosination guides chromosomes during mitosis. *Science* **348**, 799-803.

Barra H, Rodriguez J, Arce C, Caputto R. 1973. A soluble preparation from rat brain that incorporates into its own proteins [^{14}C] arginine by a ribonuclease‐sensitive system and [^{14}C] tyrosine by a ribonuclease‐insensitive system. *Journal of neurochemistry* **20,** 97-108.

Bensadoun A, Weinstein D. 1976. Assay of proteins in the presence of interfering materials. *Analytical Biochemistry* **70**, 241-250.

Berghöfer T, Eing C, Flickinger B, Hohenberger P, Wegner LH, Frey W, Nick P. 2009. Nanosecond electric pulses trigger actin responses in plant cells. *Biochemical and biophysical research communications* **387**, 590-595.

Brants J, Semenchenko K, Wasylyk C, Robert A, Carles A, Zambrano A, Pradeau-Aubreton K, Birck C, Schalken JA, Poch O. 2012. Tubulin tyrosine ligase like 12, a TTLL family member with SET-and TTL-like domains and roles in histone and tubulin modifications and mitosis. *PloS One* **7**, e51258.

Buschmann H, Dols J, Kopischke S, Peña EJ, Andrade-Navarro MA, Heinlein M, Szymanski DB, Zachgo S, Doonan JH, Lloyd CW. 2015. Arabidopsis KCBP interacts with AIR9 but stays in the cortical division zone throughout mitosis via its MyTH4-FERM domain. *Journal of Cell Science* **128**, 2033-2046.

Cai G. 2010. Assembly and disassembly of plant microtubules: tubulin modifications and binding to MAPs. *Journal of experimental botany* **61**, 623-626.

Cautrecasas P. 1970. Protein purification by affinity chromatography. *The Journal of Biological Chemistry* **245**, 3059.

Chan J, Calder GM, Doonan JH, Lloyd CW. 2003. EB1 reveals mobile microtubule nucleation sites in Arabidopsis. *Nature Cell Biology* **5**, 967-971.

Creppe C, Malinouskaya L, Volvert M-L, Gillard M, Close P, Malaise O, Laguesse S, Cornez I, Rahmouni S, Ormenese S. 2009. Elongator controls the migration and differentiation of cortical neurons through acetylation of α-tubulin. *Cell* **136**, 551-564.

Cuatrecasas P. 1970. Protein purification by affinity chromatography. *The Journal of Biological Chemistry* **245**, 3059.

de Keijzer J, Kieft H, Ketelaar T, Goshima G, Janson ME. 2017. Shortening of microtubule overlap regions defines membrane delivery sites during plant cytokinesis. *Current Biology* **27**, 514-520.

Dhonukshe P, Laxalt AM, Goedhart J, Gadella TWJ, Munnik T. 2003.

Phospholipase D Activation Correlates with Microtubule Reorganization in Living Plant Cells. *The Plant Cell* **15**, 2666-2679.

Dhonukshe P, Mathur J, Hülskamp M, Gadella TW. 2005. Microtubule plus-ends reveal essential links between intracellular polarization and localized modulation of endocytosis during division-plane establishment in plant cells. *BMC Biology* **3**, 11.

Durst S. 2009. Funktionelle Analyse einer mutmaßlichen Tubulinyl-Tyrosin-Ligase aus Reis. Diploma thesis.

Erck C, Peris L, Andrieux A, Meissirel C, Gruber AD, Vernet M, Schweitzer A, Saoudi Y, Pointu H, Bosc C. 2005. A vital role of tubulin-tyrosine-ligase for neuronal organization. *Proceedings of the National Academy of Sciences* **102**, 7853-7858.

Ersfeld K, Wehland J, Plessmann U, Dodemont H, Gerke V, Weber K. 1993. Characterization of the tubulin-tyrosine ligase. *The Journal of Cell biology* **120**, 725-732.

Frey N, Klotz J, Nick P. 2010. A kinesin with calponin-homology domain is involved in premitotic nuclear migration. *Journal of Experimental Botany* **61**, 3423-3437.

Gao N, Wadhwani P, Mühlhäuser P, Liu Q, Riemann M, Ulrich AS, Nick P. 2016. An antifungal protein from Ginkgo biloba binds actin and can trigger cell death. *Protoplasma* **253**, 1159-1174.

Gardiner J. 2013. The evolution and diversification of plant microtubule‐associated proteins. *The Plant Journal* **75**, 219-229.

Gardiner J. 2019. Posttranslational modification of plant microtubules. *Plant Signaling and Behavior* **14**, e1654818.

Gardiner J, Barton D, Marc J, Overall R. 2007. Potential role of tubulin acetylation and microtubule‐based protein trafficking in familial dysautonomia. *Traffic* **8**, 1145-1149.

Gardiner JC, Harper JD, Weerakoon ND, Collings DA, Ritchie S, Gilroy S,

Cyr RJ, Marc J. 2001. A 90-kD phospholipase D from tobacco binds to microtubules and the plasma membrane. *The Plant Cell* **13**, 2143-2158.

Gianì S, Qin X, Faoro F, Breviario D. 1998. In rice, oryzalin and abscisic acid differentially affect tubulin mRNA and protein levels. *Planta* **205**, 334-341.

Gilmer S, Clay P, MacRae TH, Fowke L. 1999. Acetylated tubulin is found in all microtubule arrays of two species of pine. *Protoplasma* **207**, 174-185.

Gong P, Riemann M, Dong D, Stoeffler N, Gross B, Markel A, Nick P. 2019. Two grapevine metacaspase genes mediate ETI-like cell death in grapevine defence against infection of Plasmopara viticola. *Protoplasma* **256**, 951-969.

Green PB. 1962. Mechanism for plant cellular morphogenesis. *Science* **138**, 1404-1405.

Gundersen GG, Khawaja S, Bulinski JC. 1987. Postpolymerization detyrosination of alpha-tubulin: a mechanism for subcellular differentiation of microtubules. *Journal of Cell Biology* **105**, 251-264.

Gunning B, Wick S. 1985. Preprophase bands, phragmoplasts, and spatial control of cytokinesis. *Journal of Cell Science* **1985**, 157-179.

Guo X, Liu D, Chong K. 2018. Cold signaling in plants: Insights into mechanisms and regulation. *Journal of Integrative Plant Biology* 60, 745-756.

Hashimoto T. 2003. Dynamics and regulation of plant interphase microtubules: a comparative view. *Current opinion in plant biology* **6**, 568-576.

Hashimoto T. 2015. Microtubules in plants. The Arabidopsis Book/American Society of Plant Biologists **13**.

Hiei Y, Ohta S, Komari T, Kumashiro T. 1994. Efficient transformation of rice (Oryza sativa L.) mediated by Agrobacterium and sequence analysis of the boundaries of the T-DNA. *The Plant Journal* **6**, 271-282.

Hohenberger P, Eing C, Straessner R, Durst S, Frey W, Nick P. 2011. Plant actin controls membrane permeability. *Biochimica et Biophysica Acta (BBA)-Biomembranes* **1808**, 2304-2312.

Hubbert C, Guardiola A, Shao R, Kawaguchi Y, Ito A, Nixon A, Yoshida M,

Wang X-F, Yao T-P. 2002. HDAC6 is a microtubule-associated deacetylase. *Nature* **417**, 455-458.

Hussey PJ, TRAAS JA, GULL K, LLOYD CW. 1987. Isolation of cytoskeletons from synchronized plant cells: the interphase microtubule array utilizes multiple tubulin isotypes. *Journal of Cell Science* **88**, 225-230.

Janke C, Magiera MM. 2020. The tubulin code and its role in controlling microtubule properties and functions. *Nature Reviews Molecular Cell Biology*, **1-20**.

Janke C, Rogowski K, Wloga D, Regnard C, Kajava AV, Strub J-M, Temurak N, van Dijk J, Boucher D, van Dorsselaer A. 2005. Tubulin polyglutamylase enzymes are members of the TTL domain protein family. *Science* **308**, 1758-1762.

Jovanovic AM, Durst S, Nick P. 2010. Plant cell division is specifically affected by nitrotyrosine. *Journal of Experimental Botany* **61**, 901-909.

Jovanovic AM. 2010. Functional nanlysis of a posttranslational modification of plant α-tubulin. PhD thesis.

Klotz J, Nick P. 2012. A novel actin–microtubule cross‐linking kinesin, NtKCH, functions in cell expansion and division. *New Phytologist* **193**, 576-589.

Kobe B, Kajava AV. 2001. The leucine-rich repeat as a protein recognition motif. *Current Opinion in Structural Biology* **11**, 725-732.

Krtková J, Benáková M, Schwarzerová K. 2016. Multifunctional microtubule-associated proteins in plants. *Frontiers in plant science* **7**, 474.

Krtková J, Zimmermann A, Schwarzerová K, Nick P. 2012. Hsp90 binds microtubules and is involved in the reorganization of the microtubular network in angiosperms. *Journal of Plant Physiology* **169**, 1329-1339.

Kumar N, Flavin M. 1981. Preferential action of a brain detyrosinolating carboxypeptidase on polymerized tubulin. *The Journal of Biological Chemistry* **256**, 7678-7686.

Lee Y-RJ, Li Y, Liu B. 2007. Two Arabidopsis phragmoplast-associated kinesins play a critical role in cytokinesis during male gametogenesis. *The Plant Cell* **19**, 2595-2605.

Little M, Seehaus T. 1988. Comparative analysis of tubulin sequences. Comparative Biochemistry and Physiology - Part B **90**, 655-670.

Liu Q, Qiao F, Ismail A, Chang X, Nick P. 2013. The plant cytoskeleton controls regulatory volume increase. *Biochimica et Biophysica Acta (BBA)-Biomembranes* **1828**, 2111-2120.

Lloyd CW. 1987. The plant cytoskeleton: the impact of fluorescence microscopy. *Annual Review of Plant Physiology* **38,** 119-137.

Magiera MM, Singh P, Janke C. 2018. SnapShot: functions of tubulin posttranslational modifications. *Cell* **173**, 1552-1552. e1551.

Marc J, Granger CL, Brincat J, Fisher DD, Kao T-h, McCubbin AG, Cyr RJ. 1998. A GFP–MAP4 reporter gene for visualizing cortical microtubule rearrangements in living epidermal cells. *The Plant Cell* **10**, 1927-1939.

Mizuno K, Koyama M, Shibaoka H. 1981. Isolation of plant tubulin from azuki bean epicotyls by ethyl N-phenylcarbamate-sepharose affinity chromatography. *The Journal of Biochemistry* **89**, 329-332.

Morejohn LC, Bureau TE, Molè-Bajer J, Bajer AS, Fosket DE. 1987. Oryzalin, a dinitroaniline herbicide, binds to plant tubulin and inhibits microtubule polymerization *in vitro*. *Planta* **172**, 252-264.

Munnik T, Arisz SA, De Vrije T, Musgrave A. 1995. G Protein Activation Stimulates Phospholipase D Signaling in Plants. *The Plant Cell* **7**, 2197-2210.

Murata T, Sano T, Sasabe M, Nonaka S, Higashiyama T, Hasezawa S, Machida Y, Hasebe M. 2013. Mechanism of microtubule array expansion in the cytokinetic phragmoplast. *Nature Communication* **4**, 1967.

Murata T, Wada M. 1991. Effects of centrifugation on preprophase-band formation in Adiantum protonemata. *Planta* **183**, 391-398.

Nick P, Lambert AM, Vantard M. 1995. A microtubule-associated protein in

maize is expressed during phytochrome-induced cell elongation. *The Plant Journal* **8**, 835-844.

Nick P. 2007. Control of cell axis. Plant microtubules: Springer, 3-46.

Nick P. 2012. Microtubules and the tax payer. *Protoplasma* **249**, 81-94.

Nick P. 2013. Microtubules, signalling and abiotic stress. *The Plant Journal* **75**, 309-323.

Nieuwenhuis J, Adamopoulos A, Bleijerveld OB, Mazouzi A, Stickel E, Celie P, Altelaar M, Knipscheer P, Perrakis A, Blomen VA. 2017. Vasohibins encode tubulin detyrosinating activity. *Science* **358**, 1453-1456.

North BJ, Marshall BL, Borra MT, Denu JM, Verdin E. 2003. The human Sir2 ortholog, SIRT2, is an NAD+-dependent tubulin deacetylase. *Molecular Cell* **11**, 437-444.

Ohkawa N, Sugisaki S, Tokunaga E, Fujitani K, Hayasaka T, Setou M, Inokuchi K. 2008. N‐acetyltransferase ARD1‐NAT1 regulates neuronal dendritic development. *Genes to Cells* **13**, 1171-1183.

Parrotta L, Cresti M, Cai G. 2014. Accumulation and post-translational modifications of plant tubulins. Plant Biology (Stuttgart, Germany) **16**, 521-527.

Peris L, Thery M, Fauré J, Saoudi Y, Lafanechère L, Chilton JK, Gordon-Weeks P, Galjart N, Bornens M, Wordeman L. 2006. Tubulin tyrosination is a major factor affecting the recruitment of CAP-Gly proteins at microtubule plus ends. *The Journal of cell biology* **174**, 839-849.

Peris L, Wagenbach M, Lafanechère L, Brocard J, Moore AT, Kozielski F, Job D, Wordeman L, Andrieux A. 2009. Motor-dependent microtubule disassembly driven by tubulin tyrosination. *Journal of Cell Biology* **185**, 1159-1166.

Prota AE, Magiera MM, Kuijpers M, Bargsten K, Frey D, Wieser M, Jaussi R, Hoogenraad CC, Kammerer RA, Janke C, Steinmetz MO. 2013. Structural basis of tubulin tyrosination by tubulin tyrosine ligase. *Journal of Cell Biology* **200**, 259-270.

Qin X, Gianì S, Breviario D. 1997. Molecular cloning of three rice α-tubulin isotypes: differential expression in tissues and during flower development1. *Biochimica et Biophysica Acta (BBA)-Gene Structure and Expression* **1354**, 19-23.

Reed NA, Cai D, Blasius TL, Jih GT, Meyhofer E, Gaertig J, Verhey KJ. 2006. Microtubule acetylation promotes kinesin-1 binding and transport. *Current Biology* **16**, 2166-2172.

Richardson DN, Simmons MP, Reddy AS. 2006. Comprehensive comparative analysis of kinesins in photosynthetic eukaryotes. *BMC Genomics* **7**, 18.

Schneider N. 2010. Tubulin Detyrosination in Plants. PhD thesis.

Schneider N, Ludwig H, Nick P. 2015. Suppression of tubulin detyrosination by parthenolide recruits the plant-specific kinesin KCH to cortical microtubules. *Journal of Experimental Botany* **66**, 2001-2011.

Schwarzerová K, Petrášek J, Panigrahi K, Zelenková S, Opatrný Z, Nick P. 2006. Intranuclear accumulation of plant tubulin in response to low temperature. *Protoplasma* **227**, 185-196.

Sharma N, Bryant J, Wloga D, Donaldson R, Davis RC, Jerka-Dziadosz M, Gaertig J. 2007. Katanin regulates dynamics of microtubules and biogenesis of motile cilia. *The Journal of cell biology* **178**, 1065-1079.

Smertenko A, Assaad F, Baluška F, Bezanilla M, Buschmann H, Drakakaki G, Hauser M-T, Janson M, Mineyuki Y, Moore I. 2017. Plant cytokinesis: terminology for structures and processes. *Trends in Cell Biology* **27**, 885-894.

Smirnova EA, Bajer AS. 1998. Early stages of spindle formation and independence of chromosome and microtubule cycles in Haemanthus endosperm. *Cell motility and the cytoskeleton* **40**, 22-37.

Song Y, Brady ST. 2015. Post-translational modifications of tubulin: pathways to functional diversity of microtubules. *Trends in Cell Biology* **25**, 125-136.

Stargell LA, Heruth DP, Gaertig J, Gorovsky MA. 1992. Drugs affecting

microtubule dynamics increase alpha-tubulin mRNA accumulation via transcription in Tetrahymena thermophila. *Molecular and Cellular Biology* **12**, 1443-1450.

Tamura K, Nakatani K, Mitsui H, Ohashi Y, Takahashi H. 1999. Characterization of katD, a kinesin-like protein gene specifically expressed in floral tissues of *Arabidopsis thaliana*. *Gene* **230**, 23-32.

Thion L, Mazars C, Thuleau P, Graziana A, Rossignol M, Moreau M, Ranjeva R. 1996. Activation of plasma membrane voltage-dependent calcium-permeable channels by disruption of microtubules in carrot cells. *FEBS Letters* **393**, 13-18.

Van Damme D, Van Poucke K, Boutant E, Ritzenthaler C, Inzé D, Geelen D. 2004. *In vivo* dynamics and differential microtubule-binding activities of MAP65 proteins. *Plant physiology* **136**, 3956-3967.

Waller F, Nick P. 1997. Response of actin microfilaments during phytochrome-controlled growth of maize seedlings. *Protoplasma* **200**, 154-162.

Wang L, Nick P. 2017. Cold sensing in grapevine—which signals are upstream of the microtubular “thermometer”. *Plant cell and environment* **40**, 2844-2857.

Wang L, Sadeghnezhad E, Nick P. 2020. Upstream of gene expression: what is the role of microtubules in cold signalling? *Journal of Experimental Botany* **71**, 36-48.

Wang L, Sadeghnezhad E, Riemann M, Nick P. 2019. Microtubule dynamics modulate sensing during cold acclimation in grapevine suspension cells. *Plant Science* **280**, 18-30.

Wang W, Vignani R, Scali M, Sensi E, Cresti M. 2004. Post-translational modifications of alpha-tubulin in Zea mays L are highly tissue specific. *Planta* **218**, 460-465.

Wasylyk C, Zambrano A, Zhao C, Brants J, Abecassis J, Schalken JA,

Rogatsch H, Schaefer G, Pycha A, Klocker H. 2010. Tubulin tyrosine ligase like 12 links to prostate cancer through tubulin posttranslational modification and chromosome ploidy. *International Journal of Cancer* **127**, 2542-2553.

Watts DI, Monteiro MJ, Cox RA. 1988. Identification of EcoRV fragments spanning the Nα-tubulin gene of Physarum. *FEBS Lett* **241**, 229-233.

Weisenberg RC, Broisy GG, Taylor EW. 1968. Colchicine-binding protein of mammalian brain and its relation to microtubules. *Biochemistry* 7, 4466-4479.

Wiesler B, Wang QY, Nick P. 2002. The stability of cortical microtubules depends on their orientation. *The Plant Journal* **32**, 1023-1032.

Xiong X, Xu D, Yang Z, Huang H, Cui X. 2013. A Single Amino‐Acid Substitution at Lysine 40 of an Arabidopsis thalianaα‐tubulin Causes Extensive Cell Proliferation and Expansion Defects. *Journal of Integrative Plant Biology* **55**, 209-220.

Yoshikawa M, Yang G, Kawaguchi K, Komatsu S. 2003. Expression analyses of β-tubulin isotype genes in rice. *Plant and cell physiology* **44**, 1202-1207.

Zekert N, Fischer R. 2009. The Aspergillus nidulans kinesin-3 UncA motor moves vesicles along a subpopulation of microtubules. *Molecular Biology of the Cell* **20**, 673-684.

Zhang D, Wadsworth P, Hepler PK. 1990. Microtubule dynamics in living dividing plant cells: confocal imaging of microinjected fluorescent brain tubulin. *Proceedings of the National Academy of Sciences* **87**, 8820-8824.

Zhang Q, Lin F, Mao T, Nie J, Yan M, Yuan M, Zhang W. 2012. Phosphatidic Acid Regulates Microtubule Organization by Interacting with MAP65-1 in Response to Salt Stress in Arabidopsis. *The Plant Cell* **24**, 4555-4576.

Zhang Q, Qu Y, Wang Q, Song P, Wang P, Jia Q, Guo J. 2017. Arabidopsis phospholipase D alpha 1-derived phosphatidic acid regulates microtubule organization and cell development under microtubule-interacting drugs treatment. *Journal of Plant Research* **130**, 193-202.

Zhu C, Dixit R. 2012. Functions of the Arabidopsis kinesin superfamily of microtubule-based motor proteins. *Protoplasma* **249**, 887-899.

Appendix

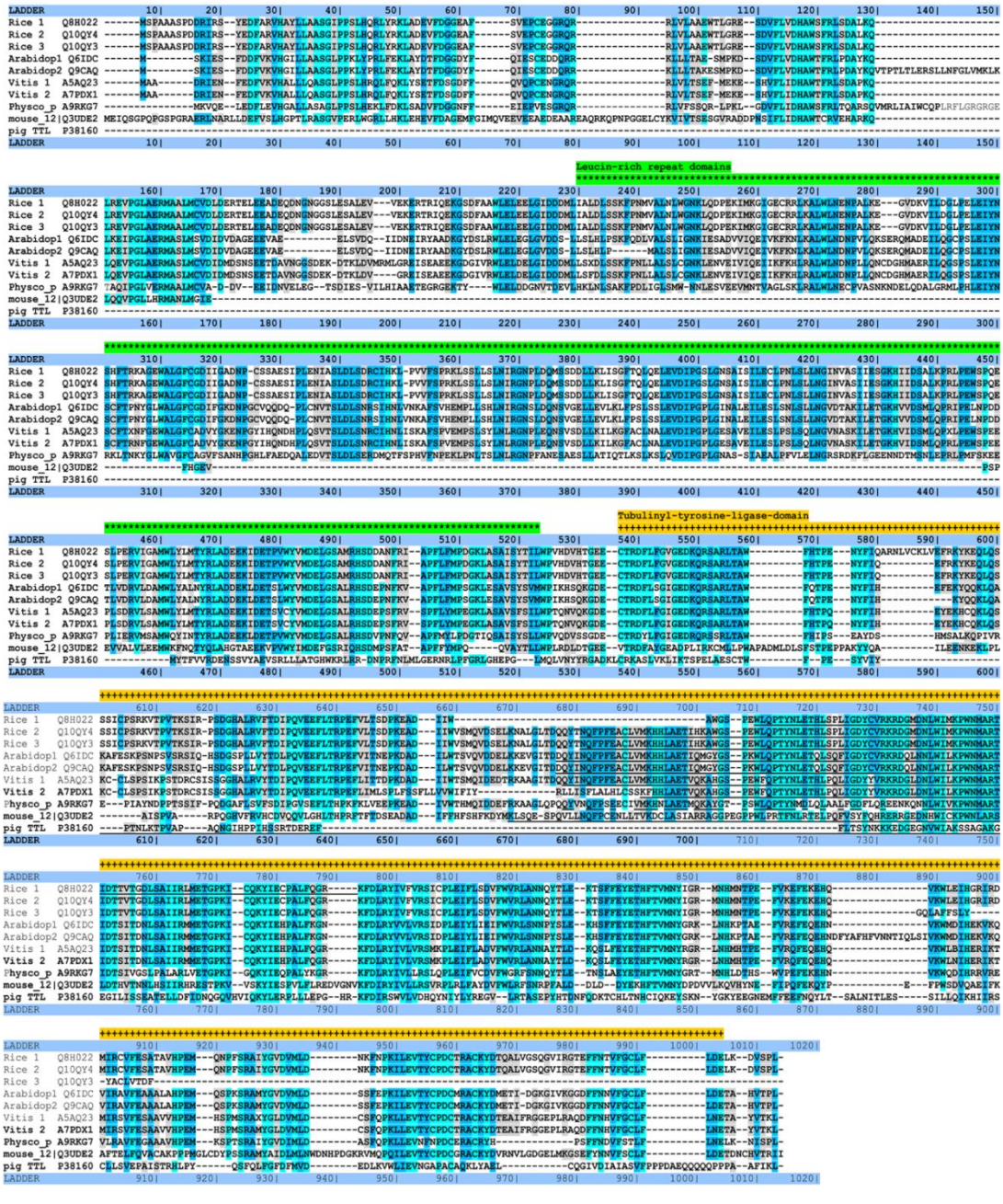

Fig.S1. Multiple alignment of TTL homologues from different eukaryotes.

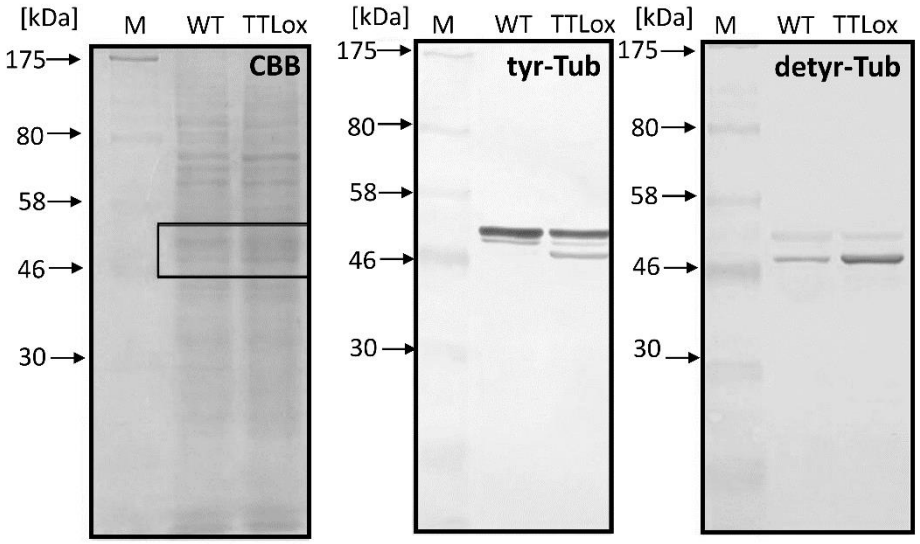

Fig.S2. Tyrosinated and detyrosinated α-tubulin detected by western blot in WT and TTLox BY-2 cell. Coomassie brilliant blue (CCB) stained SDS-gel as control (left); tyrosinated α-tubulin detected by ATT (middle); detyrosinated α-tubulin detected by DM1A (right).

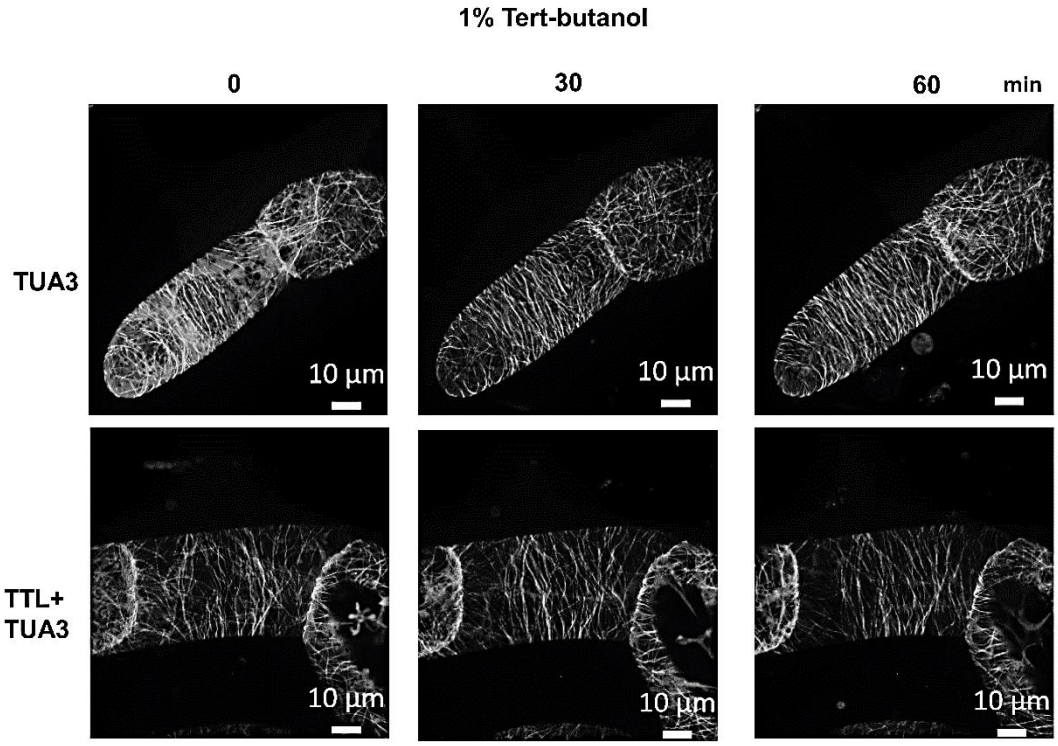

Fig.S3. Comparation of microtubular responses to 1% tert-butanol in BY-2 cell expressing NtTUA3-GFP (TUA3) and overexpression of OsTTL-RFP in NtTUA3-GFP BY-2 cell line (TTL+TUA3). Representative images of responses of cortical microtubules to 1% tert-butanol in both BY-2 cell lines are shown in a time series, respectively. Scale bar: 10 µm.

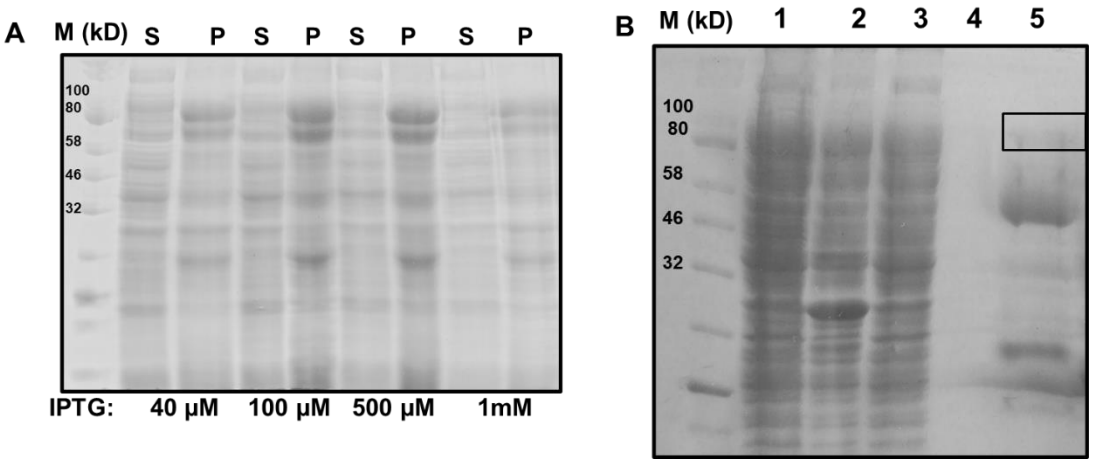

Fig.S4. Recombinant expression of OsTTL fused with His-tag in E. coli *Rosetta*-Gami competent cell and purification. The weight of recombinant OsTTL was around 98 kD. M: Marker of protein size.

A. Representative images of searching for optimize conditions for OsTTL expression under 18℃ incubation after various concentrations of IPTG induction: 40 μM, 100μM, 500μM, 1mM. S: proteins collected in the supernatant after cell broken down; P: proteins collected in the pellet after cell broken down. The weight of recombinant OsTTL was around 98 kD.

B. Purification of 3 L culture of recombinant OsTTL expression in E. coli *Rosetta*-Gami competent cell under 18℃ incubation after 40μM IPTG induction by Nikel-column. The lane in the gel represented:

1: proteins in supernatant after french press;

2. proteins in pellet after precipitation with Ammonium sulfate;

3. proteins collected from washing buffer flowing through Nikel-column binding;

4. proteins collected from washing buffer flowing through Nikel-column binding just before adding elution buffer;

5. proteins collected from elution buffer flowing through Nikel-column.